# 1.15 Analysis of 2-D Crystals of Membrane Proteins by Electron Microscopy

**PD Abeyrathne, M Arheit, F Kebbel, D Castano-Diez, KN Goldie, M Chami, and H Stahlberg,** University of Basel, Basel, Switzerland
**L Renault,** University of Alberta, Edmonton, AB, Canada
**W Kühlbrandt,** Max-Planck-Institute of Biophysics, Frankfurt am Main, Germany





## Abbreviations

| | |
|---|---|
| CCD | charge-coupled device |
| CMC | critical micelle concentration |
| CTF | contrast transfer function |
| DMPC | 1,2-dimyristoyl-sn-glycero-3-phosphocholine |
| HAADE | high-angle annular dark field |
| IPTG | isopropyl-$\beta$-D-1-thiogalactopyranoside |
| LHC | light harvesting complex |
| LPR | lipid-to-protein ratio |
| NMR | nuclear magnetic resonance |

| | |
|---|---|
| **PAGE** | polyacrylamide gel electrophoresis |
| **STEM** | scanning TEM |
| **TEM** | transmission electron microscopy |
| **VDAC** | voltage-dependent anion-selective channel |
| **XRD** | X-ray diffraction |

## Glossary

**Charge-coupled device** An electronic camera in an electron microscope that is used to record images and diffraction patterns.
**Contrast transfer function** The characteristic function by which a microscope transfers the information from the structure of the sample into the image. This is unfortunately not a 1:1 transfer, but can be a quite complicated function.
**Critical micellar concentration** The detergent concentration, above which the detergent starts to form micelles. Detergent is only effective at this concentration or higher.
**Cryo-transmission electron microscopy (Cryo-EM)** A method applying TEM to frozen hydrated specimens.
**Lipid-to-protein ratio** For 2-D crystallization, lipids and proteins are mixed at this ratio.
**Nuclear magnetic resonance** An alternative method to determine membrane protein structures. NMR does not require crystals, but requires high protein concentrations.
**Transmission electron microscopy** The instrument used to record high-resolution images and diffraction patterns of the samples.
**X-ray diffraction** A strong method to determine membrane protein structures. It requires 3-D crystals of the samples.

## 1.15.1 Introduction

X-ray crystallography, nuclear magnetic resonance (NMR), and electron crystallography of 2-D crystals have been used to resolve the structure of soluble and membrane proteins, contributing greatly to the understanding of their function. Among the three methods, electron crystallography has the unique property of determining the structure of the membrane proteins that are embedded in a single layer of a lipid membrane. This facilitates the crystallization of membrane proteins in a near-native state, while preserving their function.[1] Electron crystallography has been employed to study membrane protein structure for several decades (Table 1).[2–4] Genome-wide analysis indicates that up to 30% of proteins encoded by eukaryotic cells are membrane proteins, most of which are likely to contain membrane-spanning alpha helices. The architecture of these proteins is diverse, ranging from membrane proteins with a single transmembrane span to those with multiple transmembrane helices.[5] Membrane proteins fulfill a wide range of biological functions, including energy conversion, nutrient uptake, drug efflux, protein secretion, and signal transduction. Because membrane proteins are crucial for cellular functions, their malfunction can lead to severe diseases. Structural information of membrane proteins will facilitate the study of their interactions with substrates and inhibitors, which may aid researchers in finding effective treatments for many medically important diseases.

## 1.15.2 Membrane Protein 2-D Crystallization

Crystallization of membrane proteins involves several critical steps, which are all important for obtaining high-quality crystals. In this section, the methods, challenges, and recent improvements in each step (Figure 1) that are necessary to attain highly ordered 2-D crystals suitable for electron crystallography are discussed.

### 1.15.2.1 Isolation of Membrane Proteins

The first step involves the production of sufficient amounts of pure and homogenous protein. Three methods are used. The first is to isolate membrane proteins from native tissues or membranes. There are several examples of native membrane proteins that have been successfully produced using this method, such as porins (including mitochondrial voltage-dependent anion-selective channel (VDAC)), photosynthetic proteins (including light harvesting complex (LHC)-II, photosystems, b6f complex, bacterial antenna complexes), respiratory chain proteins (including cytochrome oxidase, complex I), connexins, bovine rhodopsin, the nicotinic acetylcholine receptor (nAChR) from *Tropedo marmorata*, aquaporins, tetraspanin MP20 from sheep lens, and the respiratory complex 1 from *Escherichia coli* (for a more detailed list, see Table 1). Most eukaryotic and prokaryotic membrane proteins are present in native tissues or membranes in minor quantities. Moreover, isolating human membrane proteins from native tissues is not an option.

The limited availability of membrane proteins from native sources is overcome by expressing membrane proteins in homologous or heterologous host organisms. A great deal of work has been carried out to develop expression vectors containing regulated promoters to produce high levels of recombinant proteins. Since a variety of regulated promoters are available for this purpose, a few examples are described below.

The tac promoter (PTAC) is one of the most widely used promoters in expression systems, and is induced by isopropyl $\beta$-D-1-thiogalactopyranoside (IPTG) and lack of tryptophane in the medium. The expression levels from PTAC are proportional to the concentration of IPTG added: Low concentrations of IPTG result in relatively low expression from PTAC and high concentrations of IPTG result in high expression. Therefore, the gene of interest, which is cloned downstream of the PTAC promoter, can be regulated by changing the IPTG concentration. However, several potential problems can occur when expressing a cloned gene product from PTAC. The cell

**Table 1** Structures of membrane proteins analyzed by electron crystallography, and the protein production, purification, and crystallization conditions. Future, updated versions of this table will be maintained at http://2dx.org.

| *Family* | *Protein* | *Resolution 2-D (Å)* | *Resolution 3-D (Å)* | *PDB/EMDB* | *Origin* | *Expressed in* | *Conc (mg ml$^{-1}$)* | *Lipid added* | *LPR (w/w)* | *Detergent* | *Temp (°C)* | *pH* | *Salts (mM unless stated otherwise)* | *Nonionic agents (%)* | *Time* | *Crystallization method* | *Crystal type* | *Reference* |
|---|---|---|---|---|---|---|---|---|---|---|---|---|---|---|---|---|---|---|
| Ion channels | AmtB – ammonium gas ion channel | 12 | | | *E. coli* | *E. coli* | 0.4 | DMPC | 1 | DM | 20 | 8 | 250 NaCl, 0.6 $NaN_3$ | – | 10 d | DI | S | 160 |
| | Annexin A5 – $Ca^{2+}$ specific ion channel | 6.5 | | | Rat | *E. coli* | 0.1 | DOPC/DOPS | – | None | 20 | 7.4 | 150 NaCl, 2 $CaCl_2$, 3 $NaN_3$ | – | 3–4 d | LM | S | 161 |
| | MscL – mechanosensitive ion channel | 15 | | | *E. coli* | *E. coli* | 1 | *E. coli* lipid | 0.45 | Triton X-100 | 4 | 8 | 100 KCl | – | 5 h | BB | V | 162 |
| | VDAC – voltage dependent anion channel | 18 | | | Potato | | | | | | | | | | | – | T | 163 |
| Potassium channels | KcsA potassium channel | 6 | | | *S. lividans* | *E. coli* | 1–2 | DMPC/sodium cholate | – | DDM | RT | 7.5 | 100 KCl, 1 EDTA | – | 3 d | DI | – | 164 |
| | KirBac3.1 potassium channel | 9 | | | *M. magnetotacticum* | *E. coli* | 1 | DOPC | 0.6–1 | DM | 20/37 | 8 | 100 KCl, 3 $NaN_3$, 75 $MgCl_2$ | – | 7 d | BB | S | 165 |
| | MloK1 – cyclic nucleotide–modulated K–channel | 16 | | | *M. loti* | *E. coli* | 0.5 | *E. coli* lipid | | DM | 25/37 | 6.7 | 20 KCl, 1 $BaCl_2$ | – | 5 d | DI | S | 166 |
| Ion antiporters | ClC–ec1 – chloride proton antiporter from *E. coli* | 6.5 | | | *E. coli* | *E. coli* | | POPC | 0.4 | DM | 4 | 7 | 25 NaCl, 20 $MgCl_2$, 0.8 $NaN_3$ | – | several days | DI | S | 167 |
| | NhaA–$Na^+$ – H+ antiporter from *E. coli* | 4 | | | *E. coli* | *E. coli* | 0.8 | *E. coli* lipid | 0.2–0.5 | DDM | 37 | 4 | 25 KAc, 150 KCl, 0.1 $GdCl_3$, 3 $NaN_3$ | 5–10 glycerol | 4–6 d | DI | T | 58 |
| | | | 7 | | *E. coli* | *E. coli* | 0.5 | *E. coli* lipid | 0.2–0.5 | DDM | 37 | 4 | 25 KAc, 150 KCl, 0.1 $GdCl_3$, 3 $NaN_3$ | 5–10 glycerol | 4–6 d | DI | T | 63 |
| | | 7 | | 3FI1 | *E. coli* | *E. coli* | 0.5 | *E. coli* lipid | 0.2–0.5 | DDM | 37 | 4 | 25 KAc, 150 KCl, 0.1 $GdCl_3$, 3 $NaN_3$ | 5–10 glycerol | 4–6 d | DI | T | 168 |
| | NhaP1 – $Na^+$ – $H^+$ antiporter from *M. jannaschii* | 6 | | | *M. jannaschii* | *E. coli* | 1 | *E. coli* lipid | 0.4–0.55 | DDM | 37 | 4 | 200 NaCl, 25 acetate | 10 glycerol | 5–7 d | DI | T | 169 |
| | | | 7 | | *M. jannaschii* | | | | | | | | | | | | | 64 |
| | TetA – secondary tetracycline transporter | 17 | | | *E. coli* | | 1 | DMPC/POPC | 0.5 – 1.5 | DDM (lipids in DM) | | 7.4 | 10 Tris, 150 NaCl, 40 $MgCl_2$ | | | DI | | 88 |
| | Phospholipase A | 7.4 | | | *E. coli* | *E. coli* | 3 | Soybean PC | 0.37–0.44 | OG | 25 | 7.5 | 30 NaCl, 2 $NaN_3$ | 10–20 glycerol | 10–16 d | DI | T | 170 |
| Major facilitator superfamily (MFS) | Lactose permease | 20 | | | *E. coli* | *E. coli* | >1 | DMPC/POPC | 0.5–1.5 | DDM | 13–37 | 7.4 | 150 NaCl, 25–50 $MgCl_2$ | – | 6 d | DI | S | 171 |
| | | 6 | | | | *E. coli* | 1–2 | POPC | 0.2–0.4 | Cymal–7 | 27 | 4.5 | | 20 glycerol | 3 d | DI | T | 172 |

(*Continued*)

**Table 1** Continued

| Family | Protein | Resolution 2-D (Å) | Resolution 3-D (Å) | PDB/EMDB | Origin | Expressed in | Conc (mg $ml^{-1}$) | Lipid added | LPR (w/w) | Detergent | Temp (°C) | pH | Salts (mM unless stated otherwise) | Nonionic agents (%) | Time | Crystallization method | Crystal type | Reference |
|---|---|---|---|---|---|---|---|---|---|---|---|---|---|---|---|---|---|---|
| | OxlT – oxalate transporter | | | | *Oxalobaster formigenes* | | | | | | | | 50 KAc, 100 potassium oxalate | | | | | |
| | | | 6.5 | EMD–1098 | *Oxalobaster formigenes* | *E. coli* | 1–2 | POPC | 0.2–0.4 | Cymal–7 | 27 | 4.5 | 50 KAc, 100 potassium oxalate | 20 glycerol | 3 d | DI | V | [173] |
| | | 3.4 | | | *Oxalobaster formigenes* | *E. coli* | 1–2 | POPC/*E. coli* lipid | 0.15–0.4 | Cymal–7 | 27–37 | 4.5 | 50 KAc/KCit, 100 potassium oxalate | 20 glycerol | 3 d | DI | T/S | [87] |
| Transporters | BetP – glycine betaine uptake system | 7.5 | | | *Corynebacterium glutamicum* | *E. coli* | 1 | *E. coli* lipid | 0.15–0.25 | DDM/$C_{12}E_9$ | 20 | 7.5 | 200 NaCl, 1.5 $MgCl_2$, 3 $NaN_3$ | 10 glycerol | 14 d | DI/BB | T/S | [174] |
| | CTR1 – copper transporter | | 6 | | Human | *P. pastoris* | 0.3–0.5 | DOPC | 0.7 | DM | 26 | 7.4 | 280 NaCl, 2 EDTA | – | 1–2 d | DI | S | [175] |
| | | 7 | 15 | EMD–1593 | Human | *P. pastoris* | 1 | DOPC | 0.7 | OG | 26 | 7.4 | 280 NaCl, 2 EDTA | | 1–2 d | DI | S | [176] |
| | UT – urea transporter: *A.* | | | | *pleuropneumoniae* | | 24 | | *Actinobacillus* | | | | | | | | | |
| | | | | | *pleuropneumoniae* | *E. coli* | 1 | DMPC/DOPC | 0.1–1.5 | DDM | 30 | 6 | 200 NaCl, 3 $NaN_3$ | – | 7 d | DI | S | [12] |
| | Mannitol transporter enzyme II | 5 | | | *E. coli* | *E. coli* | 0.7–1.4 | *E. coli* lipid | 1 | CHAPS/DM | 4 | 7.5 | 150 NaCl, 5 EDTA, 3 $NaN_3$ | – | 14 d | DI | S | [57] |
| | MelB – melibiose permease | 8 | | | *E. coli* | *E. coli* | 1 | *E. coli* lipid | 25–40 (molar) | DDM | 22 | 6 | 200 NaCl | 10 glycerol | 9 d | DI/BB | T | [177] |
| | GalP – galactose permease | 18 | | | *E. coli* | *E. coli* | 0.5–1 | DMPC | 0.2–0.6 | DM | RT | 8 | 150 NaCl, 25 $CaCl_2$, 1.5 $NaN_3$ | – | ? | DI | V | [178] |
| Transporters | IICP–glucose transporter | 12 | | | *E. coli* | *E. coli* | 1 | *E. coli* lipid | 0.4 | DDM | 24 | 9.5 | 20 mM Tris-HCl, 150 NaCl, 5 $MgCl_2$ | 0.01 $NaN_3$ | 7 d | DI | T | [179] |
| Antiporter | AdiC (amino acid/polyamine/organocation transporter superfamily) | 6.5 | | | *E. coli* | *E. coli* | 1 | *E. coli* lipid | 0.3 | DDM | RT | 5 | 250 NaCl, 1.5 $NaN_3$ | 10 glycerol | 14 d | DI | T | [180] |
| ABC transporters | MsbA – ABC transporter | | 20 | | *Vibrio cholerae*/ *Salmonella typhimurium* | *E. coli* | 0.6 | DOPS/DMPC | 1 | Cymal–7/ UDM | RT | 5–6/9 | 50 NaCl, 5 $MgCl_2$, 5 sodium orthovanadate | – | 12–36 h | BB | T | [181] |
| | EmrE – small multidrug resistance transporter | 7 | | | *E. coli* | *E. coli* | 0.5 | DMPC | 0.1–0.4 | DM/CHAPS | 25 | 7 | 50 NaCl, 20 $NaN_3$ 2 $MgCl_2$, 1 EDTA | – | 10–14 d | DI | T/V | [182] |
| | | 7 | | | *E. coli* | *E. coli* | 1 | DMPC | 0.1–0.4 | DM/CHAPS | 25 | 7–7.5 | 100 NaCl, 20 $NaN_3$, 2 $MgCl_2$, 1 EDTA | – | 10–14 d | DI | T/V | [183] |
| | | | 7.5 | EMD–1087 | *E. coli* | *E. coli* | 1 | DMPC | 0.1–0.4 | DM/CHAPS | 25 | 7–7.5 | 100 NaCl, 20 $NaN_3$, 2 $MgCl_2$, 1 EDTA | – | 10–14 d | DI | T/V | [184] |

| | | | | | | | | | | | | | | | | | |
|---|---|---|---|---|---|---|---|---|---|---|---|---|---|---|---|---|---|
| | | 7 | | | *E. coli* | *E. coli* | 0.5–1 | DMPC | 0.3–0.4 | DM/CHAPS | 25 | 7.5 | 100 NaCl, 20 $NaN_3$, 2 $MgCl_2$, 1 EDTA | – | 10–14 d | DI | T/V | [185] |
| | BmrA – multidrug ABC transporter | 20 | | | *Bacillus subtilis* | *E. coli* | 0.25 | DOPC/DOPG | 0.5–1 | DDM | 4 | 8 | 150 KCl, 5 $MgCl_2$ | – | 2 d | LM/BB | S | [186] |
| | Pgp – P–glycoprotein | 22 | | | Mouse | *P. pastoris* | 0.1 | DOGS–NiNTA/ egg PC | – | DM | 37 | 8 | 50 Tris–HCl 100 NaCl | – | 1 d | LM/BB | | [187] |
| Anion exchangers | Band 3 – erythrocytes anion exchanger | 23 | | | Human erythrocytes | – | 0.75–1.0 | DMPC | – | octylPOE | 22/37 | – | 25–50 NaCl 20 $MgCl_2$ | – | ~2 d | DI | V | [93] |
| | | | 20 | | Human erythrocytes | – | – | DMPC/ cholesterol | – | $C_{12}E_8$ | – | 8 | 100 NaCl 10 $MgCl_2$ 5 sodium phosphate | 10 PEG 200 | – | – | S | [188] |
| | AE1 – human erythrocyte anion exchanger | | 7.5 | EMD–1645 | Human blood | | 2.5 | DOPS | 0.15 | $C_{13}E_8$, $C_{12}E_8$ | 26 | 8 | 10 Tris, 100 NaCl, 100 $Na_4P_2O_7$ | | 13 d | DI | S | [189] |
| Aquaporins | Aqp0 – water channel from eye lenses | 9 | | | Sheep eye lens fiber | | 1 | *E. coli* | 1 | DM | 24,37,24 | 7.2 | 100 NaCl, 50 $MgCl_2$ | – | 3 d | DI | V/S | [190] |
| | | 4 | | | Sheep lens fiber cells | – | – | DMPC | – | DM | RT | 6 | 10 MES 50 $MgCl_2$ 150 NaCl, 5 DTT 0.02% $NaN_3$ | – | – | DI | V/S | [191] |
| | | | 3 | 1SOR | Sheep lens | – | – | DMPC | – | DM | RT | 6 | 10 MES 50 $MgCl_2$ 150 NaCl 5 DTT, 0.02% $NaN_3$ | – | – | DI | S | [152] |
| | | | 1.9 | 2B6O | Sheep lens | – | 0.25 | DMPC | – | DM | RT | 6 | 10 MES, 50 $MgCl_2$, 150 NaCl, 5 DTT, 0.02% $NaN_3$ | – | – | DI | S | [77] |
| | | | 2.5 | 3M9I | Sheep lens | – | 0.25 | *E. coli* lipid | – | OG | 37 | 6 | 10 MES, 50 $MgCl_2$, 150 NaCl | – | 7 d | DI | S | [78] |
| | Aqp1 – water channel from erythrocytes | | 16 | | Human red blood cells | – | 0.5 | *E. coli* lipid | 0.1–2.0 | Laur-oylsarco-sine/TX–100/OG | 25–35 | 5.8–8.8 | 20 Tris–HCl, 0.25 NaCl, 1 DTT, 1 sodiumazide | – | 2 d | DI | V/S | [1] |
| | | | 6 | | Human red blood cells | – | – | *E. coli* lipid | 2 | Laur-oylsarco-sine/TX–100/OG | 25–35 | – | – | – | 2 d | DI | – | [192] |
| | | | 3.8 | 1FOY | Human red blood cells | – | – | *E. coli* lipid | 2 | Laur-oylsarco-sine/TX–100/OG | 25–35 | – | – | – | 2 d | DI | – | [89] |
| | | | 4 | | Human red blood cells | – | 1 | DOPC | 0.28–0.33 | OG | – | 7.2 | 20 $NaH_2PO_4$/ $Na_2HPO_4$, 100 NaCl, 0.1 EDTA 0.03% $NaN_3$ | – | – | – | – | [193] |
| | | | 3.7 | 1IH5 | Human erythrocytes | – | – | – | – | – | – | – | 20 $NaH_2PO_4$, $Na_2HPO_4$ (pH 7.1),100 | – | – | – | – | [150] |

(*Continued*)

**Table 1** Continued

| Family | Protein | Resolution 2-D (Å) | Resolution 3-D (Å) | PDB/EMDB | Origin | Expressed in | Conc (mg $ml^{-1}$) | Lipid added | LPR (w/w) | Detergent | Temp (°C) | pH | Salts (mM unless stated otherwise) | Nonionic agents (%) | Time | Crystallization method | Crystal type | Reference |
|---|---|---|---|---|---|---|---|---|---|---|---|---|---|---|---|---|---|---|
| | | | | | | | | | | | | | NaCl,0.1 EDTA, 0.025% NaN3 | | | | | |
| | | 3.5 | | | Bovin erythrocytes | – | 1 | DMPC | – | Laur-oylsarco-sine/OG | – | 7.4 | – | – | – | DI | V | 194 |
| | | | 3.8 | 1H6I | | – | – | – | – | – | – | – | – | – | – | – | | 195 |
| | Aqp2 – mammalian water channel | | 4.5 | | Human | sf9 | 0.7 | Heart polar lipids or *E. coli* lipids | 0.5 | OG | 20–37 | 6 | 20 MES, 100 NaCl, 5 $MgCl_2$, or $MgSO_4$, 5 histidine | | 2 d | DI | S | 196 |
| | Aqp4 – mammalian water channel (Aqp4M23) | | 3.2 | 2-D57 | Rat | sf9 | 1 | *E. coli* lipid | – | OG | 20–37 | 6 | 10 MES (pH 6.0), 100 NaCl, 50 $MgCl_2$, 2 DTT, 1% (v/v) glycerol | 1 Glycerol | 3 d | DI | S | 153 |
| | | | 2.8 | 2ZZ9 | Rat | sf9 | NS | *E. coli* lipid | 1.4 | OG | 20–37 | 6 | 10 4-morpholineetha-nesulfonic acid (pH 6.0), 75 NaCl, 50 $MgCl_2$, 2 DTT | 1% Glycerol | 3 d | DI | S | 197 |
| | | | 10.0 | 3IYZ | Rat | sf9 | NS | *E. coli* lipid | 1.4 | OG | 20–37 | 6 | 10 4-morpholineetha-nesulfonic acid (pH 6.0), 75 NaCl, 50 $MgCl_2$, 2 DTT | 1% Glycerol | 3 d | DI | S | 198 |
| | Aqp9 – mammalian glycerol (and water-) channel | 7 | | | Rat | sf9 | 1–3 | DMPC | 0.4–0.6 | OG | 25 | 6 | 20 MES (pH 6), 150 NaCl, 50 $CaCl_2$, 1 dithiothreitol | | 7 d | DI | V | 53 |
| | AqpZ – *E. coli* waterchannel | 8 | | | *E. coli* | *E. coli* | 0.5 | POPC-DMPC | 0.3–2 | OG | RT | 6 | 20 citrate (pH 6.0) buffer containing 200 NaCl, 100 $MgCl_2$, 3 $NaN_3$ | 1% Glycerol | 2–3 d | DI | S | 199 |
| | SOPIP2;1 – plant aquaporin waterchannel | | 5 | | Spinach leaf | *P. pastoris* | NS | *E. coli* lipid | 0.3 | OG | NS | 8 | 20 Tris-HCl (pH 8), 100 NaCl, 50 $MgCl_2$, 2 DTT, 0.03% (w/v) $NaN_3$ | | 3 d | DI | S | 200 |
| | PM28A, C | – | – | | spinach leaf | | 1.33 | *E. coli* lipid | 1 | OTG | 24–37 | 6 | 10 MES-NaOH, 100 NaCl, 100 $MgCl_2$, 2 DTT | | 3 d | DI | S | 201 |
| | AtTIP3;1 – plant vacuole membrane aquaporin | 7.7 | | | *P. vulgaris L. cv. Greensleeves* | – | – | – | – | DHPC | 27–28 | 7.5 | 25 TEA (pH 7.5), 100 NaCl, 3 $NaN_3$, 1 DTT, 0.1 butylated hydroxytoluene, 0.1 EDTA | 10 Glycerol | 10–15 d | DI | T | 202 |
| | GlpF – *E. coli* glycerol channel | | 6.9 | | *E. coli* | *E. coli* | – | *E. coli* lipid | – | OG | – | – | 10 tricine (pH 8.5), 4 $MgCl_2$, 100 NaCl, 10 DTT | – | – | DI | S | 203 |
| | | 3.7 | | | *E. coli* | *E. coli* | 1 | *E. coli* lipid | 0.6–1.4 | OG | 25–40 | 8.5 | 10 tricine (pH 8.5), 4 $MgCl_2$, 100 NaCl, 10 DTT | - | 2 d | DI | S | 204 |
| Receptors | nAChR – nicotinic acetylcholine receptor | | | | *T. marmorata* | – | – | Native lipids | – | – | 4–17 | 6.8 | 100 Tris–HCl | – | 2–3 d | Dilution | T | 205 |

| | | | | | | | | | | | | | | | | | | |
|---|---|---|---|---|---|---|---|---|---|---|---|---|---|---|---|---|---|---|
| | | | 17 | | *T. marmorata* | – | – | Native lipids | – | – | – | 6.8 or 11 | 100 Sodium cacodylate or 100 sodium phosphate | – | – | DI | T | 206 |
| | | | 9 | | *T. marmorata* | – | – | Native lipids | – | – | 4–17 | 6.8 | 100 Tris-HCl | acetylcholine | – | Dilution | T | 207 |
| | | | 4 | 1OED | *T. marmorata* | – | – | Native lipids | – | – | | 6.8 | 100 Sodium cacodylate, 1 $CaCl_2$ | – | – | – | T | 151 |
| | | | 4 | 2BG9 | *T. marmorata* | – | – | Native lipids | – | – | – | – | – | – | – | – | T | 61 |
| | RyR–ryanodine receptor | 20 | | | New Zealand white rabbit skeletal muscle | | 0.1–1 | DOPC | – | CHAPS | – | 7.1 | 20 Na-PIPES, 100 KCl, 0.1 $CaCl_2$, 0.1 EGTA | 20 glycerol | 3–6 h | LM | S | 208 |
| Mitoch. OMP | TspO–polytopic mitochondrial OMP | | 10 | | *R. sphaeroides* | *E. coli* | 0.5–1.0 | *E. coli* lipid | 0.2–0.6 | DDM | – | 7.5 | 20 Tris, 100 NaCl, 2 EDTA | – | 3 d | DI | T | 209 |
| ADP/ATP car. | Anc2–ADP/ATP transporter (bovine mitochondria) | 18 | | | Yeast mitochondria | – | 0.03 | Egg PC | – | DDM | – | – | – | – | – | LM | S | 210 |
| GGCX | GGCX–h.s. vitamin K dependent G-glutamyl carboxylase | 12 | | | Human liver | | 0.6–1 | DMPC | 1 | DOC | 20 | 7.2 | 250 NaCl | | 1–4 d | D | T | 211 |
| Prokaryotic rhodopsins | Bacteriorhodopsin – light-driven proton pump | | 7.0 | | *H. halobium* | | | | | | | | | | | *in situ* | S | 131 |
| | | | 6.5 | | *H. halobium* | | | | | | | | | | | *in situ* | S | 212 |
| | | | 6.0 | | *H. halobium* | | | | | | | | | | | *DOC extraction* | S | 213 |
| | | | 3.5 | 1BRD | *H. halobium* | | 3 | | | OG and DTAC | 20 | 5.2 | | | ‘Several weeks’ | FU | S | 129 |
| | | | 3.5 | 2BRD | *H. halobium* | | 3 | | | OG and DTAC | | | | | 2 w–3 m | FU | S | 214 |
| | | | 3 | 1AT9 | *H. halobium* | | 3 | | | OG and DTAC | 20 | 5.2 | | | ‘Several days’ | FU | S | 215 |
| | | | 3 | 2AT9 | *H. halobium* | | | | | DTAC | | | | | Several days | FU | S | 146 |
| | | 3.5 | | | *H. halobium* | | | | | | | | | | | | | 216 |
| | | 3.5 | | | *H. halobium* | | | | | | | | | | | | | 217 |
| | | | 3.2 | 1FBB | *H. halobium* | | | | | | | | | | | | | 218 |
| | | | 3.2 | 1FBK | triple mutant | | | | | | | | | | | | | 218 |
| | | | 3.5 | | F219L mutant | | | | | OG and DTAC | 20 | 5.2 | | | ‘Several days’ | FU | S | 219 |
| | | | 6.5 (XRD) | | *H. halobium* | | | | | OG | 33 | 5 | Sodium phosphate/ammonium sulfate | | Over night | SP | N/C | 97 |
| | | | 3 | | *H. halobium* | | 3 | | | OG and DTAC | 20 | 5.2 | | | ‘Several days’ | FU | S | 220 |
| | Halorhodopsin—light-driven chloride pump | 6 | | | | | | | | | | | | | | | | 221 |
| | | | 7 | | H. HR strain D2 | | | | | | | | | | | | | 222 |
| | | | 5 | | H. HR strain D2 | | | | | | | | | | | *in situ* | S | 223 |
| Eukaryotic rhodopsins | Metarhodopsin I | | 5.5 | EMD-1079 | | | | | | LDAO | 18 | 7 | 20 HEPES, 100 NaCl, 10 $MgCl_2$, 3 $NaN_3$ | | 11 d | D | S | 224 |
| | Bovine rhodopsin | 9 | | | | | | | | | | | | | | | | 225 |
| | | 9.5 | | | Bovine rods outer segments | | 1 | | | $C_8E_4$ | | 7 | 20 HEPES, 100 NaCl, 10 $MgCl_2$, 3 $NaN_3$ | | 5–20 d | D | V | 226 |

(*Continued*)

**Table 1** Continued

| *Family* | *Protein* | *Resolution 2-D (Å)* | *Resolution 3-D (Å)* | *PDB/EMDB* | *Origin* | *Expressed in* | *Conc (mg ml$^{-1}$)* | *Lipid added* | *LPR (w/w)* | *Detergent* | *Temp (°C)* | *pH* | *Salts (mM unless stated otherwise)* | *Nonionic agents (%)* | *Time* | *Crystallization method* | *Crystal type* | *Reference* |
|---|---|---|---|---|---|---|---|---|---|---|---|---|---|---|---|---|---|---|
| | | 5 | | | Bovine rods outer segments | | | | | LDAO | 18 | 7 | 20 HEPES, 100 NaCl, 10 $MgCl_2$, 3 $NaN_3$ | | 11 d | D | T | 227 |
| | | | 5.5 | | Bovine rods outer segments | | | | | LDAO | 18 | 7 | 20 HEPES, 100 NaCl, 10 $MgCl_2$, 3 $NaN_3$ | | 11 d | D | T | 228 |
| | Squid rhodopsin | 8 | | | Squid retina | | | Squid photoreceptor lipids | | OG | 20 | 5.9 | 20 MES, 100 NaCl, 1 $MgCl_2$ | | 5 d | D | S | 229 |
| | | | 8 | | Squid retina | | | Squid photoreceptor lipids | | OG | 20 | 5.9 | 25 MES, 100 NaCl, 1 $MgCl_2$ | | 5 d | D | S | 230 |
| | | | 7.5 | | Frog retina | | 1 | | u | Tween 80 | ~21 | 7.5 | 100 NaCl | | 16–30 h | *in situ* | T/V | 231 |
| | | 8 | | | Squid retina | | ~0.9 | Squid photoreceptor | u | OG | 20 | 5.9 | 100 NaCl, 1 $MgCl_2$ | | 5 d | D | V | 229 |
| | | | | | Bovine retina | | 1 | | u | LDAO | 18 | 7 | 100 NaCl, 10 $MgCl_2$ | | 11 d | D | T/V | 231 |
| | Sensory rhodopsin | 6.9 | | | *N. pharaonis* | *H. salinarium* | 1.4 | *H. salinarium* | 0.4 | OG | 8 | 5.5 | 300 NaCl | | >40 h | D | T/V | 232 |
| Eukaryotic rhodopsin | channelrodopsin-2 | 6 | | | *C. reinhardtii* | *P. pastoris* | 1–3 | DMPC, E *coli* lipid | 1.25, 8.75 | DM | 25–28 | 7 | 20 mM HEPES, 100 mM NaCl, 10 mM $MgCl^2$ | 20 Glycerol | 2–6 w | DI | T | 233 |
| Translocases | SecYEG – bacterial core protein translocase | 9 | | | *E. coli* | *E. coli* | 0.4–0.15 | DOPG PE | 0.2 | $C_{12}E_9$ | 23 | 8 | 5 $MgCl_2$, 120 NaCl, 1 EDTA | | Weeks | D | T | 55 |
| | | | 8 | | | | | | | | | | | | | | | 234 |
| | YidC – membrane insertase | 10 | | | *E. coli* | *E. coli* | 0.5 | DPPG | 0.05–0.2 (w/w) | DM | 30 | 5.6 | 100 NaCl $_2$, $NaN_3$ | | | D | T/S | 235 |
| Membrane-associated protein with functions in eicosanoid and glutathione metabolism (MAPEGs) | MGST1 (rat microsomal glutathione-S transferase 1) | 3 | | | Rat liver | | 1 | Bovine liver lecithin | 3 | | 21 | 8 | 50 KCl | | 8 d | D | S | 236 |
| | | 3 | | | Rat liver | | 1 | Bovine liver phosphatidylcholine | 3 | TX-100/ cholate | 4.0–20 | 6.5–10.2 | KCl | | 4–10 d | D/B | V/S | 237 |
| | | 3 | | | Rat liver | | | Bovine liver lecithin in cholate | 2.0–3.0 | TX-100 | 21 | 7 | 50 KCl | | 8 d | D | S | 238 |
| | | | 6 | | Rat liver | | 1 | Bovine liver phosphatidylcholine | 3 | TX-100/ cholate | 4.0–20 | 6.5–10.2 | KCl | | 4–10 d | D | S | 239 |
| | | | 6 | | Rat liver | – | 0.5–1.75 | DOPC | 0.15–0.3 | TX-100 | RT | 7 | 50 KCl | 20 glycerol, Glutathione 1 GSH | 7 d | DI | S | 240 |
| | | | 3.2 | 2H8A | Rat liver | – | 0.5–1.75 | DOPC | 0.15–0.3 | TX-100 | RT | 7 | 50 KCl | 20 glycerol, 1 GSH | 7 d | DI | S | 154 |
| | MPGES1 (h.s. microsomal prostaglandin E2 synthase 1) | | 3.5 | 3-DWW | Human | *E. coli* | 1 | Bovine liver lecithin | 0.5 | TX-100 | RT | 7.5 | 50 NaCl | 20 glycerol, 1 GSH | 7 d | DI | S | 155 |

| | | | | | | | | | | | | | | | | |
|---|---|---|---|---|---|---|---|---|---|---|---|---|---|---|---|---|
| | LTC(4)S – leukotriene C4 synthase | 4.5 | | Human | *S. pombe* | 1 | DMPC | 1 | TX-100/DOC | RT | 7.6 | 50 KCl, 50 HEPS, 1 EDTAE | 20 glycerol, 10 bM, 10 GSH | 10–14 d | DI | S | 241 |
| | | 7.5 | | Human | *S. pombe* | 0.3–several mgs | DOPC DMPC | 0.05–0.5 | TX-100/DOC | 23–24 | – | 50 KCl, 50 HEPS, 1 EDTAE | 20 glycerol, 10 bM, 10 GSH | 8–21 d | DI | S/V | 242 |
| Photosynthesis proteins (bacteria) | RC – photosynthetic reaction center | 20 | | *R. viridis* | – | 1–2 | – | U | LDAO | 23 | 5.3 | 100 Pi | 100 $NaH_2PO_4$ | >24 h | DI | S/V | 243 |
| | LHC1 – light harvesting complex 1 | 8.5 | | *R. rubrum* | | 1.7 | DOPC | ~0.1 | OG | 4 | 7.8 | 50 NaCl, 5 $MgCl_2$ | – | 5 d | DI | V | 244 |
| | LHC1-RC – light harvesting complex 1 with photosynthetic reaction center | 25 | | *R. sphaeroides* | | 0.5 | DOPC | 0.4–0.9 | DHPC/ OG | 20–35 | 7.5 | 150 NaCl, 2 $MgCl_2$ | – | 64 h | DI | S/V | 245 |
| | | 16 | | *R. rubrum* | | 1 | DOPC | 0.75–1.33 | DHPC | 8 | 7.9 | 200 NaCl, 10 $MgCl_2$ | – | 7 d | DI | S/V | 246 |
| | | 10 | | *R. viridis* | | 0.5 | Soybean PC | 1 | CHAPS | 25–30 | 8 | 1 EDTA | 5 glycerol | 4–7 d | DI | S | 247 |
| | | 8.5 | | *R. rubrum* | | 0.5 | DOPC | 1–1.2 | DHPC | 20–35 | 7.5 | 100 NaCl | – | 64 h | DI | S | 248 |
| | | 9 | | *R. rubrum* | | 0.5 | DOPC | 1 | DHPC | 25–30 | 7.5 | 100 NaCl | – | 64 h | DI | S | 249 |
| | LHC1-RC-PufX | 26 | | *R. sphaeroides* | | 0.4 | PC/PA 9:1 | 0.75–1 | DTM | 4 | 7.8 | 200 NaCl | – | 24 h | BB | V | 250 |
| | | 8.5 | 30 | *R. sphaeroides* | | 0.5 | EC lipid | 0.4 | DDM | 20 | 7.5 | 100 NaCl | – | 10 d | DI | | 251 |
| | | 25 | | *R. sphaeroides* | | | | | | | | | | | *in situ* | S | 252 |
| | LHC2 – light harvesting complex 2 | 18 | | *R. sulfidophilum* | | 1 | DMPC | 0.7 | OG | 25 | 8 | | – | Several days | DI | S/T | 253 |
| | | 7 | | *R. sulfidophilum* | | 1 | DMPC | n.r. | OG | n.r. | 8 | | – | 3–10 d | DI | T | 254 |
| | | 6 | | *R. sphaeroides* | | 0.5 | DOPC | 0.4–0.9 | OG | 20,35,20 | 7.5 | | – | 64 h | DI | T | 245 |
| | | 10 | | *R. gelatinosus* | | 0.2–0.7 | PC, PC/PE 1:1 | 0.3 | LDAO | RT | 8 | 300 NaCl, 5 $MgCl_2$ | – | 4 h | BB | S | 255 |
| | Photosystem I | 15 | 25 | *Synechococcus* | | n.r. | | U | TX-100 | 4 | 6.5 | 0.5 EDTA | – | 2–3 d | BB | S/V | 256 |
| Photosynthesis proteins (plants) | PS I – photosystem I | 20 | | *Synechococcus* | | 1.6 | DMPC | 0.25 | OTG | 25–37 | 7 | 50 $MgCl_2$ | – | 60 h | DI | S/V | 94] |
| | PS II – photosystem II | 20 | | Spinach chloroplast | | 2 | | | HTG | 20 | 6.5 | 20 NaCl, 1 $CaCl_2$ | – | 4 d | DI | S/T | 80] |
| | | 20 | | Spinach chloroplast | | | DMPC | | OTG | 6–20 | 6 | 10 NaCl | – | 1–5 d | Dilution | T | 257 |
| | | | 8 | Spinach chloroplast | | 1 | No lipid added | | HTG | 20 | 6.5 | 20 NaCl, 1 $CaCl_2$, 1 ZnAc | – | 4 d | DI | T | 81 |
| | | 9 | | Spinach chloroplast | | ~2 | Thylakoid lipids | | | 22 | 6.5 | 20 NaCl, 1 $CaCl_2$, 1 ZnAc | 30 glycerol | 1 d | BB | T | 258 |
| | | 16 | | *S. elongatus* | | | *S. elongatus* thylakoid lipid | | HTG | 20 | | 5 $MgCl_2$, 5 $ZnSO_4$ | 30 glycerol | 7 d | BB | S | 259 |
| | | 20 | | *viridis zb63* | | | | | □-DM | | | | | | *in situ* | S | 260 |
| | LHC I – light-harvesting chlorophyll a/b–protein complex | 3.7 | | | | | | | TX-100/NG | 25–40 | | | – | 2 d | | | 261 |
| | | | 6 | | | | | | | | | | – | | | | 262 |
| | | 3.2 | | | – | 1.5 | | 0.25 | TX-100/NG | 25,40 | 7 | | 40 glycerol | 2 d | DI | S | 96 |
| | | | 3.4 | Pea chloroplast | – | 1.5 | | 0.25 | TX-100/NG | 25,40 | 7 | | 40 G | 2 d | DI | S | 149 |
| | LHC II – light harvesting complex II | 18 | | *Rhodovulum (Rhv.) sulfidophilum* | – | 1 | DMPC | | OG | 25 | 8 | 50 Tris-HCl, 3 sodium azide | – | 3–10 d | DI | T | 253 |
| | | 18 | | *Ectothiorhodospira* sp. | – | 0.1 | PC | 1:3–4 | LDAO/DDM | 22 | | | – | – | DI | V | 263 |
| | | 27 | | *Rhodobacter capsulatus* | – | 2 | PC | 1–1.4 | LDAO/DDM | 22 | | | – | – | DI | V | 263 |
| Electron transport chain | Cytochrome $b_6f$ complex | 8 | | *C. reinhardtii* chloroplast | – | 0.5 | Egg PC/DOPG | 0.2 | Hecameg | 4 | 8 | 245 AP, 2 $CaCl_2$ | 0.3 glycerol | Days | BB | m | 69 |
| | | 8 | | Spinach chloroplast | – | 1 | Egg PC/DOPG | 0.5 | Hecameg | 4 | 8 | 400 AP, 2 $CaCl_2$ | 1 glycerol | 6 d | BB | V | 56 |
| | | 9 | | *C. reinhardtii* | – | 0.5–1.0 | Egg PC/PG | 0.3 | Hecameg | 4 | | | | | SM2-Bio Beads | | 68 |
| | | 25 | | | – | 0.5–1.0 | PC, PE | ~1 | | 25 | 5.5–6.0 | 0.5 EDTA | – | – | DI | T | 70 |

(*Continued*)

**Table 1** Continued

| Family | Protein | Resolution 2-D (Å) | Resolution 3-D (Å) | PDB/EMDB | Origin | Expressed in | Conc (mg $ml^{-1}$) | Lipid added | LPR (w/w) | Detergent | Temp (°C) | pH | Salts (mM unless stated otherwise) | Nonionic agents (%) | Time | Crystallization method | Crystal type | Reference |
|---|---|---|---|---|---|---|---|---|---|---|---|---|---|---|---|---|---|---|
| | Cytochrome $bc_1$ complex | | 16 | | *Neurospora* mitochondria | – | – | – | – | TX-100, $C_{12}$POE – | – | – | – | – | – | – | – | 264 |
| | Cytochrome *bo* | 6 | | | *E. coli* | *E. coli* | 1 | Egg PC/brain PS | 0.29 | TX-100 | 37 | 10 | | – | Days | DI | T | 265 |
| | Cytochrome *c* oxidase – Cyt $aa_3$ | | 20 | | Bovine heart mitochondria | – | 2 | – | – | TX-100 | 0–5 | 7.2 | 1000 KCl | S | – | *in situ* | V | 266 |
| | Cytochrome *c* oxidase – Cyt $aa_3$ | 25 | | | *P. debitrificans* | – | 0.2 | Egg PC brain PS | – | DDM | 12 | 7 | 20 bistris-propane | – | – | DI | T | 267 |
| | Cytochrome *c* oxidase – Cyt *bo* | 25 | | | *E. coli* | – | 0.35 | Soybean PC brain PS | – | LDAO | – | 6.9 | 20 bistris-propane | – | – | DI | T | 267 |
| | Cytochrome *c* oxidase – Cyt *bo* | 25 | | | *E. coli* | – | 0.35 | Egg PC brain PS | – | TX-100 | – | – | 20 bistris-propane | – | – | DI | S | 267 |
| | Cytochrome c oxidase – Cyt *bo* | 40 | | | *E. coli* | – | 1.5 | PC | – | DDM | 24 | 8 | 20 Tris/HCl | – | | DI | T | 267 |
| | Cytochrome c oxidase – Cyt $aa_3$ | 25 | | | *R. sphaeroides* | – | 0.1–0.2 | Egg PC brain PS | – | DDM | – | 7 | 20 bistris-propane 2.5% isopropanol | – | 24 h | – | V/S | 267 |
| | Cytochrome *c* reductase | 25 | | | *N. crassa* mitochondrial membrane | – | 2.5–3.0 | POPC POPS | 1.7 | TX-100 | – | 7 | 50 Tris-acetate | – | Over night | DI | V | 268 |
| | Complex 1 | 13 | | | Bovine | – | 1 | DOPC | 0.4 | t-DOC | 4 | 7.5 | 200 NaCl | – | 10 d | BB | T | 269 |
| | Complex 1 membrane subcomplex | 20 | | | Bovine mitochondria | – | 1 | DOPC | 0.4 | t-DOC | 22 | 9 | 600 NaCl, 10 $CaCl_2$, 2 $NAD^+$ | – | 2 w | BB | V | 269 |
| ATPases | F1Fo-ATP synthase | 30 | | | | | 0.01–0.15 | DOPC | 0.5–0.75 | DDM | – | – | – | – | 1 d | LM | S | 102 |
| | | 4 | | | *I. tartaricus* | *I. tartaricus (DSM 2382)* | 1 | POPC | 0.5 | OG | 20, 37 | 7.5 | 10 Tris-HCl, 200 NaCl, 3 $NaN_3$ | – | 2 d | DI | V | 62 |
| | KdP-ATPase | 22 | | | *E. coli* | *E. coli* | 3 | – | – | – | – | 7.5 | 150 $Na_3VO_4$ | – | 3–14 d | *in situ* | V | 270 |
| | | 29 | | | Bovine | | 0.8 | DOPC/DOPA | 1.2 | DDM | 4–20 | 7.3 | 50 HEPES, 300 NaCl, 5 $MgCl_2$ | – | 2 d | LM | S | 271 |
| | V-ATPase | 23 | | | *T. thermophilus* | *T. thermophilus* | 2 | POPC | 0.2 | Triton X-100 | 4 | 8.7 | – | – | – | DI | S | 272 |
| | Rotor ring of the V-ATPase | 7 | | | *T. thermophilus* | *T. thermophilus* | 2 | POPC | 0.25 | Triton X-100 | – | 8 | – | – | – | DI | V | 273 |
| | Rotor ring of the $Na^+$ F-ATPase | 6 | | | *I. tartaricus* | | 0.8 | POPC | 1.5 | OG | | 7 | 10 Tris, 200 NaCl | – | 2.5 d | DI | S | 274 |
| | | | 4 | | *I. tartaricus* | | 1 | POPC | 0.5 | OG | 20.0–37.0 | 7.5 | 10 Tris, 200 NaCl | – | 2 d | DI | S | 62 |
| | | 7 | | | *C. paradoxum* | DSM 7308 | 1 | POPC | | Zwittergent 3-12 | 25.0–37.0 | 7 | 10 Tris, 200 NaCl, 3 $NaN_3$ | – | 2 d | DI | V | 275 |
| | | 5 | | | *A. Woodii* | DSM 1030 | 2 | POPC | 0.5–1.0 | OG | 25.0–37.0 | 8 | 10 Tris, 200 NaCl, 3 $NaN_3$ | – | 2 d | DI | V | 276 |
| | Membrane-bound rotor ring of the $H^+$ F-ATPase | 6 | | | *Bacillus* sp. | TA2.A1 | 1 | POPC | 0.3–1.2 | DDM | 4 | 7.5 | 10 Tris, 200 NaCl, 3 $NaN_3$ | – | 28 d | DI | V | 277 |
| P-type ATPases | $H^+$ ATPase | | 8 | | *N. crassa* | – | 1 | – | – | DDM | – | – | 100 AmSulphate, 0.1% trehalose, 10.5% PEG4000- | – | – | Growth on C-film grid | St | 72 |
| | | 8 | | | | | 1 | Egg PC | 0.2 | – | – | – | – | 20 glycerol | – | – | – | 106 |
| | | 8 | | | *Arabidopsis* plasma membrane | *S. cerevisiae* | 0.2 | Egg PC | 0.33 | DDM | 20 | 6.5 | 150 KCl | 20 glycerol | 48 h | FL | S | 105 |
| | | | 7 | 1MHS | *A. aeolicus* | *E. coli RP-codon plus cells* | 2 | DPPC | 0.4 | DDM | 20 | 7.5 | 20 Tris, 50 NaCl, 0.05 $NaN_3$ | | 14 d | DI | S | 278 |
| | CtrA3 – copper-transporter | 7 | | | *A. aeolicus* | *E. coli* | 2 | DPPC | 0.4 | DDM | 30 | 7.5 | 20 Tris, 50 NaCl | | 14 d | DI | V | 279 |

| | | | | | | | | | | | | | | | | | |
|---|---|---|---|---|---|---|---|---|---|---|---|---|---|---|---|---|---|
| | CopA – copper-transporter | | 17 | 2VOY | *A. fulgidus* | *E. coli* | 0.5 | DOPC | | DDM | 45–55 | 6.1 | 50 MES, 25 $Na_2SO_4$, 25 $K_2SO_4$, 10 $MgSO_4$ | | 5 d | DI | T | [280] |
| | Gastric $H^+/K^+$ ATPase | 14 | | | Pig gastric | | 1 | – | – | OG | 4.0–20.0 | 3.9 | 10 propionate, 1–5 $MgCl_2$, AlF, and ADP | 40 glycerol | 2.5 d | DI | V | [281] |
| | | | 6.5 | 3IXZ | Pig gastric | | – | DOPC | 0.5 | DM | 0–3.0 | 4.87–5.5 | 10 MES, 1 $MgCl_2$, 0.5 $AlCl_3$, 4 NaF, 0.3 ADP, 3 DTT | 10 glycerol | 12 d | DI | V | [282] |
| | | | 7 | 2XZB | Pig stomach | | | DOPC | 1 | $C_{12}E_8$ | | 5.5 … 4.8 | 10 MES, 10 $MgCl_2$, 1 $BeSO_4$, 4 NaF, 1 ADP, 3 DTT | 10 glycerol | 4 d | | | [156] |
| | $Ca^{2+}$ ATPase | 8 | | | Rabbit sarcoplasm reticulum | | 2 | Egg yolk PC | 0.6–1.2 | $C_{12}E_8$ | 4.0–25.0 | 6 | 20 Mes, 100 KCL, 10 $CaCl_2$, 3 MgCl2, 5 DTT, 0.1 mg $mL^{-1}$ C12E8 | 20 glycerol | 7 d | DI | S | [283] |
| | | | 8 | | Rabbit sarcoplasm reticulum | | – | Egg yolk PC | 0.6–1.2 | $C_{12}E_8$ | 0 | 7.3 | 10 imidazole, 100 KCl, 5 $MgCl_2$, 5 $Na_3VO_4$, 30 dansyl thapsigargin | 20 glycerol | 1 d | – | T | [284] |
| | | | 6 | 1KJU | Rabbit sarcoplasm reticulum | | – | Egg yolk PC | 0.6–1.2 | $C_{12}E_8$ | 4 | – | 100 KCl, 5 $MgCl_2$ 0.5 , $Na_3VO_4$, 30 dansyl thapsigargin | – | 5 d | DI | – | [285] |
| | | | 8 | | | | | | | | | 7.2 | 20 imidazole, 100 KCl, 5 $MgCl_2$, 0.5 decavanadate | | | Freeze-thaw | T | [286] |
| | | 10 | | | | | | | | | | 7.4 | 20 imidazole, 100 KCl, 35 $MgCl_2$, 0.25 $Na_3VO_4$ | | | Freeze-thaw | T | [287] |
| | E2 state | | 8 | | Rabbit sarcoplasm reticulum | | 1 | Egg yolk PC, PA, PE | 0.5 | $C_{12}E_8$ | 4.0–20.0 | 7.4 | 20 imidazole, 100 KCl, 5 $MgCl_2$, 0.5 EGTA, and 0.5 $Na_3VO_4$ | 10 glycerol | 4–7 d | BB | T | [288] |
| | $Na^+/K^+$ ATPase | 11 | | | Dog kidney medulla | Dog kidney medulla | ? | – | ? | – | On ice | 3.0–6 | 150 NaAc or 150 $Na_3PO_4$ | – | Few days | DI | S | [289] |
| | | 25 | | | Dog kidney medulla | Dog kidney medulla | 0.5–1 | DEPC/DOPC | 0.25 | $C_{12}E_8$ | 4 | 5.5 | 10 KCl, 2. 5 $MgCl_2$, 0.5 $Na_3VO_4$ | 20 glycerol | 1–2 w | BB/DI | V/S | [290] |
| | | 9.5 | | | Dog kidney medulla | Dog kidney medulla | – | – | – | | 4 | 7.3 | 1 $NH_4VO_3$, 5 $MgCl_2$, 5 $CaCl_2$ | – | 1 d | DI | S | [291] |
| | | | 11 | | Supraorbital glands of salt-adapted ducks | Supraorbital glands of salt-adapted ducks | 1 | DHPC | 0.35 | /DHPC | | 7.5 | 10 KCl, 2.5 $MgCl_2$, 0.5 $Na_3VO_4$ | – | – | – | T | [292] |
| | Kdp – FABC complex, $K^+$ pump | | 24 | | *E. coli* | *E. coli* | 0.8–1 | DOPC/DOPE | 0.5 | $DM/C_{12}E_9$ | | 7.5 | 100 NaCl | – | 3–4 h | BB | T | [293] |
| Beta-barrel membrane proteins | OmpF – porin | 3.2 | | | *E. coli* | – | 1 | DMPC | 1 | $C_sPOE$ | 20, 37 | 7 | 100 NaCl | – | 24 h | DI | V | [294] |
| | | 3.5 | | | *E. coli* | | | | | | | | | | | | | [295] |
| | OmpF – colicin complex | 25 | | | *E. coli* | | | | | | | | | | | | | [296] |

(*Continued*)

**Table 1** Continued

| *Family* | *Protein* | *Resolution 2-D (Å)* | *Resolution 3-D (Å)* | *PDB/EMDB* | *Origin* | *Expressed in* | *Conc (mg ml$^{-1}$)* | *Lipid added* | *LPR (w/w)* | *Detergent* | *Temp (°C)* | *pH* | *Salts (mM unless stated otherwise)* | *Nonionic agents (%)* | *Time* | *Crystallization method* | *Crystal type* | *Reference* |
|---|---|---|---|---|---|---|---|---|---|---|---|---|---|---|---|---|---|---|
| | FhuA – porin | 15 | | | *E. coli* | *E. coli* | 0.01–0.15 | *E. coli* lipid | 0.6 | TX-100 | 20 | 8 | 100 NaCl | – | ~18 h | LM | S | 102 |
| | | 8 | | | *E. coli* | *E. coli* | 1 | *E. coli* lipid | 0.5 | LDAO, OTG | 21 | 8 | 100 NaCl | – | 5–6 h | BB | V/S | 297 |
| | Maltoporin | 25 | | | | – | 0.1–1.0 | *E. coli* lipid | – | Octyl-POE | 37 | – | 20 HEPES (pH 7.0), 0.1 M NaCl, 10 $MgCl_2$, 0.2 DTT, 0.2 EDTA, 3 $NaN_3$ | – | – | DI | V | 298 |
| | KdgM – outer membrane porins | 7 | | | *E. chrysanthemi* | *E. coli* | 1.4–1.8 | DMPC | 0.1–0.15 | LDAO | – | 9 | 200 NaCl | – | – | CNBD and DI | T | 299 |
| | KdgN – outer membrane porins | 7 | | | *E. chrysanthemi* | *E. coli* | 1.4–1.8 | DMPC | 0.2 | OG | – | 7.4 | 100 KCl | – | – | CNBD and DI | V | 299 |
| | NanC – outer membrane porins | 7 | | | *E. coli* | *E. coli* | 1.4–1.8 | DMPC | 0.1–0.15 | LDAO | – | 9 | 200 NaCl, 1 $MgCl_2$ | – | – | CNBD and DI | T | 299 |
| | OmpG – monomeric Porin | 6 | | | *E. coli* | *E. coli* | 1 | *E. coli* lipid | 0.25–1.5 | $C_{12}E_8$ | 20 | 7 | 100 KCl, 25 $MgCl_2$ | – | 8 w | DI | V/S | 300 |
| | LamB | 25 | | | *E. coli* | | 1 | *E. coli* lipid | 1 | octyl-POE | 37 | 7 | 100 NaCl | – | n.r. | DI | V | 298 |
| | Omp21 | 18 | | | *C. acidovorans* | *E. coli* | 1 | PE | 0.7 | LDAO,C8En | 35 | 9 | n.r. | – | 5 d | DI | V | 301 |
| | OpcA | 30 | | | *N. meningitidis* | | | DMPC | 0.1 | $C_8E_5$ | 20 | 4.5 | 50 $ZnCl_2$ | | Days | DI | V | 302 |
| | PhoE – porin | 3.4 | | | *E. coli* | | 1.5 | DMPC | 0.25 | | 25, 38 | 7.5 | 100 NaCl | – | 2–3 d | DI | V | 303 |
| LPS assembly proteins | $Wzz^{st}$ O-antigen chain length regulator | 14 | | | *S. enterica* serovar Typhimurium LT2 | *E. coli* | 0.5 | DMPC | 0.5–1.0 | DDM | RT | – | – | – | – | Hydrophobic beads | V | 8 |
| Peptide transporter | DtpD (YbgH) | 19 | | | *E. coli* | BL21(DE3) pLysS | 2.7 | *E. coli* PE | 0.3–0.4 | DM | RT | 8 | 300 NaCl, 250 mannitol, 20 Tris-HCl | 10 glycerol | 5 d | DI | T | 304 |
| Gap junctions | alphaCx43 – connexin gap junction channel | | 20 | | Rat liver gap junctions | | – | – | – | DOC | 4 | 8 | 5 HEPES, 5 EGTA, + 0.5 $MgCl_2$ or 0.05 $CaCl_2$ | – | 3 d | *in situ* | S | 305 |
| | | | 16 | | Rat liver gap junctions | | | | | | | | | | | | | 306 |
| | | | 7.5 | | Rat cardiac gap junctions | BHK cells | 1 | DHPC | – | Tween 20 | 27 | 7.5 | 2.8% Tween 20, 200 KI, 2 sodium thiosulfate, 100 μg ml$^{-1}$ oleamide, 1 μg ml$^{-1}$ triβuoromethylketone, 140 μg ml$^{-1}$ phenylmethylsulfonyl fluoride, 50 μg ml$^{-1}$ gentamycin in 10 HEPES containing 0.8% NaCl | – | 0.5 d | *in situ* | S | 307 |
| | | | 7.5 | | Rat cardiac gap junctions | BHK cells | 1 | DHPC | – | Tween 20 | 27 | 7.5 | 2.8% Tween 20, 200 KI, 2 sodium thiosulfate, 140 μg ml$^{-1}$ phenylmethylsulfonyl | – | 0.5 d | *in situ* | S | 308 |

| | | | | | | | | | | | | | | | | | | |
|---|---|---|---|---|---|---|---|---|---|---|---|---|---|---|---|---|---|---|
| | | | | | | | | | | | | | fluoride, 50 μg $ml^{-1}$ gentamycin in 10 HEPES containing 0.8% NaCl | | | | | |
| | | 7.5 | | | Rat cardiac gap junctions | BHK cells | 1 | DHPC | – | Tween 20 | 4 | 7.5 | 2.8% Tween 20, 200 KI, 2 sodium thiosulfate, 140 μg $ml^{-1}$ phenylmethylsulfonyl fluoride, 50 μg $ml^{-1}$ gentamycin in 10 HEPES containing 0.8% NaCl | – | 0.5 d | *in situ* | S | [309] |
| | Cx26–connexin gap junction channel | | 10 | | | SF9 insect cells | 1 | DOPC | 1 | DM | 20–37 | 5.8 | 10 MES (pH 5.8), 100 NaCl, 50 $MgCl_2$, 5 CaCl2, 2 DTT | | 6 d | DI | V | [310] |
| | | | 6 | 3IZ1, 3IZ2 | | SF9 insect cells | 1 | DOPC | 1 | DM | 20–37 | 5.8 | 10 MES (pH 5.8), 100 NaCl, 50 $MgCl_2$, 5 $CaCl_2$, 2 DTT | 1 glycerol | 6 d | DI | V | [311] |
| | a1 connexin-43 fragment | 7.5 | | | Cardiac gap junctions | BHK cells | 1 | DHPC | | Tween 20 | 27 | 7.5 | 200 KI 2 $Na_2S_2O_3$ | | ~2 d | *in situ* | S | [312] |
| | | 10 | | | | SF9 insect cells | 1 | DOPC | 0.8–1 | DDM | 20–37 | 5.8 | 10 MES (pH 5.8), 100 NaCl, 50 $MgCl_2$, 5 $CaCl_2$, 2 DTT | – | 6 d | DI | – | [313] |
| Bladder proteins | Uroplakins | | 12 | | Mouse bladder | | | | | | | | | | | *in situ* | S | [314] |
| Toxins | Cry4Ba delta-endotoxin complex | 17 | | | *Bacillus thuringiensis* | *E. coli* | 0.5–1 | DMPC | 1 | OG | 25 | 10.5 | 50 $Na_2CO_3$ | – | 1–2 d | DI | S | [315] |
| | StnII–sticholysin II actinoporin | | 15 | | *Stichodactyla helianthus* | *Stichodactyla helianthus* | 1 | Sphingomyelin, egg PC, cholesterol | 0.15 | – | 4 | 7 | 100 NaCl | – | 2–7 h | LM | S | [316] |
| | | | 18 | | *Stichodactyla helianthus* | *Stichodactyla helianthus* | 1 | Sphingomyelin,DOPC, cholesterol | 0.15 | – | 4 | 7 | 100 NaCl | – | 12 h | LM | S | [317] |
| | Aerolysin | | 25 | | *Aeromonas hydrophila* | *Aeromonas hydrophila* | ? | *E. coli* PE | 0.2–5 | Octyl-POE | 4 | 7.4 | 100 NaCl, 1 $CaCl_2$ | – | 13 h | DI | S/T | [318] |

Abbreviations: AP, ammonium phosphate; BB, Bio-beads; conc, concentration; bM, Beta-mercaptoethanol; C, cubes; CsPOE; d, day; DDM, *n*-dodecyl-β-D-maltoside; DHPC, diheptanoyl-*sn*-glycero-3-phosphocholine; DI, dialysis; DM, *n*-decyl-β-D-maltopyranoside; DMPC, dimyristoylphosphatidylcholine; DOPC, dioleoyl phosphatidylcholine; DOPG, dioleoylphosphatidylglycerol; DOPS, 1,2-dioleoyl-*sn*-glycero-3-phosphoserine; DPPC, 1,2-dipalmitoyl-*sn*-glycero-3-phosphocholine; DPPG, dipalmitoyl phosphatidylglycerol; DTAC, dodecyl-trimethyl-ammonium chloride; DTM, *n*-decyl-β-D-thiomaltoside; DTT, dithiotheritol; EDTA, ethylenediaminetetraacetic acid; EGTA, *ethylene glycol tetraacetic acid*; EMDB, Electron Microscopy Data Bank; FU, fusion; h, hour; GSH, Glutathionine; HEPES, N′-2-Hydroxy ethylpiperazine-N′-2-ethanesulphonic acid; HTG, *n*-heptyl-β-D-thioglucopyranoside; LDAO, lauryldimethylamine oxide; LM, lipid monolayer; LPR, lipid-to-protein ratio; m, month; MES, 2-(*n*-morpholino)ethanesulfonic acid; N, needles; n.r. not reported; NS, not specified; OG, *n*-octyl-β-D-glucopyranoside; OTG, *n*-octyl-β-D-thioglycopyranoside; PC, phosphatidyl choline; PDB, Protein Data Bank; PE, Phosphatidyl ethanolamine; Pi, Sodium phosphate buffer; PMSF, Phenylmethanesulfonyl fluoride POPC, 1-palmitoyl-2-oleoyl-*sn*-glycero-3-phosphocholine; RT, room temperature; SDS, sodium dodecyl sulfate; S, Sheets; SP, salt precipitation; St, Stacks; T, Tubes; UDM, *n*-undecyl-β-D-maltoside; V, Vesicles; w, week.

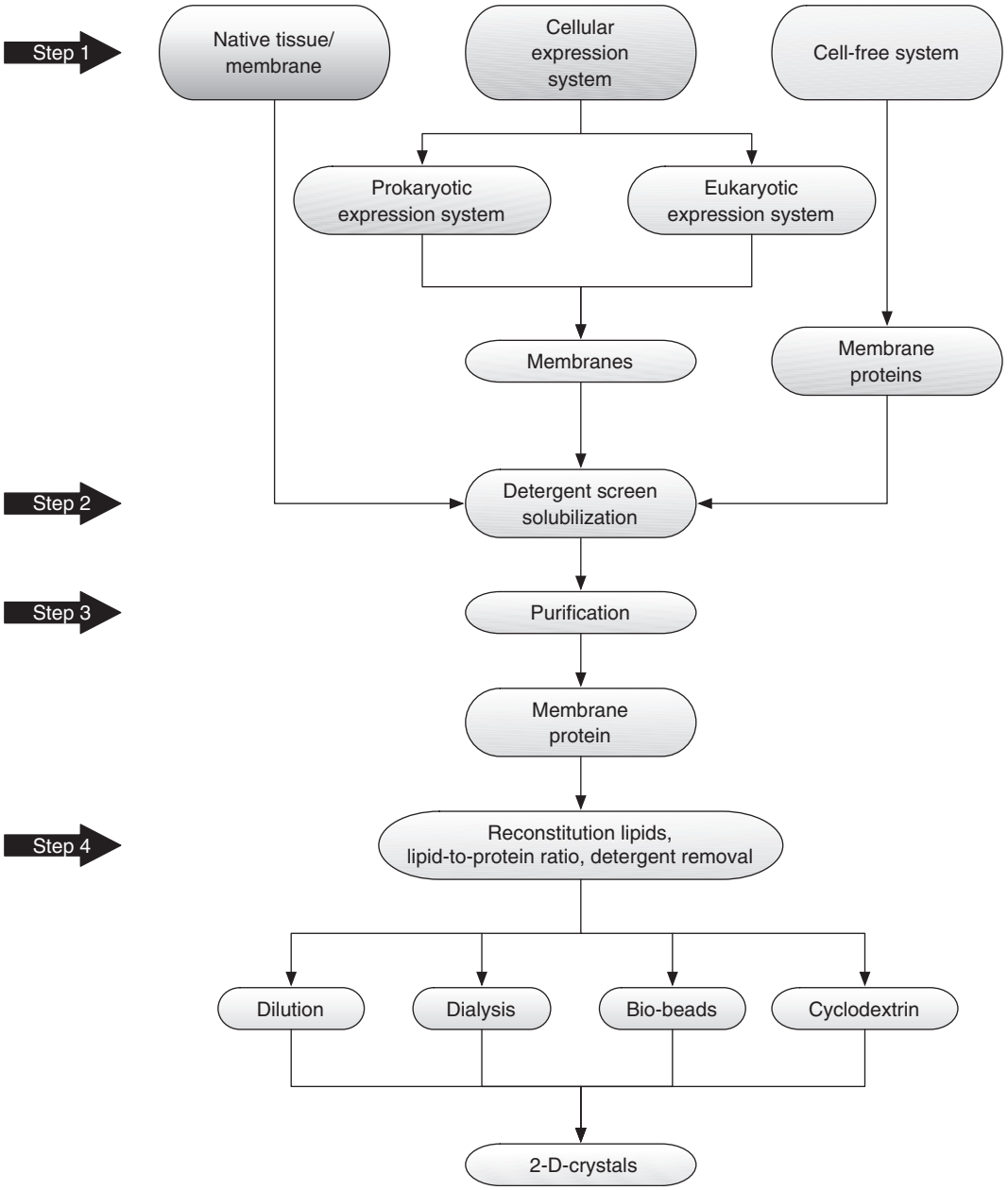


**Figure 1** Schematic representation of membrane protein crystallization steps.

viability should be monitored at different concentrations of IPTG, because high-level expression of some membrane proteins results in inclusion bodies[6] or inhibits cell growth; even when the gene is fully repressed, some residual expression from PTAC can still occur. If this leaky expression causes problems, it may be necessary to clone the gene into an alternative expression vector that is more tightly controlled. Interestingly, more than 30 prokaryotic membrane transport proteins have been successfully overexpressed in *E. coli* using the plasmid pTTQ18[7] with PTAC and have achieved expression levels ranging from 5 to 50% of inner membrane proteins.

The promoter for the *E. coli* arabinose operon ($P_{BAD}$ or PARA) is a useful alternative to PTAC. When a gene is cloned behind the $P_{BAD}$ promoter, expression of the gene is controlled by the AraC activator. High-level expression from PARA is inducible by using media containing arabinose. Moreover, expression from PARA can be tightly shut off by using media containing glucose but lacking arabinose. The $P_{BAD}$ expression system (Invitrogen(New York, USA)) has been successfully used to produce prokaryotic membrane proteins.[8,9]

Another commonly used promoter for protein expression is a regulated phage promoter. A gene of interest is cloned downstream of the promoter, which relies on a phage encoded ribonucleic acid (RNA) polymerase. Many phages produce a specific RNA polymerase that recognizes a promoter sequence, which is quite different from *E. coli* promoter sequences. Three phage-specific RNA polymerase/promoter systems that are commonly used in expression vectors include T7, SP6, and T3.

In addition to recognizing unique promoters, these systems result in very high transcription levels of the downstream gene. Such high-level transcription can be useful for overproducing membrane proteins, but the expression is often so high that it is toxic to the host cell. To avoid this, the phage RNA polymerase is only induced when overexpression is desired. For example, the phage RNA polymerase may be itself cloned behind a regulated promoter, or the polymerase may be introduced to the cell on a defective phage. The T7 expression system (pET system from Novagen (Madison, USA) and pQE system from Qiagen (California, USA)) has been widely used for the expression of soluble proteins but also for both prokaryotic and eukaryotic membrane proteins.[10–13]

To maximize the expression level for a protein of interest, it is important to optimize some key parameters: The expression levels of the protein of interest between minimal (M9) and complex (LB) media, the concentration of inducers such as IPTG and arabinose, and the incubation period for the inducers (2–24 hours). The most common difficulties associated with membrane protein expression are toxicity and a reduction in host-cell viability after induction. In such cases, overexpression can still be achieved by a careful choice of media, host strain (such as mutants of BL2 (DE3),[14] C41 (DE3), or C43 (DE3) (Lucigen (Heidelberg, Germany))), growth temperature, titration of inducer, and time period of induction.

Many bacterial membrane proteins have been produced in large quantities by overexpression.[15,16] However, attempts to produce eukaryotic membrane proteins in prokaryotic systems have had only limited success. One likely reason is that many eukaryotic proteins need posttranslational modifications and the cellular machineries for these modifications are absent in prokaryotes. In many cases, overexpressed membrane proteins will accumulate in inclusion bodies, although there are a few exceptions such as the neurotensin receptor[17,18] and human adenosine $A_{2a}$ receptor,[19] which are both G protein-coupled receptors (GPCRs). There are some reports of successful protein refolding from inclusion bodies,[20] but these techniques need to be carefully optimized for each protein and cannot be easily generalized.

The use of eukaryotic expression systems is an alternative choice for eukaryotic membrane proteins. The most commonly used eukaryotic expression systems include yeasts, insect cells, and mammalian cells. Yeast systems are particularly convenient because they contain all of the appropriate posttranslational modification machinery, but yet are easier to handle and less expensive than mammalian or insect cell expression systems. Three yeast strains, *S. cerevisiae*, *Schizosaccharomyces pombe (S. pombe)*, and *Pichia pastoris* (*P. pastoris*), have been regularly used for heterologous expression of eukaryotic membrane proteins. Many different expression vectors are available for use in *S. cerevisiae*, since recombinant DNA can be introduced either as self-replicating episomal plasmids or stably integrated into the yeast genome via homologous recombination. An advantage of *S. pombe* over *S. cerevisiae* is that initiation of transcription is similar to that in higher eukaryotes.[21] In addition to yeast-specific promoters, some mammalian promoters, such as SV40 and human cytomegalovirus (hCMV), are active in *S. pombe*.[22] However, the *S. pombe* expression system is much less developed than those of *E. coli* or *S. cerevisiae*; several *S. pombe* expression vectors have become available for recombinant protein production.[23] In contrast to *S. cerevisiae* system, only vectors for genomic integration are available in *P. pastoris* and mainly utilize the methanol-inducible alcohol oxidase promoter (AOX1). A number of membrane proteins have already been successfully produced in these yeast systems.[24–31]

Nevertheless, some points need to be considered when choosing yeast as an expression system. A major problem with yeast systems is the proteases present in vacuoles that can interfere with the production of recombinant protein. This can be eliminated to a certain extent by using protease-deficient yeast strains lacking one or more proteases. When using yeast for heterologous expression, it has to be taken into consideration that differences in codon usage can result in reduced production levels of the protein of interest, so that codon usage may need to be optimized. It was also shown that some membrane proteins from higher eukaryotes are not compatible with the yeast secretory pathway, which results in a reduced yield of functional membrane proteins. The lipid and sterol composition of yeast membranes differs from that in higher eukaryotes, which may affect the expression of recombinant membrane proteins compared to the native systems. *P. pastoris* is especially suited for high cell-density fermentation, yielding up to 500 $OD_{600}$ units $l^{-1}$,[32] thus helping to obtain large quantities of a homogenous protein preparation. Examples of successful structural determination of membrane proteins expressed in yeast systems include a voltage-sensitive K-channel that was used for single particle analysis and 2-D crystallization;[33] monoamine oxidase B (MAO-B), for which the crystal structure was determined to a 1.7 Å resolution;[34] and yeast aquaporin Aqy1 from *P. pastoris* at 1.15 Å resolution.[35]

In some cases, the levels of proteins expressed in eukaryotic systems are either undetectable or only detectable in small amounts by Western blot analysis. Reasons include: Toxic effects of the insertion of membrane proteins into cellular membranes, inefficient transport of the overexpressed membrane proteins to the membrane, poor growth of overexpressing strains, or a generally unfavorable impact on cellular metabolism. Some of these problems, such as inefficient transport or toxicity, are eliminated by a third method of protein production: Cell-free expression systems. Cell-free systems may be an alternative to established cellular expression systems.[36] Cell-free systems have been used to resolve the protein production problem for many membrane proteins[37–44] and some of these proteins have been successfully used for structural analysis by NMR.[45] However, cell-free expressed membrane proteins have not yet been successfully crystallized.

### 1.15.2.2 Detergent Screening and Solubilization of Membrane Proteins

Since native and *in-vivo* expressed recombinant membrane proteins are embedded in a lipid bilayer, detergents are necessary to remove the proteins from those membranes. This step is called 'solubilization' and it is the second critical step in membrane protein crystallization. Choosing the ideal detergent is critical. The detergent determines the efficiency of extracting the membrane protein from the bilayer, as well as the stability, solubility, and homogeneity of the purified

proteins and thereby the probability of obtaining useful crystals. During the solubilization process, the concentration of detergent increases to levels at or above the critical micelle concentration (CMC): Detergent monomers assemble into micelles that surround the hydrophobic parts of membrane proteins, keeping them in solution.[46,47] This process disintegrates the lipid bilayers, which start to break and generate mixed micelles of protein/detergent, protein/detergent/lipid, lipid/detergent, and detergent alone. Individual membrane proteins may have different solubilization requirements, especially with regard to detergent concentration, pH, and salt concentration. Therefore, the most suitable compound should be selected carefully, trying a wide range of detergents at concentrations above the CMC, and protein concentrations ranging from 1 to 10 mg $ml^{-1}$. Many different detergents (ionic, nonionic, and zwitterionic) are available (**Table 2**), and therefore choosing the right detergent can be difficult and time consuming, but is often important. Solubilization efficiency can be monitored using sodium dodecyl sulfate polyacrylamide gel electrophoresis (-PAGE) and Western blotting. Often, it may not be possible to select a detergent suitable for both solubilization and purification. In such cases, detergent exchange may be necessary before or during subsequent purification steps.[48] Once the solubilization conditions are optimized, the protein is ready for purification.

### 1.15.2.3 Purification of Membrane Proteins

The third critical step is the purification of the detergent-solubilized membrane protein. It is important to keep the detergent concentration above the CMC throughout the purification steps to prevent precipitation of the proteins. The final detergent concentration of the purified protein should be as low as possible, ideally just above the CMC, since the detergent has to be removed in the subsequent 2-D crystallization step. Purification methods for membrane proteins from native tissues or membranes and from overexpression systems are well established. There are many different affinity tags available that can facilitate the purification of overexpressed membrane proteins. Most widely used are histidine tags, either as hexa-histidine, octa-histidine, or deca-histidine tags, depending on the desired binding strength. Addition of a histidine tag to a membrane protein enables its rapid purification by nickel ($Ni^{2+}$) or cobalt ($Co^{2+}$) affinity chromatography.[49–52] Histidine tags are small and generally do not interfere with the expression level, protein folding, or membrane insertion. In some cases, it is important to remove the histidine tag after protein purification to improve crystal packing.[53] In addition to the histidine tag, there are some other tags such as strep-tag, tap-tag, and flag-tag, that are also available and can be used for protein purification. Antibodies to the affinity tags are often commercially available, which facilitates the detection of the membrane protein by Western blotting without the necessity of raising novel antibodies.

### 1.15.2.4 Reconstitution of Membrane Proteins into Lipid Bilayers

The fourth critical step is the reconstitution of the purified membrane proteins into a lipid bilayer.[54] This is achieved by decreasing the detergent concentration of the protein solution in the presence of lipids. When the detergent is removed, the hydrophobic surface areas of the membrane protein strongly prefer to be in contact with the lipid fatty acid chains or with one another, rather than becoming exposed to the aqueous solvent, which would be highly unfavorable. The equilibrium between a single membrane protein molecule (or a lipid) exposed to water or embedded in a lipid environment is far on the bilayer side. The hydrophobic surfaces are therefore forced to join together, so as to exclude water, thus preventing unfavorable interaction with the aqueous medium. During this process, the small micellar structures join together to form vesicles, tubes, and/or sheets (**Figure 2**), and the protein incorporates into these during or after their formation. At the right conditions, this can result in 2-D crystal formation of the membrane proteins in the reconstituted membranes. These can be in the form of planar crystalline sheets, crystalline vesicles, or tubes. From the energetic point of view, vesicles are more stable, as they do not have open edges, at which the lipid or hydrophobic protein is exposed to the aqueous medium. The open hydrophobic edge around a crystalline sheet is energetically unfavorable, so it tends to close into a cylinder or sphere, unless the protein has a strong predisposition for planar layers. This appears to be the case for bacteriorhodopsin, LHC-II, and the aquaporins. If the protein does not have this predisposition – which would be difficult to predict, and even more difficult to influence – it usually forms tubular vesicles that are most often 0.5 to 1 μm wide. Crystalline vesicles can be spherical or can have a variety of other shapes. Frequently, they adopt the shape of tubes in which the 2-D lattice describes the surface of a cylinder, which is closed on both sides by a more or less hemispherical cap. Occasionally, they seem to grow from protein/lipid aggregates.[55–58] The degree of curvature of a tubular vesicle must depend on the tightness of the crystal lattice and the strength of crystal contacts. Tubular crystals are easily distorted by surface forces, which preclude helical processing. They flatten on the support film and can then be treated as two superposed 2-D lattices.

An example for a membrane protein that was studied from tubular crystals is the nAChR, a ligand-gated ion channel from the postsynaptic membrane, which, besides tubulin,[59,60] is so far the only high-resolution structure of a membrane protein to have been determined from tubular crystals. The receptor forms ~1000-Å-wide tubes, with the 2-D lattice on the wall of a cylinder. The tubes are narrow and strong enough not to be flattened by surface forces in the thin layer of buffer on a holey support film, and therefore can be processed as helical arrays, so the grid does not need to be tilted in the electron microscope. However, the tubes are far too narrow for electron diffraction, so the structure has to be determined without the aid of high-resolution electron diffraction amplitudes. Nonetheless, helical processing of images of a large number of tubular crystals recoded at liquid helium temperature have yielded the structure of nAChR in several different states, most recently at 4-Å resolution,[61] a real accomplishment of crystallographic electron image processing.

To date, none of the flattened tubular crystals have produced a map of similar quality; the best collapsed tubular vesicles, such as the bacterial sodium/proton antiporter NhaA[58] or ATP synthase c-rings[62] go to ~4 Å, but the 3-D

**Table 2** Detergents used in membrane protein solubilization and crystallization trials. The data in this table were compiled from several sources, including: http://www.affymetrix.com, http://www.sigmaaldrich.com, and Bhairi (2001)[316]

| *Name* | *Abbreviation* | *M.W. (anhydrous)* | *CMC (mM)* | *CMC (%)* | *Aggregation number* | *Average micellar weight (Da)* |
|---|---|---|---|---|---|---|
| ***Nonionic detergents*** | | | | | | |
| APO-10 | | 218.3 | 4.6 | 0.100 | 131 | 28 000 |
| APO-12 | | 246.4 | 0.568 | 0.013 | 2232 | 500 000 |
| Big CHAP | | 878.1 | 2.9 | 0.25 | 10 | 8800 |
| Big CHAP, Deoxy | | 862.1 | 1.1–1.4 | 0.12 | 8–16 | 10 500 |
| BRIJ® 35 | Brij-35 | 627 | 0.09 | 0.005 6 | 40 | 49 000 |
| $C_{12}E_5$ | | 406.6 | 0.064 | 0.002 | - | - |
| $C_{12}E_6$ | | 450.7 | 0.087 | 0.003 9 | - | - |
| $C_{12}E_8$ | $C_{12}E_8$ | 538.8 | 0.11 | 0.005 9 | 123 | 66 000 |
| $C_{12}E_9$ | $C_{12}E_9$ | 582.8 | 0.08 | 0.004 6 | - | 83 000 |
| 2-Cyclohexyl-*n*-ethyl-β-D-maltoside | Cymal-2 | 452.5 | 120 | 5.43 | - | - |
| 6-Cyclohexyl-*n*-ethyl-β-D-maltoside | Cymal-6 | 508.6 | 0.56 | 0.028 4 | 91 | 32 000 |
| 1-Cyclohexyl-*n*-ethyl-β-D-maltoside | Cymal-1 | 438.5 | 340 | 14.9 | - | - |
| 7-Cyclohexyl-1-heptyl-β-D-maltoside | Cymal-7 | 522.5 | 0.19 | 0.009 92 | 150 | 78 300 |
| *n*-Decanoylsucrose | | 496.6 | 2.5 | 0.124 | - | - |
| *n*-Decyl-β-D-maltopyranoside | DM | 482.6 | 1.6 | 0.087 | 69 | - |
| *n*-Decyl-β-D-thiomaltoside | DTM | 498.6 | 0.9 | 0.044 8 | - | - |
| Digitonin | | 1229.3 | $<0.5$ | | 60 | 74 000 |
| *n*-Dodecanoylsucrose | | 524.6 | 0.3 | 0.015 7 | - | - |
| *n*-Dodecyl-β-D-glucopyranoside | | 348.5 | 0.19 | 0.006 6 | 200 | 70 000 |
| *n*-Dodecyl-β-D-maltoside | DDM | 510.6 | 0.1–0.6 | 0.009 | 98 | 50 000 |
| Dodecyl-trimethyl-ammonium chloride | DTAC | 264 | 17.0 | 0.488 | 50 | 13 200 |
| *n*-Heptyl-β-D-glucopyranoside | | 278.3 | 70 | 1.9 | - | - |
| *n*-Heptyl-β-D-thioglucopyranoside | HTG | 294.4 | 79 | 2.32 | - | - |
| *n*-Nonyl-β-D-glucopyranoside | NG | 306.4 | 6.5 | 0.2 | 133 | - |
| Methyl 6-O-(*n*-heptylcarbamoyl)-α-D-glucopyranoside | Hecameg | 335.4 | 19.5 | 0.654 | | |
| Nonidet P-40 (octylphenoxypolyethoxyethanol), now IGEPAL CA-630 | Nonidet P-40 | 558.7 | 0.25 | 0.014 | 149 | 90 000 |
| NP-40 (nonylphenoxypolyethoxyethanol) | NP-40 | 603.0 | 0.05–0.3 | 0.05–0.3 | 100–155 | 76 600 |
| *n*-Octanoyl-β-D-glucosylamine | NOGA | 305.4 | 80 | 2.44 | - | - |
| *n*-Octanoylsucrose | | 468.5 | 24.4 | 1.14 | - | - |
| *n*-Octyl-β-D-glucopyranoside | OG | 292.4 | 10–21 | 0.3–0.6 | 84 | 25 000 |
| *n*-Octyl-β-D-maltopyranoside | | 454.5 | 19.5 | 0.89 | 84 | 38 000 |
| *n*-Octyl-β-D-thioglycopyranoside | OTG | 308.4 | 9 | 0.277 | - | - |
| *n*-Octylpolyoxyethylene | Octyl-POE | 174.3 | 6.6 | 0.115 | | |
| TRITON® X-100 | TX-100 | 625 | 0.01-0.016 | 0.015 | 100–155 | 80 000 |
| TWEEN® 20 | Tween 20 | 1228 | 0.059 | 0.007 2 | - | - |
| TWEEN® 80 | Tween 80 | 1310 | 0.012 | 0.001 57 | 60 | 79 000 |
| *n*-Undecyl-β-D-maltoside | UDM | 496.6 | 0.59 | 0.029 2 | - | - |
| ***Ionic detergents*** | | | | | | |
| Amphipol A8-35 | | 9–10 | - | 20 | - | - |
| Cetyltrimethylammonium bromide | CTAB | 364.5 | 1.0 | 0.036 4 | 170 | 62 000 |
| Cholic acid, sodium salt | Cholate | 430.6 | 9–15 | | 2.0 | 900 |
| Deoxycholic acid, sodium salt, Na-deoxycholate | DOC | 414.6 | 4–8 | 0.24 | 22 | 1600–4100 |
| Lauroylsarcosine, sodium salt | | 293.4 | 14.57 | 0.427 | 2.0 | 600 |
| Taurocholic acid, sodium salt | | 537.7 | 3–11 | | 4 | 2100 |
| ***Zwitterionic detergents*** | | | | | | |
| CHAPS | CHAPS | 614.9 | 6-10 | 0.49 | 10 | 6000 |
| CHAPSO | | 630.9 | 8 | 0.5 | 11 | 7000 |
| Diheptanoyl-*sn*-glycero-3-phosphocholine | DHPC | 481.5 | 1.4 | 0.07 | 100 | 50 000 |
| Lauryldimethylamine oxide, 30% solution | LDAO | 229.4 | 1–2 | 0.023 | 76 | 17 000 |
| ZWITTERGENT® 3-08 detergent | | 279.6 | 330 | 10.9 | - | - |
| ZWITTERGENT® 3-10 detergent | | 307.6 | 25–40 | 1.2 | 41 | 12 500 |
| ZWITTERGENT® 3-12 detergent | | 335.6 | 2–4 | 0.094 | 55 | 18 500 |
| ZWITTERGENT® 3-14 detergent | | 363.6 | 0.1–0.4 | 0.007 | 83 | 30 000 |
| ZWITTERGENT® 3-16 detergent | | 391.6 | 0.01–0.06 | 0.001 1 | 155 | 60 000 |

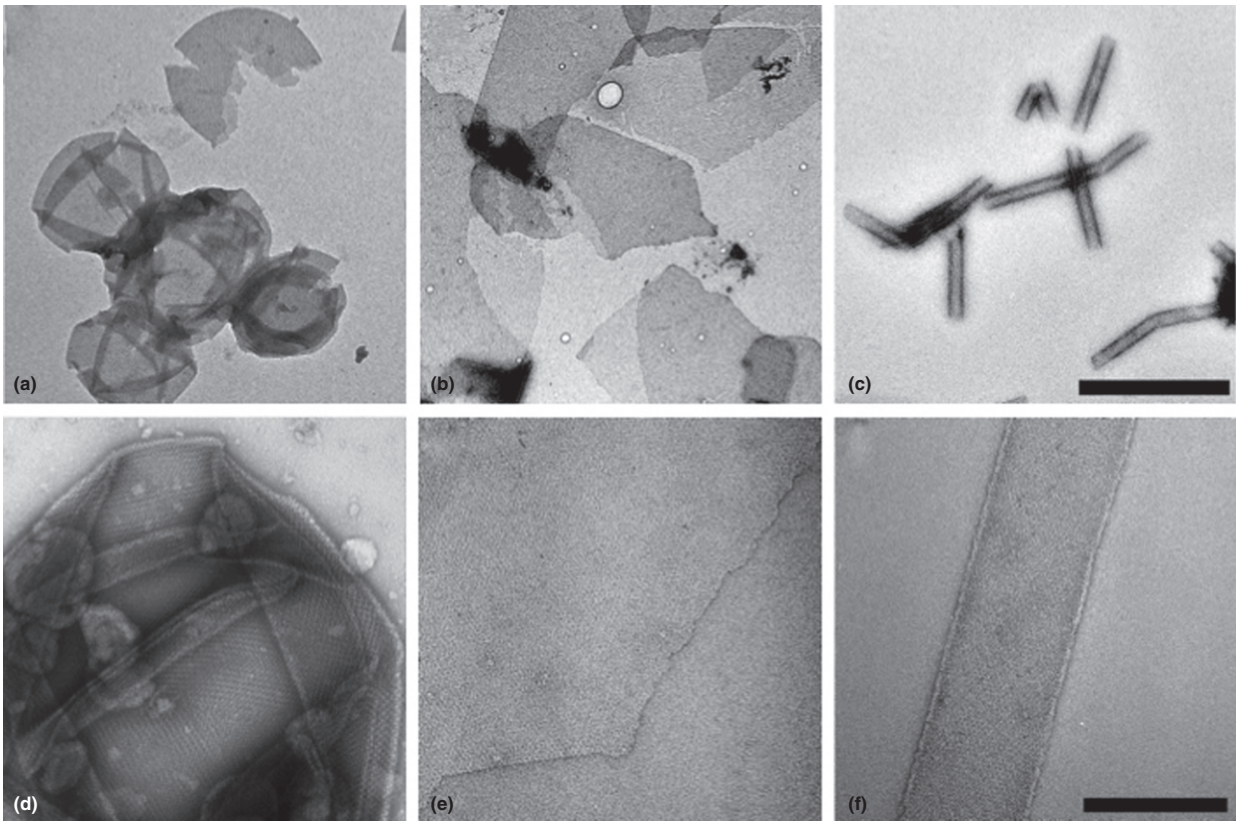


**Figure 2** TEM analysis of 2-D crystallization trials by negative staining. (a), (b), and (c) Low magnification micrograph showing vesicles, sheets, and tubes of reconstituted protein into lipid bilayer (scale bar represents 1 μm). (d), (e), and (f) are corresponding high-magnification images (scale bar represents 100 nm). (a) and (d) from HasA-HasR-Heme complex in DOPC:DOPS:POPE (60:20:20) at 0.5 LPR, (b) and (e) from OmpF in *E. coli* lipids in 0.2 LPR, and (c) and (f) from OmpF in PC:PS (80:20) at 0.2 LPR.

maps of these proteins[62,63] have not resolved side chains. More often, 3-D maps from this type of crystal go to ~6–8 Å inplane. At this resolution, trans-membrane alpha helices show up clearly, and the maps can serve as an excellent template for molecular modeling, if a high-resolution structure of a related protein is available, as in the example of the archaeal sodium/proton antiporter NhaP1.[64]

The most likely reason why vesicular 2-D crystals are less well ordered is that, due to weak lattice forces, the crystal contacts are not strong enough to prevent small rotations or distortions of individual molecules. In principle, these rotations and distortions can be detected by cross correlation with a reference and then corrected, as in lattice unbending, but the signal/noise ratio of low-dose electron micrographs is too low to do this for individual proteins, as would be necessary to correct rotations in 3-D, or to sort out distorted protein molecules. Perhaps electron-optical phase plates that should improve the signal/noise ratio of the image, or new detectors with a quantum efficiency better than film will make this possible in future. At present, lattice distortions can be reliably corrected only in 2-D, with a reference comprising several unit cells, which accounts for the limited resolution achieved with less-than-perfect 2-D crystals.

Crystalline sheets are in many ways preferable to vesicle crystals. Their size is not constrained by the cylindrical geometry of a tubular vesicle, and they are more likely to lie flat on the support film. 2-D crystalline sheets seem to form preferably under equilibrium conditions[2] in the presence of a small amount of detergent. Although many membrane proteins have a tendency to form 2-D lattices in a lipid bilayer, some of them also tend to interact with one another in the orthogonal direction. This circumstance will lead to form multilamellar crystals rather than true 2-D crystals. Multilamellar crystals consist of stacks of 2-D crystals, often in precise register, so that thin stacks can be difficult to distinguish from proper, unilamellar 2-D crystals by transmission electron microscopy (TEM) and image analysis. They can sometimes be detected by careful inspection of the edges of crystalline areas in negatively stained specimens, which may show distinct steps in gray levels or contrast. Scanning TEM (STEM) in high-angle annular dark field (HAADF) mode can be used to measure the mass per area of such crystals, which would then reveal the number of layers in such 2-D crystal stacks.[65] Membrane proteins that occur naturally in stacked membranes, such as LHC-II[66] or the cytochrome $b_6f$ complex,[67–69] have a tendency to form multilamellar crystals. Both complexes come from chloroplast grana membranes, which form extensive stacks *in vivo*. Membrane proteins that are designed to bind extramembraneous subunits may also tend to form stacked multilayers, if those subunits are absent. The membrane portion of the enzyme II mannitol transporter from *E. coli*[57] is a good example. Naturally, there is a risk of

multilayer formation with proteins that have extensive extramembraneous domains, such as the cytochrome $bc_1$ complex,[70] Ca ATPase,[71] and Neurospora proton ATPase,[72] which have the highest potential for hydrophilic crystal contacts in the orthogonal direction and all form multilamellar membrane crystals. In the case of LHC-II, naturally involved in the control of thylakoid stacking, the tendency to form multilayers is suppressed at low ionic strength both *in vivo* and *in vitro*. Mono- and divalent cations screen the surface charges, thus enabling stacks to form by nonpolar interactions. Unfortunately, this simple trick does not seem to work with other systems, though it should be possible to control the formation of multilayers at least to some extent through the variation of parameters that interfere with polar interactions, in particular ionic strength and pH. In some cases it may be worth modifying accessible surface residues to reduce the capacity for orthogonal interaction, an approach that is untried but seems promising.

In general reconstitution of membrane proteins into the bilayer depends on the choice of lipids, the lipid-to-protein ratio (LPR), the buffer conditions, possible additives like, for example, cholesterol, temperature, and the method and speed of detergent removal.

#### 1.15.2.4.1 Choice of lipids

Crystallization is more likely to occur when the lipid bilayer is in the fluid phase, permitting some lateral mobility of the embedded membrane proteins. Since lipids are a major part of the natural environment of all membrane proteins, native lipids are often ideal for crystallization. They contain a mixture of mostly charged lipid head groups, which are likely to interact with the protein at the interface region between the hydrophobic and hydrophilic phases and the molecular geometries of these lipids are similar to those found under physiological conditions. Most natural lipids have unbranched C18 or C16 fatty acid chains that are either fully saturated, or singly or multiply unsaturated. The length and saturation of the fatty acid tails determine the fluidity of the lipid bilayer, and in particular the transition temperature at which they change from a liquid-crystalline to a fluid state. Lipids with unbranched, fully saturated fatty acid chains of more than 14 carbon atoms have transition temperatures above 20 °C, whereas natural lipids with unsaturated C16 and C18 fatty acid chains have transition temperatures below 0 °C.[2,73] It has often been shown that the 2-D crystallization of membrane proteins in a lipid bilayer requires the latter to be fluid, and for this reason slightly elevated temperatures may be needed. Usually, the incorporated protein lowers the effective transition temperature of the system, and the requirement for higher temperatures therefore may influence the crystal quality. Some examples of proteins crystallized with native lipids include bacteriorhodopsin,[74] the cytochrome $bc_1$ complex,[75] and photosystem I.[76]

In addition to native lipids, the most commonly used lipids for 2-D crystallization are synthetic lipids, often phospholipids. Many of them are zwitterionic lipids (phosphatidyl cholines (PC), phosphatidyl ethanolamines (PE), phosphatidyl serines (PS), sphingomyelin (SM)) and the charge of their head groups depends on the pH, making them important to cover a wide range of pH in 2-D crystallization trials. Examples of negatively charged lipids at neutral pH include phosphatidyl glycerols (PG), phosphatidyl inositols (PI), and phosphatidic acids (PA). Charged head groups of lipids may give rise to strong repulsive forces, which would tend to interfere with micelle fusion and protein incorporation. The ceramides and gangliosides are uncharged sphingolipids and are important constituents of complex lipid extracts, such as brain lipids. The head groups of the typical plant glycolipids monogalactosyldiacylglycerol (MGDG) and digalactosyldiacylglycerol (DGDG) are hydrophilic but uncharged, except sulfoquinovosyl diacylglycerol (SQDG), which carries a polar sulfuryl group.

High-resolution X-ray and 2-D electron crystallography structures have shown that the head groups and fatty acid tails of lipids have special interaction with membrane proteins.[77] Therefore, it is important to select the suitable lipid for the crystallization process. Biological membranes have an effective hydrophobic core thickness of ~35 Å. Native membrane lipids with their high content of unsaturated C16 and C18 chains produce bilayers of suitable thickness for reconstitution of most membrane proteins. Interestingly, dimyristoyl phosphatidylcholine (DMPC), which has shorter saturated C14 chains end-to-end, forms bilayers of exactly the required hydrophobic diameter of 35 Å. DMPC was successfully employed in many reconstitution and 2-D crystallization experiments, as, for example, for photosystem I, photosystem II, aquaporin, KcsA K channel, porin, as well as with mixtures of DMPC with a second lipid, generally one containing longer hydrocarbon chains (such as in the cases of lactose permease, AqpZ). Furthermore, synthetic lipids, *E. coli* lipids,[78] soybean lecithin, and egg lecithin have also been successfully used for 2-D crystallization. A study of AQP0 2-D crystals in two different lipids suggests that the lipid adapts to the hydrophobic domain of the membrane protein,[78] rather than the other way round.

Frequently, isolated membrane proteins bind one or several lipids from their native membrane environment, and the presence of these lipids is often essential for the integrity and stability of the protein. Sometimes these native lipids are required for the 2-D crystal formation. A well-documented example is LHC-II, which requires the glycolipid DGDG[79] and a photosystem II subcomplex.[80,81] Such tightly bound lipids should not be removed by excessive purification, for example, by ion exchange chromatography, which exposes the protein to high salt concentrations and a large excess of detergent. The lipid content of a purified membrane protein fraction can be monitored by 1-D or 2-D thin-layer chromatography (TLC) of a small sample (2–4 μl) of concentrated detergent-protein solution (for details see Christie, 1982[82]). However, is not always easy to identify membrane lipids, or to determine the exact amounts of each lipid present. Laser-desorption mass spectroscopy is a useful method for identifying lipids by comparison against known standards, although the fatty acid chain heterogeneity of natural lipids may cause complications.[83,84]

No general recommendations can be made as to which lipid or lipid mixture is most suitable for any particular membrane protein. Nevertheless, some rules for choosing and handling lipids can be provided. First, polyunsaturated lipids with fatty acid chains containing unconjugated double bonds

are easily oxidized; therefore they must be stored under argon or nitrogen at low temperature (–20 °C) in the dark. Second, it is advisable to work in an inert-gas atmosphere or to add an enzymatic oxygen scavenging system such as glucose oxidase to the crystallization mix. Third, prior to their use for 2-D crystallization trials, lipids must be transferred to detergent-containing water or appropriate buffer solution.[69] Mono-unsaturated synthetic lipids such as 1,2-dioleoyl-*sn*-glycero-3-phosphocholine (DOPC), 1,2-dioleoyl-*sn*-glycero-3-phospho-(1′-rac-glycerol) (DOPG), and 1-palmitoyl-2-oleoyl-*sn*-glycero-3-phosphocholine (POPC) are less sensitive to oxidation than the polyunsaturated natural lipids, yet have suitably low transition temperatures. Therefore, they have become increasingly popular as an alternative to natural lipids.

#### 1.15.2.4.2 Ratio of lipid to protein

When the amount of lipid exceeds that of protein (wt/wt), the protein mainly incorporates into the lipid bilayer in a geometry that is similar to its native state. When the amount of protein exceeds that of lipid, some of the protein will aggregate, most likely in a denatured form. An important parameter for crystal packing during reconstitution is therefore the LPR, which should be low enough to promote crystal contacts between protein molecules, but not so low that the protein will begin to aggregate. This ratio is not always easy to predict: More often than not, the purified membrane protein will carry some native lipids from its biological membranes, and in some cases, lipid is added to the solubilized membrane protein during purification. Therefore, the LPR must be determined empirically by carefully designed reconstitution experiments.

#### 1.15.2.4.3 Crystallization buffer and additives

2-D crystal formation is driven by hydrophobic interactions of the membrane-embedded hydrophobic portions of the protein, and by polar interactions between the hydrophilic surface areas. The polar interactions are sensitive to the exact composition of the crystallization buffer, its ionic strength, and pH. Specific additives, which bind to the hydrophilic- or solvent-exposed surface regions of protein, can therefore improve its crystallization behavior.

#### 1.15.2.4.4 Temperature

Temperature affects 2-D crystal formation in several ways: First, if the detergent is removed from the crystallization mixture by dialysis, the rate of detergent removal is obviously temperature dependent. Higher temperatures will speed up the process, and lower temperatures will slow it down. Second, the temperature has an effect on lipid fluidity, and therefore the rate of 2-D diffusion of the protein and lipid. Third, the CMC of the detergent is likely to be temperature dependent. Finally, the strength of hydrophobic interactions increases with increasing temperature. Therefore, the interactions between the hydrophobic surface areas of the protein with one another, and with the lipid, as well as the strength of lipid-lipid interactions increase as the temperature rises. For these reasons, slightly elevated temperatures are generally beneficial for growing 2-D crystals of membrane proteins, and by far the most have been grown at room temperature or above (e.g., Ringler et al., 2000;[85] Mosser, 2001[86]). In some cases, a temperature ramp between room temperature and 37 °C, applied once or repeatedly over a period of several hours, has proved to be advantageous, probably because of a gradual transition across the temperature-dependent CMC of the detergent in both directions. If the protein is stable enough, it may be best to keep the temperature high throughout the experiment, as in the case of the sodium/proton antiporter, NhaA,[58] the oxalate transporter OxlT,[78] and the tetracycline transporter.[88] However, there is no reason not to drop the dialysis temperature if protein stability requires it, although this will increase the dialysis time. Once the crystals are formed, they are usually quite stable at lower temperatures and may be kept at 4 °C for weeks or months. The structure of Aqp1, for example, was determined from one single 2-D crystallization sample of 100 µl initial volume, which was stored and maintained in the fridge at 4 °C for several years, until the structure was determined from it.[89] Complete detergent removal may be advisable for improved crystal stability.[85]

#### 1.15.2.4.5 Removal of detergent

The final step of the reconstitution process involves lowering the detergent concentration, which induces protein insertion into the lipid membrane. This can be achieved by several different methods: Dilution, dialysis, and addition of Bio-beads or addition of cyclodextrin.

##### 1.15.2.4.5.1 Dilution method

Diluting a solution of protein, lipid, and detergent decreases the concentrations of all components by equal factors and is probably the most reproducible way to achieve crystallization, as the final concentration of the detergent can be fixed in a highly reproducible manner. This method is useful for samples prepared with high-CMC detergents because detergents with low CMC have a higher fraction bound to the proteins and lipids, and therefore membrane reconstitution requires a dilution factor that is too large to maintain usable protein concentrations. The dilution method has been used with great success in the cases of PhoE,[90,91] OmpF, band3, and photosystem I.[92]

##### 1.15.2.4.5.2 Dialysis method

Dialysis is the most commonly used method in electron crystallography of membrane proteins. In this method, detergent slowly passes through the pores of the dialysis membrane, which creates a local gradient that may favor crystallization. Indeed, the dialysis membrane may generate crystallization nuclei, and the detergent gradient produced by the slow removal of detergent could stimulate the growth of large crystals. The major drawback of this method is the long time it takes to remove low-CMC detergents. Therefore, the method is more practical for medium- to high-CMC detergents (typically CMC > 1 mM). In the case of low-CMC detergent dialysis, it is necessary to optimize the buffer conditions such that the protein remains stable for long dialysis times. Interestingly, the best crystals reported so far have been obtained by the dialysis method with high-CMC detergents; they include cytochrome $b_o$ ubiquinol oxidase, photosystem II, CHIP, rhodopsin, glutathione transferase, NhaA transporter, mannitol transporter enzyme II, and AQPs.[86]

Special equipment has been designed to improve the dialysis method. A temperature-controlled, continuous-flow dialysis apparatus has the advantage of providing precise control of the temperature profile, which was found to be quite critical in some cases.[54,93,94] Additionally, this system maintains a maximal detergent gradient across the dialysis membrane, which improves the reproducibility of the crystallization process.

#### 1.15.2.4.5.3 Bio-Beads method

Adsorption of detergent to polystyrene beads (e.g., Bio-Beads SM2, Bio-Rad) is another approach for 2-D crystallization. Hydrophobic absorption removes the detergent from the protein solution, thus promoting the incorporation of the protein into lipid bilayers to form 2-D crystals. This method was, for example, used for the cytochrome *b6f* complex.[69] Bio-Beads have two important properties: They can be used for small sample volumes and they have higher affinities for detergents than for lipids. It has been shown that nonspecific adsorption of lipids is about 100 to 200 times lower than the specific adsorption of detergent. Since crystallization experiments are generally performed at low LPRs, weak lipid adsorption may have some effects. However, lipid adsorption can be reduced by pre-incubating the beads with an excess of sonicated liposomes.[95] Crystallization trials can be performed using either a one-step addition of Bio-Beads, resulting in fast removal of the detergent, or by addition of the same Bio-Bead mass progressively, resulting in a slower process. The rate of detergent removal is not directly linked to the weight of Bio-Beads used but to the working temperature; the rate of detergent adsorption doubles every 15 °C. To maintain a reproducible adsorption property, the freshly prepared Bio-Beads must be precisely weighed (wet, but not soaked or dry, and at an appropriate detergent-to-Bio-Beads ratio), properly prepared (washed three times in methanol and then three times in deionized water while stirring), and must not be allowed to dry out.[86,95]

#### 1.15.2.4.5.4 Equilibrium methods

In the case of LHC-II[96] and bacteriorhodopsin,[97] large 2-D sheets have been obtained by simply incubating a mixture containing the protein, lipid, and detergent in crystallization buffer. Crystals form in suspension by stepwise addition of solubilized protein to a growing edge of the crystalline sheets. The crystallization process resembles that of 3-D crystallization in batch. Clearly this requires precisely controlled conditions of all factors that can influence crystal formation, in particular the concentrations of protein, lipid, and detergent(s), as well as pH, temperature, and ionic strength (see Kühlbrandt, 1992[2]).

#### 1.15.2.4.5.5 Cyclodextrins

An alternative approach to removing detergent during the reconstitution process is to use cyclodextrin. Cyclodextrins are ring-shaped molecules, composed of six, seven, or eight glucose molecules. Since the nonpolar environment inside the ring enables cyclodextrins to engulf detergents, the interaction between cyclodextrins and the detergent relies on molecular interactions rather than on diffusion or adsorption properties. An appropriate combination of detergent and cyclodextrins enables detergent removal regardless of the charge of the detergent (anionic, zwitterionic, or nonionic) or its CMC. Cyclodextrin has a higher affinity for detergents than for lipids, thus preventing changes in the LPR during reconstitution. These properties make cyclodextrins particularly useful for 2-D crystallization trials. Initially, cyclodextrins were used to reconstitute active membrane proteins into proteoliposomes at high LPR for functional studies.[98–100] Later on, the same approach was used for the 2-D crystallization of OmpF and SoPIP2;1. Both proteins yielded quality crystals suitable for cryo-electron microscopy (cryo-EM).[101]

#### 1.15.2.4.5.6 2-D crystallization on a lipid monolayer

Another method of growing 2-D crystals of membrane proteins uses the lipid monolayer method.[86,102] In this method, a lipid monolayer is spread on the surface of a small ($\sim$40 µl) volume of crystallization buffer in a clean Teflon well. It is important to use an excess of lipid by a factor of $\sim$1.5 over the amount that would cover the well surface to allow for partial solubilization by the detergent. After 4 hours the monolayer is stabilized and a few microliters of detergent-solubilized protein is injected into the cell through a small opening at the side. The protein attaches rapidly to the monolayer surface and the detergent is absorbed by Bio-Beads, which are introduced one by one through the side opening.[102] The monolayer with attached protein is incubated for up to 3 days, during which the protein has time to crystallize. Finally, the surface layer is transferred to the specimen support grid for examination in the electron microscope. In principle, any lipid that interacts with the hydrophilic surface area of a protein can be used, but functionalized lipids with head groups that are designed to interact specifically with a particular part of the protein are most promising. Nickel-nitrilotriacetic acid (Ni-NTA) lipids bind Ni ions to interact with a histidine tag on the protein, as an increasing number of membrane proteins are expressed with such a tag for purification. This elegant technique was first developed for soluble proteins.[103,104] Ni-NTA-lipids are now commercially available from Avanti (Alabaster, Alabama, USA). The NTA lipid is diluted with a regular lipid that forms fluid monolayers such as *E. coli* polar lipid. As in 2-D crystallization by dialysis, the LPR of the injected protein solution is important. In practice, this procedure has been limited to detergents with low CMC such as *n*-dodecyl-beta-D-maltoside (DDM) which are easier to balance against the tendency to dissolve the monolayer.

#### 1.15.2.4.5.7 2-D crystallization on functionalized, fluoridated lipids

In a similar, but potentially even more general approach, Ni-NTA derivatized, partly perfluoridated lipids have been developed by Mioskowski and colleagues.[105] These special lipids do not mix with membrane lipids and do not dissolve in any detergent. These lipids are therefore, in principle, ideal substrates for membrane protein 2-D crystallization. The CMC of the detergent, and the amount added to the subphase is therefore not a concern with these lipids, as the monolayers have been shown to be resistant to high concentrations of a variety of detergents. The procedure is very similar to the one just described for regular lipids. It has yielded large 2-D crystals of recombinant plant proton ATPase, expressed with a his tag

in yeast.[105] These crystals were very similar to the vesicular crystals of the same protein,[106] except that the unit cell was larger by about 5%. Surprisingly, both crystals had the same inplane twofold screw axis, whereas it may be expected that 2-D arrays grown by specific attachment of the protein to the lipid would yield crystals without inplane symmetry. Indeed, the 2-D crystals of FhuA and TFoF1 ATPase grown on Ni-NTA-derivatized lipid monolayers were of this expected asymmetrical type.[102] This may be taken to suggest that the proton ATPase crystals grew on the fluorinated lipid from small crystalline vesicles forming in suspension, which then merged into large lattices upon attachment to the monolayer via the his tag. Indeed small vesicles can be found at the periphery of larger sheets.[105] Against this hypothesis is the observation that the protein clearly attaches to the monolayer before lattices appear. The method works fairly reproducibly with the plant proton ATPase but has so far not yielded crystals of proteins that had not been crystallized in suspension before. The lipid properties, and in particular the ability to bind his-tagged proteins, seem to deteriorate over several months. Possibly this is due to the loss of Ni ions. Recharging the lipid with fresh Ni solution seemed to restore the original binding properties. More work is needed to improve the reproducibility and general applicability of these promising compounds.

One great advantage of lipid monolayer crystallization is that it requires only very small amounts of protein. Unfortunately, this advantage is outweighed by the difficulties of controlling the crystallization process, of transferring the very fragile surface layers onto specimen support grids and preparing them for high-resolution electron microscopy (EM). So far, none of the 2-D crystals grow on lipid layers have yielded high-resolution electron diffraction patterns, even though they were certainly large enough.

#### 1.15.2.5 EM Microscopy Screening of 2-D Crystals

For many decades the electron microscope (EM) has been an extraordinarily versatile instrument for ultrastructural investigations in material sciences and biology. Biological samples are more difficult to work with, because they are prone to radiation damage, scatter electrons weakly, and are susceptible to dehydration in high vacuum. It is important to use proper conditions during sample preparations, which will preserve the structural integrity during TEM data collection. Sample preparation techniques for 2-D crystals, together with their advantages and disadvantages, will be discussed in the following sections.

##### *1.15.2.5.1 Negative staining: 2-D crystals screening*

After reconstitution into a lipid bilayer, the electron microscope is used to screen for the formation of 2-D crystals, their shapes, and degree of order. Preparation of 2-D crystals for TEM is the next key step. The quickest method for preparing specimens for screening 2-D crystals is by negative staining (**Figure 2**). The method of negative staining was introduced by Brenner and Horne in 1959,[107] and is rapid and simple, requires a small amount of sample (less than 5 µl), and can provide structural information at high signal-to-noise ratio to a resolution of about 16 Å.

Most biological materials show little image contrast compared to their surroundings, unless they are stained. In EM, electrons are absorbed very little by biological samples and contrast is obtained mainly by electron scattering. To increase the contrast between the protein and the background, electron-dense stains are utilized. These are usually water-soluble heavy metal (U, W, Au, Pt, Pb, and Os) salts or compounds that scatter the electrons strongly in regions surrounding and partly penetrating the protein of interest. Heavy metal salts are more tolerant to electron irradiation than the biological samples. The most commonly used heavy metal salts are uranyl acetate or uranyl formate, as well as sodium or potassium phosphotungstate. Uranyl salts are more suitable for protein samples, while phosphotungstate is useful for lipid structures. The optimal stain for a particular specimen has to be chosen and evaluated by trial and error.

Copper grids (available from many TEM suppliers) are the most commonly used specimen support grids for biological EM. They are coated with a specimen support film (usually a thin carbon film). To obtain optimal staining and to enhance the absorption of sample to the carbon surface of the specimen grids, the grids are usually glow-discharged under reduced air pressure prior to adsorption of the specimen.

The ionic conditions of the sample buffer and the presence of remaining detergents strongly interfere with the stain absorption by the specimen. To avoid this, the number of washing steps is increased (from two to six) prior to adding the negative stain solution to the specimen.

Grids of negatively stained 2-D crystal trials can then be imaged in the TEM. This is commonly done with a TEM operated at 80 to 120 kV at nominal magnifications ranging from 2000× to 50 000×. An experienced operator can recognize 2-D crystals directly through the binoculars of the TEM. Alternatively, automated systems have been developed that assist in screening for 2-D crystals,[108] or that even can recognize 2-D crystals via online image processing.[109] Recorded low-dose images (see below) allow the determination of the projection map from the negatively stained crystals at resolutions of 16 Å. For 3-D work, or for higher resolution, the frozen hydrated sample has to be investigated, which is called cryo-electron microscopy (cryo-EM).

### 1.15.3 EM Data Collection for 2-D Crystals

#### 1.15.3.1 Cryo-EM Sample Preparation for 2-D Crystals

Biological membranes are at home in an aqueous environment. It is essential to minimize perturbations to the molecular structure of the membrane proteins when preparing the protein 2-D crystals for visualization and structural investigation in the electron microscope. The method of cryo-EM was established in the 1970–1980s[110–112] as a means to avoid sample fixation and decrease electron damage while imaging.

Cryo-EM allows faithful preservation of structural details at the molecular or even atomic level by rapid freezing and maintaining the specimen in a frozen hydrated state under close-to-native condition in the electron microscope. Imaging specimens at cryogenic temperatures (below −170 °C) in the

TEM provides increased radiation protection from the electron beam during data collection.

Cryo-EM methods involve the rapid freezing of the sample, commonly employing a plunge-freezing device that rapidly immerses the specimen into either liquid ethane or liquid propane. Freezing rates faster than 10 000 K $s^{-1}$ produce a vitreous ice layer of ~100 nm thickness from the solute buffer that essentially embeds the sample in amorphous, vitrified buffer. This has numerous advantages over negative staining. For example, the sample is not dried in a heavy metal salt or exposed to the acidic pH of 4.3, as is the case for negative staining with uranyl acetate. The sample retains its water content, whereas by negative staining the sample is dehydrated by air drying. Preserved hydration means that the protein or 2-D crystal retains its 3-D shape within the vitreous ice layer. In addition, if the sample is suspended within a hole in a carbon film, the biological sample does not come into direct contact with the carbon surface so that any charge interactions or surface forces that otherwise occur between sample and support film are avoided.

For 2-D crystal imaging, in most cases the sample is nevertheless adsorbed to a continuous carbon film, to keep the crystalline array as flat and undistorted as possible,[113] and to minimize sample movement under the electron beam. This can be achieved by the so-called back-injection method.[114] An even better protection and also a reduction of beam-induced specimen movement and/or charging is achieved by the so-called carbon sandwich method.[115] In order to retain high-resolution structural information from 2-D crystals, meticulous sample preparation techniques must be employed for cryo-EM.[116,117]

Sugar embedding is currently considered the best method to prepare 2-D crystals of membrane proteins reconstituted into lipid bilayers. The type of sugar used, the concentration of sugar, freezing time, and freezing media vary from crystal to crystal, but a dilute (1–20%) solution of trehalose in buffer or water is used most commonly. It is important to screen the suitable conditions for the crystal of interest prior to data collection.

### 1.15.3.2 Cryo-EM Imaging and Data Acquisition

The ability to image 2-D crystalline arrays in the electron microscope places stringent demands on data collection. Many factors may degrade the attainable resolution, including beam-induced specimen drift or the absence of complete and uniform specimen flatness on the TEM grid, which can lead to resolution loss with the current generation of image processing software. (Future image processing approaches that accommodate for variations of sample tilt throughout a single image of a flattened 2-D crystal may remove this limitation.)

Due to the sensitivity of 2-D crystals to radiation damage, low-dose procedures are necessary.[118] This requires specialized software for beam blanking and microscope control. Data collection on 2-D crystals by cryo-EM imaging is done in the same way as other (e.g., single-particle) samples would be imaged. The specimen grid is routinely screened at a low magnification to allow selection of areas with good ice or sugar thickness (as thin as possible without actually drying the crystal) and with a well-dispersed sample distribution. Once a promising area is identified, an image shift is applied that moves the beam away from the position of interest and sets this area at a higher magnification so that the sample can be carefully focused. Usually a degree of defocus is applied to enhance image contrast. Then the software will shift the electron beam back to the area of interest and a single image is taken at a predetermined exposure time and magnification. Normally, each 2-D crystal is imaged only once and therefore at only one preset specimen tilt angle. This is done to maximize the amount of recorded high-resolution information in one image. Successive images are then acquired from other 2-D crystals from different areas across the grid.

The method of spot scanning can be applied to reduce the amount of beam-induced image drift that can occur during image acquisition on tilted specimens.[119] Additional alignment procedures together with optimizing microscope parameters are needed to minimize electron beam exposure during imaging and data acquisition. Out-of-focus spot-scan imaging of 2-D crystals requires a TEM with a parallel beam at small spot sizes, such as the JEOL 3000, FEI Titan, or ZEISS Libra.

### 1.15.3.3 Electron Diffraction of Frozen Hydrated Crystals

In addition to imaging, data collection of 2-D crystals can be done by electron diffraction using TEM with low-dose techniques and microscope control software. Electron diffraction for data collection from 2-D crystals is unaffected by the phase contrast transfer function (CTF) of the instrument, and does not suffer from specimen vibration or drift. The resulting diffraction data are also less sensitive to specimen charging during the exposure. Even though electron diffraction usually requires well-ordered, large 2-D crystals (at least 1 μm in diameter, depending on the unit cell size), data collection can be used in an efficient way to obtain a high-resolution data set from tilted samples.[120] The electron diffraction patterns enable reliable determination of the structure amplitudes of the sample, but they lack the phase information. With respect to recording diffraction patterns, the search and diffraction record modes are needed. These two modes and the current improvements of data collection of 2-D crystals using electron diffraction are discussed below.

#### *1.15.3.3.1 Search mode*

The 'search mode' is used to search for and identify the position of target crystals without exposing crystals to a high dose electron beam. When high-resolution data in the order of a few Angstroms of resolution are to be recorded, the maximum exposure that proteins can tolerate is 10–20 e $Å^{-2}$ over the usual electron energy range of 100–300 keV. Therefore, the intensity used in the search mode is usually around 1 e $Å^{-2}$ $minute^{-1}$. Due to this low intensity, it is important to work at very low magnification, even when using a sensitive charge-coupled device (CCD) camera and working in a high contrast mode of the microscope (e.g., by using the so-called shadow image mode, when operating in strongly defocused diffraction mode). The local electron dose can be reduced by spreading the beam over a larger area (20–100 μm diameter).

#### 1.15.3.3.2 Diffraction mode

The 'diffraction mode' is used to collect the diffraction data of the crystals. The diffraction focus must be carefully set to optimize the spot sharpness without saturating the detector while recording diffraction patterns. It is important to control the illumination of crystals, for which the diameter of the illuminated area depends on the average size of the monocrystalline crystal areas. The beam should illuminate the whole crystal, when the crystals are of moderate size. While large crystals are almost always advantageous, there is an upper limit to the beam diameter that can be used, since lens aberrations prevent obtaining a sharp focus from an area more than a certain diameter. This size may vary widely among different microscopes. Particularly when the beam and crystal sizes are about the same, it is important to make sure that the diffraction mode is correctly aligned with the target selected in the search mode. To test if the beam in diffraction mode is correctly centered on the crystal, the operator can slightly overfocus the diffraction pattern to produce a strongly defocused shadow image. This should then show the chosen 2-D crystal. The beam should also expand concentrically as the diffraction focus is changed, indicating that it is properly positioned on the optical axis of the instrument.

The use of slow-scan CCD cameras has had a major influence on diffraction data recording.[121] CCDs offer much greater linearity and dynamic range than photographic films, which need digitizing for fine spots on a transparent background.[122] However, the major problem that CCDs present is blooming, or spreading of the signal from the very intense central spot region and its surrounding areas. The unspread beam highly oversaturates the CCD, since it is several orders of magnitude stronger than diffraction spots from a typical protein crystal. To avoid this, it is important to use a beam stop to block the central beam, which otherwise may damage the CCD camera. Hence, the beam stop blocks a significant portion of the diffraction pattern. Some CCD cameras have a special antiblooming feature, which thermally generates electron-hole pairs within the CCD, but these are only slowly generated under the usual operating conditions. Therefore, a longer exposure time of 20–60 s is an alternative way to achieve antiblooming capability. In addition, long exposures also reduce the influence of the streak that often shows up from the central beam as the pattern is deflected in and out by the beam blocker. Proper intensity can be achieved by using a small condenser aperture and high spot size setting.

Another problem occurring in electron diffraction is that the higher-resolution spots tend to fade substantially faster than those at lower resolution and the total exposure must be set to capture the greatest intensity without adding too much noise. The use of an energy filter can greatly improve the quality of diffraction data.[122,123]

## 1.15.4 Image Processing for 2-D Crystals

TEM imaging of biological samples is affected by a very low signal-to-noise ratio, which makes the distinction of the molecular arrangement in a single protein difficult, if not impossible. For samples that organize in a crystalline arrangement, the systematic repetition can be exploited to extract the underlying common signal from the multitude of noisy realizations. The availability of an enormous number of naturally 'aligned' (i.e., equally oriented and regularly distributed) copies of the same protein makes trivial the averaging of the different realizations of the same view, and thus the recovery of the original signal. If further views of the protein can be extracted from differently oriented crystals, they can be integrated in the computer into a 3-D structure.

As elegantly simple as the underlying idea is, the actual workflow needs to respond to multiple additional problems: Deviations from perfect crystallinity, instrumental restrictions, limits and perturbations of the imaging system, and the scope of results attainable with reasonable computational resources, all limit the performance of the method. Specially tailored image analysis tools and concepts have evolved in order to tackle these reality constraints with increasing efficiency. The current state of the art of the algorithmic machinery, discussing both the mathematical concepts that have been established as well as the available software resources that embody them will be discussed in the following sections.

### 1.15.4.1 Mathematical Setting

#### 1.15.4.1.1 3-D reconstruction in EM

Along with electron crystallography, other electron transmission imaging techniques such as tomography and single particle reconstruction offer the potential of generating a 3-D computer model by integrating 2-D data sets recorded by the microscope. All these techniques share the same basic mathematic tool that sustains the links between experimental 2-D data and the computed 3-D model: The central section theorem.

Simple to prove, this key phenomenon states that the projection along the $z$ direction of a 3-D volume contains the same information as the central slice in the reciprocal space ($z^* = 0$) of the 3-D-Fourier transform of the volume. This implies that a full set of projections along all spatial directions is equivalent to a full sampling of the Fourier transform of the object, and therefore allows reconstructing the original volume.

This abstract mathematical result elegantly echoes in instrumental experimentation by the theory of electron optics, which establishes that the image created by a TEM corresponds (with a certain degree of approximation) to a projection of the sample. In other words, with sufficient projections of the sample imaged in different orientations with respect to the electron beam, it is possible to create an approximation to its 3-D density distribution.

#### 1.15.4.1.2 Data sets in electron crystallography

The crystalline arrangement of the proteins in the 2-D crystals that are imaged in electron crystallography gives access to high-resolution data that otherwise would be very difficult to extract. The 'biological protein alignment' in well-ordered 2-D crystals is by far superior to the 'computational protein alignment' that a cross-correlation-based image-processing single particle approach would be able to perform on noisy data.

#### 1.15.4.1.2.1 Imaging conditions

For the collection of an entire data set, different 2-D crystals of the protein are imaged in the electron microscope. In a typical cryo-EM session, 2-D crystals of 1 μm diameter or larger would be imaged at 80 000 × magnification at liquid helium temperature (4.3 K), or at 50 000 × magnification at liquid nitrogen temperature (77 K or slightly warmer). The higher magnification at liquid helium temperature reflects the additional protection from beam damage that a sugar-embedded 2-D crystal receives from the lower helium temperature.[124] Illumination with a field emission gun (FEG) microscope at 200 or 300 kV acceleration voltage, using a relatively low defocus of two to five times Scherzer defocus (e.g., 400–1000 nm underfocus), and recording images on photographic film is usually employed. This allows benefit to be obtained from the better point spread function of scanned film vs. current generations of CCD cameras at higher voltages.[125] Electron diffraction data from 2-D crystalline samples are best recorded on CCDs. A typical experiment could involve hundreds of crystals, tilted in different angles that are each only imaged once. Although tilt ranges between $-70^\circ$ and $+70^\circ$ are experimentally available in most modern microscopes, practical work is often producing better results at tilt angles between $-45^\circ$ and $+45^\circ$ of sample tilt.

### 1.15.4.1.3 Direct image and diffraction patterns

The microscope can collect images in two different operational modes: In 'direct imaging' mode, a 2-D projection of the sample is recorded in the image plane. In 'diffraction mode', the crystalline nature of the sample creates a coherent interference in the focal plane of the imaging system, which is recorded as a so-called diffraction pattern. The diffraction pattern intensities represent the squared amplitudes of the crystal structure. In contrast, a Fourier transform of a recorded image contains spots that encode the amplitude and also the phase of the protein structure, but these are modulated by the instruments CTF, which has regions of lower signal-to-noise ratio at its Thon rings, and which is resolution-limited due to the envelope function of the CTF. For this reason, the best resolution is usually obtained from a 2-D crystal sample by first recording and processing direct image data to obtain a ~5-Å 3-D map with amplitudes and phases, and then improving on the quality and resolution of the amplitudes by collecting electron diffraction data. However, electron diffraction requires the availability of well-ordered large 2-D crystals, because a computational crystal lattice unbending procedure can only be used to improve the quality of direct images, but not of electron diffraction patterns.

### 1.15.4.1.4 3-D reconstruction in electron crystallography

Direct imaging provides a direct way to exploit the crystalline structure of the sample. All the repetitions of the protein available in each projection can be averaged, yielding an ideal view of the particle for those particular orientations. With an appropriately large set of ideal views a 3-D reconstruction can be created. In fact, the starting position is very similar to the situation in single particle reconstruction, with the valuable difference that much more a priori information is available. It is thus possible to follow the single particle methodology to compensate for perturbations of the crystalline ordering, as well as for the inaccuracy in the determination of the projection geometry. This fact has been exploited in several applications,[126] including a maximum likelihood-based single particle approach to 2-D crystal images.[127]

For the processing of diffraction patterns, the Fourier space is the most natural setting. In the 3-D case, the Fourier transform of a crystal is given by the Fourier transform of the repeating unit sampled by the Fourier transform of the lattice. For 2-D crystals, periodicity occurs only in the horizontal directions. In the vertical direction there is no systematic repetition, and the Fourier components are not restricted to discrete points, but continuously distributed. The transform can therefore be viewed as a set of 'lattice lines' ($h$, $k$, $z^*$), where the indices $h$ and $k$ define a discrete lattice in the Fourier space. According to the central section theorem, the diffraction spots from an untilted crystal contain all the amplitudes of the ($h$, $k$, 0) Fourier components of the crystal. For tilted crystals, each diffraction spot in a pattern corresponds to the value of the lattice line at a height $z^*$ determined by the tilt angle, the inplane orientation of the crystal and the indices of the examined lattice line. The more data from different tilts are recorded, the denser is the sampling of the amplitudes in each lattice line. At this stage, phase information gained from direct imaging, molecular replacement or *ab initio* computation enables the use of Fourier inversion to construct an approximation to the original density map.

Extracting a 3-D model from an irregularly sampled Fourier space is a mathematically involved task (as Fourier space interpolation is not as straightforward as the homologous operation in direct space and a careful formulation as a combination of *sinc* function is required). However, this enables the incorporation of additional boundary constraints that model available a priori information, as for instance the vertical thickness of the crystal. Extended formulations of this kind can dramatically increase the quality of the reconstruction as in Gipson et al.[128]

### 1.15.4.1.5 Analysis of individual images

Before information from different images can be combined, each individual image needs a separate analysis and preprocessing. This involves the extraction of the lattice parameters and orientation, identification, and correction of crystalline defects and the compensation for image distortions introduced by the imaging system.

#### 1.15.4.1.5.1 Lattice parameter determination

Both experimental diffraction patterns and amplitude maps of computed Fourier transform of direct space images give a direct insight into the structure of the crystal. Correct identification and indexing of diffraction spots determines basic lattice information as size and orientation of the unit cell, and might also be used to detect the presence of several layers, to identify a possible underlying higher order symmetry, or to infer the precise tilt geometry.

#### 1.15.4.1.5.2 CTF correction

The physics of the interaction of electrons with matter and the subsequent image contrast formation process in the TEM introduces different kinds of distortions and modulations in the image. Although an experienced operator can reduce the impact of some optical aberrations (astigmatism, barrel and

pincushion distortions) the coherent misrepresentation of frequencies of different ranges is inherent to the image formation model. This effect can be viewed in the Fourier space as a modulation of the original signal with a radially symmetrical, oscillating function (called CTF).

The dependence of the quantitative behavior of this function on features of the imaging system (as defocus value, electrostatic potential) has been successfully modeled, enabling to some extent the computational correction of this effect. However, full correction is an open question, as distorted tilted samples do not lend themselves to an efficient mathematical treatment.[129,130] Further, for non-tilted samples the frequency components of the original signal that are close to the zeros of the CTF are irremediably lost in a single image. Their recovery would require further data, recorded with different parameters in the experimental design so that different frequency ranges are accessed.

#### *1.15.4.1.5.3 Unbending*

The underlying idea of electron crystallography is to benefit from the extensive repetition of the unit cell in a structured manner. As real crystals might depart from perfect periodicity, it is frequently necessary to perform a numerical correction on the recorded images to enhance the crystalline nature of the data. In direct imaging, this requires first identifying the perturbation that is deforming the ideal lattice, a task that can be performed by cross correlating an idealized reference on the whole image, and then comparing the obtained maxima with the spots predicted by translational symmetry. The image can then be computationally corrected according to the so obtained deformation map, and the whole procedure can be iterated extracting a new reference from the corrected, 'unbent' image.[129,131–133]

This list is an enumeration rather than a pipeline of sequential steps, as these aspects are severely intertwined with each other, and the actual implementation requires integrating the interaction among these elements.

#### *1.15.4.1.6 Merging and reconstruction*

Individual images must still undergo a further preprocessing step, which, in contrast to the previous ones, addresses a collective issue of the whole data set: The different absolute intensity scales in each image or diffraction pattern. As each one stems from a different crystal imaged under slightly different conditions, their intensities need to be rescaled to a common reference.

#### *1.15.4.1.7 Reconstruction and refinement*

After rescaling, the data set can be used to create a first 3-D reconstruction using one of the frameworks described above: Filling of the lattice lines in the Fourier space or direct space processing. In both cases, the obtained reconstruction can be used as a first reference to go back some steps and incorporate this model as a priori information for the 2-D processing. This allows, for instance, the accuracy in the determination of the tilt geometry to be increased, which typically is not reliable for high tilts. This refined geometry will in turn yield a reconstruction of higher quality, so that this procedure can be iterated until convergence. Upon publication, final reconstruction maps should be deposited in the EMDataBank.org.[134]

### 1.15.4.2 Software Resources

Several different software approaches assist in each step in the processing of 2-D crystal data.[135] In general, the technically involved aspects of the algorithms are to a large extent transparent to the user, who is not dependent on a perfect command of the mathematical details. Instead, he or she needs to control or at least supervise the flow of the data throughout the different steps of the processing pipeline. While current software tools allow automating most aspects of the data analysis, optimizing the quality of the final result usually requires the experience and intuition of a trained human operator, which is still the better analysis tool.

Since the 1970s, there has been one major software package creating, defining, and enabling the field of electron crystallography: The so-called MRC program suite that was created by Richard Henderson (MRC, Cambridge, UK) and coworkers.[136] This suite consists of a large set of image-processing programs for 2-D crystals. The software offers a robust implementation of all the algorithms needed in the dataflow described in the previous section. Over the years a few other groups have developed software to facilitate the use of the MRC programs, with different solutions depending on the imaging mode (e.g., SPECTRA,[137] ICE,[138] CRISP,[139–141] or *2dx*, see below).

For the processing of direct images, the most prominent outcome is *2dx*,[142–144] a software system that provides a user interface to visualize and process 2-D crystals, while mostly relying on the MRC programs as underlying kernel. In addition, *2dx* offers user-guidance and optionally fully automatic processing of 2-D crystal images,[145] and also incorporates a maximum-likelihood-based single particle processing tool for 2-D crystal images.[127] *2dx* provides the user with an intuitive system for data management, default processing parameters, and a broad documentation integrated in the front end.

For the processing of electron diffraction data, the MRC software package offers robust programs that automatically index diffraction patterns and evaluate the data from those patterns. The XDP software tool[146] can be used to facilitate the use of the MRC programs by adding a front-end software system for diffraction pattern evaluation.

A new development for electron crystallography data processing for images and diffraction patterns is IPLT,[147,148] a package that does not make use of the MRC software suite, but provides a reimplementation of existing algorithms as well as newly developed algorithms for 2-D crystal processing in a modular way.

These software systems were reviewed by Schenk et al. (2010).[135]

## 1.15.5 Conclusion

Membrane protein structure determination has received a major boost through the availability of the complete genome sequence of many bacterial genomes. Genome sequences of diverse range bacteria (e.g., thermophilic, hyperthermophilic, and/or mesophilic) can now be screened for homologous membrane protein genes, which might give better expression levels or are more amenable for crystallization, while still

allowing the analysis of the mechanism of function. In addition, recent developments have led researchers to successfully obtain structural information of many eukaryotic membrane proteins, which are more laborious to express, solubilize, purify, and crystallize.

Electron crystallography of 2-D membrane protein crystals has been used to determine the structure of membrane proteins for several decades now. This method has been used to resolve the structure of nine membrane proteins and tubulin, but near-atomic resolutions in 3-D are still rare (BR,[129] LHCII,[149] AQP1,[89,150] nAChR,[151] AQP0,[77,152] AQP4,[153] MGST,[154] prostaglandin E2,[155] $H^+/K^+$-ATPase,[156] and tubulin[59]). Nevertheless, large numbers of membrane protein structures have been determined to 5 to 9 Å resolution (**Table 1**), which allows determining the α-helices present in the membrane protein.[157,158] The low-resolution maps together with biochemical and evolutionary data and hydropathy plots allowed in several cases building rational models for the structures (e.g., EmrE[159]). The current methodologies of membrane protein expression, purification, and sample preparation techniques for EM, together with recent and new developments for automation in 2-D crystallization, data collection, and data-processing software will open new structural information of many membrane proteins in near future.

## References


[1] Walz, T.; Smith, B.; Zeidel, M.; Engel, A.; Agre, P. Biologically active two-dimensional crystals of aquaporin CHIP. *J. Biol. Chem.* **1994**, *269*(3), 1583–1586.

[2] Kühlbrandt, W. Two-dimensional crystallization of membrane proteins. *Quart. Rev. Biophys.* **1992**, *25*(1), 1–49.

[3] Renault, L.; Chou, H. T.; Chiu, P. L.; Hill, R. M.; Zeng, X.; Gipson, B.; Zhang, Z. Y.; Cheng, A.; Unger, V.; Stahlberg, H. Milestones in electron crystallography. *J. Comput. Aided Mol. Des.* **2006**, *20*(7-8), 519–527.

[4] Glaeser, R.; Downing, K.; DeRosier, D.; Chiu, W.; Frank, J. *Electron Crystallography of Biological Macromolecules*; Oxford University Press: USA, 2007; 476 pp.

[5] Anson, L. Membrane protein biophysics. *Nature* **2009**, *459*(7245), 343.

[6] Nilsson, B.; Anderson, S. Proper and improper folding of proteins in the cellular environment. *Annu. Rev. Microbiol.* **1991**, *45*, 607–635.

[7] Stark, M. J. Multicopy expression vectors carrying the lac repressor gene for regulated high-level expression of genes in *Escherichia coli*. *Gene* **1987**, *51*(2-3), 255–267.

[8] Larue, K.; Kimber, M. S.; Ford, R.; Whitfield, C. Biochemical and structural analysis of bacterial O-antigen chain length regulator proteins reveals a conserved quaternary structure. *J. Biol. Chem.* **2009**, *284*(11), 7395–7403.

[9] Woodward, R.; Yi, W.; Li, L.; Zhao, G.; Eguchi, H.; Sridhar, P. R.; Guo, H.; Song, J. K.; Motari, E.; Cai, L.; Kelleher, P.; Liu, X.; Han, W.; Zhang, W.; Ding, Y.; Li, M.; Wang, P. G. *In vitro* bacterial polysaccharide biosynthesis: Defining the functions of Wzy and Wzz. *Nat. Chem. Biol.* **2010**, *6*(6), 418–423.

[10] Abeyrathne, P. D.; Lam, J. S. Conditions that allow for effective transfer of membrane proteins onto nitrocellulose membrane in Western blots. *Can. J. Microbiol.* **2007**, *53*(4), 526–532.

[11] Ghanei, H.; Abeyrathne, P. D.; Lam, J. S. Biochemical characterization of MsbA from *Pseudomonas aeruginosa*. *J. Biol. Chem.* **2007**, *282*(37), 26939–26947.

[12] Raunser, S.; Mathai, J. C.; Abeyrathne, P. D.; Rice, A. J.; Zeidel, M. L.; Walz, T. Oligomeric structure and functional characterization of the urea transporter from *Actinobacillus pleuropneumoniae*. *J. Mol. Biol.* **2009**, *387*(3), 619–627.

[13] Yamashita, A.; Singh, S. K.; Kawate, T.; Jin, Y.; Gouaux, E. Crystal structure of a bacterial homologue of $Na^+/Cl^-$-dependent neurotransmitter transporters. *Nature* **2005**, *437*(7056), 215–223.

[14] Miroux, B.; Walker, J. E. Over-production of proteins in *Escherichia coli*: Mutant hosts that allow synthesis of some membrane proteins and globular proteins at high levels. *J. Mol. Biol.* **1996**, *260*(3), 289–298.

[15] Bannwarth, M.; Schulz, G. E. The expression of outer membrane proteins for crystallization. *Biochim. Biophys. Acta* **2003**, *1610*(1), 37–45.

[16] Loll, P. J. Membrane protein structural biology: The high throughput challenge. *J. Struct. Biol.* **2003**, *142*(1), 144–153.

[17] Grisshammer, R.; Duckworth, R.; Henderson, R. Expression of a rat neurotensin receptor in *Escherichia coli*. *Biochem. J.* **1993**, *295*(Pt 2), 571–576.

[18] Tucker, J.; Grisshammer, R. Purification of a rat neurotensin receptor expressed in *Escherichia coli*. *Biochem. J.* **1996**, *317*(Pt 3), 891–899.

[19] Weiss, H. M.; Grisshammer, R. Purification and characterization of the human adenosine A(2a) receptor functionally expressed in *Escherichia coli*. *Eur. J. Biochem* **2002**, *269*(1), 82–92.

[20] Kiefer, H.; Krieger, J.; Olszewski, J. D.; Von Heijne, G.; Prestwich, G. D.; Breer, H. Expression of an olfactory receptor in *Escherichia coli*: Purification, reconstitution, and ligand binding. *Biochemistry* **1996**, *35*(50), 16077–16084.

[21] Bharathi, A.; Ghosh, A.; Whalen, W. A.; Yoon, J. H.; Pu, R.; Dasso, M.; Dhar, R. The human RAE1 gene is a functional homologue of *Schizosaccharomyces pombe* rae1 gene involved in nuclear export of Poly(A)+ RNA. *Gene* **1997**, *198*(1-2), 251–258.

[22] Wood, V.; Gwilliam, R.; Rajandream, M. A.; Lyne, M.; Lyne, R.; Stewart, A.; Sgouros, J.; Peat, N.; Hayles, J.; Baker, S.; Basham, D.; Bowman, S.; Brooks, K.; Brown, D.; Brown, S.; Chillingworth, T.; Churcher, C.; Collins, M.; Connor, R.; Cronin, A.; Davis, P.; Feltwell, T.; Fraser, A.; Gentles, S.; Goble, A.; Hamlin, N.; Harris, D.; Hidalgo, J.; Hodgson, G.; Holroyd, S.; Hornsby, T.; Howarth, S.; Huckle, E. J.; Hunt, S.; Jagels, K.; James, K.; Jones, L.; Jones, M.; Leather, S.; McDonald, S.; McLean, J.; Mooney, P.; Moule, S.; Mungall, K.; Murphy, L.; Niblett, D.; Odell, C.; Oliver, K.; O'Neil, S.; Pearson, D.; Quail, M. A.; Rabbinowitsch, E.; Rutherford, K.; Rutter, S.; Saunders, D.; Seeger, K.; Sharp, S.; Skelton, J.; Simmonds, M.; Squares, R.; Squares, S.; Stevens, K.; Taylor, K.; Taylor, R. G.; Tivey, A.; Walsh, S.; Warren, T.; Whitehead, S.; Woodward, J.; Volckaert, G.; Aert, R.; Robben, J.; Grymonprez, B.; Weltjens, I.; Vanstreels, E.; Rieger, M.; Schafer, M.; Muller-Auer, S.; Gabel, C.; Fuchs, M.; Dusterhoft, A.; Fritzc, C.; Holzer, E.; Moestl, D.; Hilbert, H.; Borzym, K.; Langer, I.; Beck, A.; Lehrach, H.; Reinhardt, R.; Pohl, T. M.; Eger, P.; Zimmermann, W.; Wedler, H.; Wambutt, R.; Purnelle, B.; Goffeau, A.; Cadieu, E.; Dreano, S.; Gloux, S.; Lelaure, V.; Mottier, S.; Galibert, F.; Aves, S. J.; Xiang, Z.; Hunt, C.; Moore, K.; Hurst, S. M.; Lucas, M.; Rochet, M.; Gaillardin, C.; Tallada, V. A.; Garzon, A.; Thode, G.; Daga, R. R.; Cruzado, L.; Jimenez, J.; Sanchez, M.; del Rey, F.; Benito, J.; Dominguez, A.; Revuelta, J. L.; Moreno, S.; Armstrong, J.; Forsburg, S. L.; Cerutti, L.; Lowe, T.; McCombie, W. R.; Paulsen, I.; Potashkin, J.; Shpakovski, G. V.; Ussery, D.; Barrell, B. G.; Nurse, P. The genome sequence of Schizosaccharomyces pombe. *Nature* **2002**, *415*(6874), 871–880.

[23] Siam, R.; Dolan, W. P.; Forsburg, S. L. Choosing and using *Schizosaccharomyces pombe* plasmids. *Methods* **2004**, *33*(3), 189–198.

[24] Abdulaev, N. G.; Popp, M. P.; Smith, W. C.; Ridge, K. D. Functional expression of bovine opsin in the methylotrophic yeast *Pichia pastoris*. *Protein Expr. Purif.* **1997**, *10*(1), 61–69.

[25] Arkinstall, S.; Edgerton, M.; Payton, M.; Maundrell, K. Co-expression of the neurokinin NK2 receptor and G-protein components in the fission yeast *Schizosaccharomyces pombe*. *FEBS Lett.* **1995**, *375*(3), 183–187.

[26] Erlenbach, I.; Kostenis, E.; Schmidt, C.; Hamdan, F. F.; Pausch, M. H.; Wess, J. Functional expression of M(1), M(3) and M(5) muscarinic acetylcholine receptors in yeast. *J. Neurochem.* **2001**, *77*(5), 1327–1337.

[27] Mollaaghababa, R.; Davidson, F. F.; Kaiser, C.; Khorana, H. G. Structure and function in rhodopsin: Expression of functional mammalian opsin in *Saccharomyces cerevisiae*. *Proc. Natl. Acad. Sci. USA* **1996**, *93*(21), 11482–11486.

[28] Payette, P.; Gossard, F.; Whiteway, M.; Dennis, M. Expression and pharmacological characterization of the human M1 muscarinic receptor in *Saccharomyces cerevisiae*. *FEBS Lett.* **1990**, *266*(1-2), 21–25.

[29] Presland, J.; Strange, P. G. Pharmacological characterisation of the D2 dopamine receptor expressed in the yeast *Schizosaccharomyces pombe*. *Biochem. Pharmacol.* **1998**, *56*(5), 577–582.

[30] Sander, P.; Grunewald, S.; Maul, G.; Reilander, H.; Michel, H. Constitutive expression of the human D2S-dopamine receptor in the unicellular yeast *Saccharomyces cerevisiae*. *Biochim. Biophys. Acta* **1994**, *1193*(2), 255–262.

[31] Sizmann, D.; Kuusinen, H.; Keranen, S.; Lomasney, J.; Caron, M. G.; Lefkowitz, R. J.; Keinanen, K. Production of adrenergic receptors in yeast. *Receptors Channels* **1996**, *4*(3), 197–203.

[32] Cereghino, J. L.; Cregg, J. M. Heterologous protein expression in the methylotrophic yeast *Pichia pastoris*. *FEMS Microbiol. Rev.* **2000**, *24*(1), 45–66.

[33] Parcej, D. N.; Eckhardt-Strelau, L. Structural characterisation of neuronal voltage-sensitive $K^+$ channels heterologously expressed in *Pichia pastoris*. *J. Mol. Biol.* **2003**, *333*(1), 103–116.

[34] Binda, C.; Li, M.; Hubalek, F.; Restelli, N.; Edmondson, D. E.; Mattevi, A. Insights into the mode of inhibition of human mitochondrial monoamine oxidase B from high-resolution crystal structures. *Proc. Natl. Acad. Sci. USA* **2003**, *100*(17), 9750–9755.

[35] Fischer, G.; Kosinska-Eriksson, U.; Aponte-Santamaria, C.; Palmgren, M.; Geijer, C.; Hedfalk, K.; Hohmann, S.; de Groot, B. L.; Neutze, R.; Lindkvist-Petersson, K. Crystal structure of a yeast aquaporin at 1.15 angstrom reveals a novel gating mechanism. *PLoS Biol.* **2009**, *7*(6), e1000130.

[36] Schwarz, D.; Dotsch, V.; Bernhard, F. Production of membrane proteins using cell-free expression systems. *Proteomics* **2008**, *8*(19), 3933–3946.

[37] Berrier, C.; Park, K. H.; Abes, S.; Bibonne, A.; Betton, J. M.; Ghazi, A. Cell-free synthesis of a functional ion channel in the absence of a membrane and in the presence of detergent. *Biochemistry* **2004**, *43*(39), 12585–12591.

[38] Elbaz, Y.; Steiner-Mordoch, S.; Danieli, T.; Schuldiner, S. *In vitro* synthesis of fully functional EmrE, a multidrug transporter, and study of its oligomeric state. *Proc. Natl. Acad. Sci. USA* **2004**, *101*(6), 1519–1524.

[39] Ishihara, G.; Goto, M.; Saeki, M.; Ito, K.; Hori, T.; Kigawa, T.; Shirouzu, M.; Yokoyama, S. Expression of G protein coupled receptors in a cell-free translational system using detergents and thioredoxin-fusion vectors. *Protein Expr. Purif.* **2005**, *41*(1), 27–37.

[40] Klammt, C.; Lohr, F.; Schafer, B.; Haase, W.; Dotsch, V.; Ruterjans, H.; Glaubitz, C.; Bernhard, F. High level cell-free expression and specific labeling of integral membrane proteins. *Eur. J. Biochem.* **2004**, *271*(3), 568–580.

[41] Klammt, C.; Schwarz, D.; Eifler, N.; Engel, A.; Piehler, J.; Haase, W.; Hahn, S.; Dotsch, V.; Bernhard, F. Cell-free production of G protein-coupled receptors for functional and structural studies. *J. Struct. Biol.* **2007**, *158*(2), 482–493.

[42] Klammt, C.; Schwarz, D.; Fendler, K.; Haase, W.; Dotsch, V.; Bernhard, F. Evaluation of detergents for the soluble expression of alpha-helical and beta-barrel-type integral membrane proteins by a preparative scale individual cell-free expression system. *FEBS. J.* **2005**, *272*(23), 6024–6038.

[43] Spirin, A. S.; Baranov, V. I.; Ryabova, L. A.; Ovodov, S. Y.; Alakhov, Y. B. A continuous cell-free translation system capable of producing polypeptides in high yield. *Science* **1988**, *242*(4882), 1162–1164.

[44] Trbovic, N.; Klammt, C.; Koglin, A.; Lohr, F.; Bernhard, F.; Dotsch, V. Efficient strategy for the rapid backbone assignment of membrane proteins. *J. Am. Chem. Soc.* **2005**, *127*(39), 13504–13505.

[45] Koglin, A.; Klammt, C.; Trbovic, N.; Schwarz, D.; Schneider, B.; Schafer, B.; Lohr, F.; Bernhard, F.; Dotsch, V. Combination of cell-free expression and NMR spectroscopy as a new approach for structural investigation of membrane proteins. *Magn. Reson. Chem.* **2006**, *44*. Spec No, S17–S23.

[46] Byrne, B.; Jormakka, M. Solubilization and Purification of Membrane Proteins. In *Structural Genomics on Membrane Proteins*; Lundstrom, K., Ed.; CRC Press: Boca Raton, 2006; pp 179–198.

[47] Howard, T. D.; McAuley-Hecht, K. E.; Cogdell, R. J. *Crystallization of Membrane Proteins*. Blackwell Press: Oxford, 2000.

[48] Ward, A.; Sanderson, N. M.; O'Reilly, J.; Rutherford, N. G.; Poolman, B.; Henderson, P. F. J. *The Amplified Expression, Indentificaiton, Purification, Assay and Properties of Histidine-Tagged Bacterial Membrane Transport Proteins*. Blackwell Press: Oxford, 2000.

[49] Hochuli, E.; Dobeli, H.; Schacher, A. New metal chelate adsorbent selective for proteins and peptides containing neighbouring histidine residues. *J. Chromatogr.* **1987**, *411*, 177–184.

[50] Mathur, R.; Balasubramanian, A. S. Cobalt-ion chelate affinity chromatography for the purification of brain neutral alpha-D-mannosidase and its separation from acid alpha-D-mannosidase. *Biochem. J.* **1984**, *222*(1), 261–264.

[51] Pos, K. M.; Bott, M.; Dimroth, P. Purification of two active fusion proteins of the Na(+)-dependent citrate carrier of Klebsiella pneumoniae. *FEBS Lett.* **1994**, *347*(1), 37–41.

[52] Pourcher, T.; Leclercq, S.; Brandolin, G.; Leblanc, G. Melibiose permease of *Escherichia coli*: Large scale purification and evidence that $H^+$, $Na^+$, and $Li^+$ sugar symport is catalyzed by a single polypeptide. *Biochemistry* **1995**, *34*(13), 4412–4420.

[53] Viadiu, H.; Gonen, T.; Walz, T. Projection map of aquaporin-9 at 7 A resolution. *J. Mol. Biol.* **2007**, *367*(1), 80–88.

[54] Jap, B. K.; Zulauf, M.; Scheybani, T.; Hefti, A.; Baumeister, W.; Aebi, U.; Engel, A. 2-D crystallization: From art to science. *Ultramicroscopy* **1992**, *46*(1-4), 45–84.

[55] Collinson, I.; Breyton, C.; Duong, F.; Tziatzios, C.; Schubert, D.; Or, E.; Rapoport, T.; Kühlbrandt, W. Projection structure and oligomeric properties of a bacterial core protein translocase. *EMBO J.* **2001**, *20*(10), 2462–2471.

[56] Dietrich, J.; Kuhlbrandt, W. Purification and two-dimensional crystallization of highly active cytochrome b(6)f complex from spinach. *FEBS Lett* **1999**, *463*(1-2), 97–102.

[57] Koning, R. I.; Keegstra, W.; Oostergetel, G. T.; Schuurman-Wolters, G.; Robillard, G. T.; Brisson, A. The 5 A projection structure of the transmembrane domain of the mannitol transporter enzyme II. *J. Mol. Biol.* **1999**, *287*(5), 845–851.

[58] Williams, K. A.; Geldmacher-Kaufer, U.; Padan, E.; Schuldiner, S.; Kühlbrandt, W. Projection structure of NhaA, a secondary transporter from *Escherichia coli*, at 4.0 A resolution. *EMBO J.* **1999**, *18*(13), 3558–3563.

[59] Nogales, E.; Wolf, S. G.; Downing, K. H. Structure of the alpha beta tubulin dimer by electron crystallography. *Nature* **1998**, *391*(6663), 199–203.

[60] Nogales, E.; Wolf, S. G.; Khan, I. A.; Luduena, R. F.; Downing, K. H. Structure of tubulin at 6.5 A and location of the taxol-binding site. *Nature* **1995**, *375*(6530), 424–427.

[61] Unwin, N. Refined structure of the nicotinic acetylcholine receptor at 4A resolution. *J. Mol. Biol.* **2005**, *346*(4), 967–989.

[62] Vonck, J.; von Nidda, T. K.; Meier, T.; Matthey, U.; Mills, D. J.; Kühlbrandt, W.; Dimroth, P. Molecular architecture of the undecameric rotor of a bacterial Na(+)- ATP synthase. *J. Mol. Biol.* **2002**, *321*(2), 307–316.

[63] Williams, K. A. Three-dimensional structure of the ion-coupled transport protein NhaA. *Nature* **2000**, *403*(6765), 112–115.

[64] Goswami, P.; Paulino, C.; Hizlan, D.; Vonck, J.; Yildiz, Ö.; Kühlbrandt, W. Structure of the archaeal $Na^+/H^+$ antiporter NhaP1 and functional role of transmembrane helix 1. *EMBO J.* **2011**, *30*(2), 439–449.

[65] Müller, S. A.; Engel, A. Structure and mass analysis by scanning transmission electron microscopy. *Micron* **2001**, *32*(1), 21–31.

[66] Kühlbrandt, W.; Thaler, T.; Wehrli, E. The structure of membrane crystals of the light-harvesting chlorophyll a/b protein complex. *J. Cell Biol.* **1983**, *96*(5), 1414–1424.

[67] Breyton, C. Conformational changes in the cytochrome b6f complex induced by inhibitor binding. *J. Biol. Chem.* **2000**, *275*(18), 13195–13201.

[68] Bron, P.; Lacapere, J. J.; Breyton, C.; Mosser, G. The 9 A projection structure of cytochrome b6f complex determined by electron crystallography. *J. Mol. Biol.* **1999**, *287*(1), 117–126.

[69] Mosser, G.; Breyton, C.; Olofsson, A.; Popot, J. L.; Rigaud, J. L. Projection map of cytochrome b6 f complex at 8 A resolution. *J. Biol. Chem.* **1997**, *272*(32), 20263–20268.

[70] Hovmöller, S.; Leonard, K.; Weiss, H. Membrane crystals of a subunit complex of mitochondrial cytochrome reductase containing the cytochromes b and c1. *FEBS Lett.* **1981**, *123*(1), 118–122.

[71] Lacapere, J. J.; Stokes, D. L.; Olofsson, A.; Rigaud, J. L. Two-dimensional crystallization of Ca-ATPase by detergent removal. *Biophys. J.* **1998**, *75*(3), 1319–1329.

[72] Auer, M.; Scarborough, G. A.; Kühlbrandt, W. Three-dimensional map of the plasma membrane $H^+$-ATPase in the open conformation. *Nature* **1998**, *392*(6678), 840–843.

[73] Cevc, G.; Marsh, D. *Phospholipid Bilayers: Physical Principles and Models*; John Wiley & Sons: New York, 1987.

[74] Essen, L.; Siegert, R.; Lehmann, W. D.; Oesterhelt, D. Lipid patches in membrane protein oligomers: Crystal structure of the bacteriorhodopsin-lipid complex. *Proc. Natl. Acad. Sci. USA* **1998**, *95*(20), 11673–11678.

[75] Hunte, C.; Koepke, J.; Lange, C.; Rossmanith, T.; Michel, H. Structure at 2.3 Å resolution of the cytochrome bc(1) complex from the yeast *Saccharomyces cerevisiae* co-crystallized with an antibody Fv fragment. *Struct. Fold. Des* **2000**, *8*(6), 669–684.

[76] Jordan, P.; Fromme, P.; Witt, H. T.; Klukas, O.; Saenger, W.; Krau, B. N. Three-dimensional structure of cyanobacterial photosystem I at 2.5 Å resolution. *Nature* **2001**, *411*(6840), 909–917.

[77] Gonen, T.; Cheng, Y.; Sliz, P.; Hiroaki, Y.; Fujiyoshi, Y.; Harrison, S. C.; Walz, T. Lipid-protein interactions in double-layered two-dimensional AQP0 crystals. *Nature* **2005**, *438*(7068), 633–638.

[78] Hite, R. K.; Li, Z.; Walz, T. Principles of membrane protein interactions with annular lipids deduced from aquaporin-0 2-D crystals. *EMBO J.* **2010**, *29*(10), 1652–1658.

[79] Nussberger, S.; Dorr, K.; Wang, D. N.; Kühlbrandt, W. Lipid-protein interactions in crystals of plant light-harvesting complex. *J. Mol. Biol.* **1993**, *234*(2), 347–356.

[80] Nakazato, K.; Toyoshima, C.; Enami, I.; Inoue, Y. Two-dimensional crystallization and cryo-electron microscopy of photosystem II. *J. Mol. Biol.* **1996**, *257*(2), 225–232.

[81] Rhee, K. H.; Morris, E. P.; Barber, J.; Kühlbrandt, W. Three-dimensional structure of the plant photosystem II reaction centre at 8 A resolution. *Nature* **1998**, *396*(6708), 283–286.

[82] Christie, W. W. *Lipid Analysis*; Pergamon Press: Oxford, 1982.

[83] Maslennikov, I.; Kefala, G.; Johnson, C.; Riek, R.; Choe, S.; Kwiatkowski, W. NMR spectroscopic and analytical ultracentrifuge analysis of membrane protein detergent complexes. *BMC Struct. Biol.* **2007**, *7*, 74.

[84] Maslennikov, I.; Krupa, M.; Dickson, C.; Esquivies, L.; Blain, K.; Kefala, G.; Choe, S.; Kwiatkowski, W. Characterization of protein detergent complexes by NMR, light scattering, and analytical ultracentrifugation. *J. Struct. Funct. Genomics* **2009**, *10*(1), 25–35.

[85] Ringler, P.; Heymann, B. J.; Engel, A. Two-dimensional crystallization of membrane proteins. In *Membrane Transport*; Baldwin, S. A., Ed.; Oxford University Press: Oxford, UK, 2000; pp 229–268.

[86] Mosser, G. Two-dimensional crystallogenesis of transmembrane proteins. *Micron* **2001**, *32*(5), 517–540.

[87] Heymann, J. A.; Hirai, T.; Shi, D.; Subramaniam, S. Projection structure of the bacterial oxalate transporter OxlT at 3.4A resolution. *J. Struct. Biol.* **2003**, *144*(3), 320–326.

[88] Yin, C. C.; Aldema-Ramos, M. L.; Borges-Walmsley, M. I.; Taylor, R. W.; Walmsley, A. R.; Levy, S. B.; Bullough, P. A. The quarternary molecular architecture of TetA, a secondary tetracycline transporter from *Escherichia coli*. *Mol. Microbiol.* **2000**, *38*(3), 482–492.

[89] Murata, K.; Mitsuoka, K.; Hirai, T.; Walz, T.; Agre, P.; Heymann, J. B.; Engel, A.; Fujiyoshi, Y. Structural determinants of water permeation through aquaporin-1. *Nature* **2000**, *407*(6804), 599–605.

[90] Jap, B. K.; Downing, K. H.; Walian, P. J. Structure of PhoE porin in projection at 3.5 A resolution. *J. Struct. Biol.* **1990**, *103*(1), 57–63.

[91] Walian, P. J.; Jap, B. K. Three-dimensional electron diffraction of PhoE porin to 2.8 A resolution. *J. Mol. Biol.* **1990**, *215*(3), 429–438.

[92] Dolder, M.; Engel, A.; Zulauf, M. The micelle to vesicle transition of lipids and detergents in the presence of a membrane protein: Towards a rationale for 2-D crystallization. *FEBS Lett.* **1996**, *382*(1-2), 203–208.

[93] Dolder, M.; Walz, T.; Hefti, A.; Engel, A. Human erythrocyte band 3. Solubilization and reconstitution into two-dimensional crystals. *J. Mol. Biol.* **1993**, *231*(1), 119–132.

[94] Ford, R. C.; Hefti, A.; Engel, A. Ordered arrays of the photosystem I reaction centre after reconstitution: Projections and surface reliefs of the complex at 2 nm resolution. *EMBO J.* **1990**, *9*(10), 3067–3075.

[95] Rigaud, J.-L.; Mosser, G.; Lacapere, J.-J.; Olofsson, A.; Levy, D.; Ranck, J.-L. Bio-Beads: An efficient strategy for two-dimensional crystallization of membrane proteins. *J. Struct. Biol.* **1997**, *118*(3), 226–235.

[96] Wang, D. N.; Kühlbrandt, W. High-resolution electron crystallography of light-harvesting chlorophyll a/b-protein complex in three different media. *J. Mol. Biol.* **1991**, *217*(4), 691–699.

[97] Michel, H.; Oesterhelt, D. Three-dimensional crystals of membrane proteins: Bacteriorhodopsin. *Proc. Natl. Acad. Sci. USA* **1980**, *77*(3), 1283–1285.

[98] Degrip, W. J.; Vanoostrum, J.; Bovee-Geurts, P. H. Selective detergent-extraction from mixed detergent/lipid/protein micelles, using cyclodextrin inclusion compounds: A novel generic approach for the preparation of proteoliposomes. *Biochem. J.* **1998**, *330*(Pt 2), 667–674.

[99] Turk, E.; Kim, O.; le Coutre, J.; Whitelegge, J. P.; Eskandari, S.; Lam, J. T.; Kreman, M.; Zampighi, G.; Faull, K. F.; Wright, E. M. Molecular characterization of *Vibrio parahaemolyticus* vSGLT: A model for sodium-coupled sugar cotransporters. *J. Biol. Chem.* **2000**, *275*(33), 25711–25716.

[100] Zampighi, G. A.; Kreman, M.; Lanzavecchia, S.; Turk, E.; Eskandari, S.; Zampighi, L.; Wright, E. M. Structure of functional single AQP0 channels in phospholipid membranes. *J. Mol. Biol.* **2003**, *325*(1), 201–210.

[101] Signorell, G. A.; Kaufmann, T. C.; Kukulski, W.; Engel, A.; Remigy, H. W. Controlled 2-D crystallization of membrane proteins using methyl-beta-cyclodextrin. *J. Struct. Biol.* **2007**, *157*(2), 321–328.

[102] Levy, D.; Mosser, G.; Lambert, O.; Moeck, G. S.; Bald, D.; Rigaud, J. L. Two-dimensional crystallization on lipid layer: A successful approach for membrane proteins. *J. Struct. Biol.* **1999**, *127*(1), 44–52.

[103] Kubalek, E. W.; Le Grice, S. F.; Brown, P. O. Two-dimensional crystallization of histidine-tagged, HIV-1 reverse transcriptase promoted by a novel nickel-chelating lipid. *J. Struct. Biol.* **1994**, *113*(2), 117–123.

[104] Schmitt, L.; Dietrich, C.; Tampe, R. Synthesis and characterization of chelator-lipids for reversible immobilization of engineered proteins at self-assembled lipid interfaces. *J. Am. Chem. Soc.* **1994**, *116*, 8485–8491.

[105] Lebeau, L.; Lach, F.; Venien-Bryan, C.; Renault, A.; Dietrich, J.; Jahn, T.; Palmgren, M. G.; Kühlbrandt, W.; Mioskowski, C. Two-dimensional crystallization of a membrane protein on a detergent-resistant lipid monolayer. *J. Mol. Biol.* **2001**, *308*(4), 639–647.

[106] Jahn, T.; Dietrich, J.; Andersen, B.; Leidvik, B.; Otter, C.; Briving, C.; Kühlbrandt, W.; Palmgren, M. G. Large scale expression, purification and 2-D crystallization of recombinant plant plasma membrane $H^+$-ATPase. *J. Mol. Biol.* **2001**, *309*(2), 465–476.

[107] Brenner, S.; Horne, R. W. A negative staining method for high resolution electron microscopy of viruses. *Biochim. Biophys. Acta* **1959**, *34*, 103–110.

[108] Hu, M.; Vink, M.; Kim, C.; Derr, K.; Koss, J.; D'Amico, K.; Cheng, A.; Pulokas, J.; Ubarretxena-Belandia, I.; Stokes, D. Automated electron microscopy for evaluating two-dimensional crystallization of membrane proteins. *J. Struct. Biol.* **2010**, *171*(1), 102–110.

[109] Iacovache, I.; Biasini, M.; Kowal, J.; Kukulski, W.; Chami, M.; van der Goot, F. G.; Engel, A.; Remigy, H. W. The 2-DX robot: A membrane protein 2-D crystallization Swiss Army knife. *J. Struct. Biol.* **2010**, *169*(3), 370–378.

[110] Taylor, K. A.; Glaeser, R. M. Electron diffraction of frozen, hydrated protein crystals. *Science* **1974**, *186*(4168), 1036–1037.

[111] Dubochet, J.; Adrian, M.; Chang, J.-J.; Homo, J.-C.; Lepault, J.; McDowall, A. W.; Schultz, P. Cryo-electron microscopy of vitrified specimens. *Quart. Rev. Biophys.* **1988**, *21*, 129–228.

[112] Dubochet, J.; Booy, F. P.; Freeman, R.; Jones, A. V.; Walter, C. A. Low temperature electron microscopy. *Ann. Rev. Biophys. Bioeng.* **1981**, *10*, 133–149.

[113] Vonck, J. Parameters affecting specimen flatness of two-dimensional crystals for electron crystallography. *Ultramicroscopy* **2000**, *85*(3), 123–129.

[114] Wall, J. S.; Hainfeld, J. F.; Chung, K. D. In *Films That Wet Without Glow Discharge*, 35th EMSA Meeting, Louisville, San Francisco Press: Louisville, 1985.

[115] Gyobu, N.; Tani, K.; Hiroaki, Y.; Kamegawa, A.; Mitsuoka, K.; Fujiyoshi, Y. Improved specimen preparation for cryo-electron microscopy using a symmetric carbon sandwich technique. *J. Struct. Biol.* **2004**, *146*(3), 325–333.

[116] Chou, H.-T.; Evans, J. E.; Stahlberg, H. Electron crystallography of membrane proteins. *Methods Mol. Biol.* **2007**, *369*, 331–343.

[117] Abeyrathne, P. D.; Chami, M.; Pantelic, R. S.; Goldie, K. N.; Stahlberg, H. Preparation of 2-D crystals of membrane proteins for high-resolution electron crystallography data collection. *Meth. Enzymol.* **2010**, *481*, 25–43.

[118] Baker, L. A.; Rubinstein, J. Radiation damage in electron cryomicroscopy. *Methods Enzymol.* **2010**, *481*, 371–388.

[119] Downing, K. H. Spot-scan imaging in transmission electron microscopy. *Science* **1991**, *251*(4989), 53–59.

[120] Walz, T.; Grigorieff, N. Electron crystallography of two-dimensional crystals of membrane proteins. *J. Struct. Biol.* **1998**, *121*(2), 142–161.

[121] Brink, J.; Chiu, W. Applications of a slow-scan CCD camera in protein electron crystallography. *J. Struct. Biol.* **1994**, *113*(1), 23–34.

[122] Downing, K. H.; Li, H. Accurate recording and measurement of electron diffraction data in structural and difference fourier studies of proteins. *Microsc. Microanal.* **2001**, *7*(5), 407–417.

[123] Yonekura, K.; Maki-Yonekura, S.; Namba, K. Quantitative comparison of zero-loss and conventional electron diffraction from two-dimensional and thin three-dimensional protein crystals. *Biophys. J.* **2002**, *82*(5), 2784–2797.

[124] Fujiyoshi, Y. The structural study of membrane proteins by electron crystallography. *Adv. Biophys.* **1998**, *35*, 25–80.

[125] Downing, K. H.; Hendrickson, F. M. Performance of a 2k CCD camera designed for electron crystallography at 400 kV. *Ultramicroscopy* **1999**, *75*(4), 215–233.

[126] Koeck, P. J.; Purhonen, P.; Alvang, R.; Grundberg, B.; Hebert, H. Single particle refinement in electron crystallography: A pilot study. *J. Struct. Biol.* **2007**, *160*(3), 344–352.

[127] Zeng, X.; Stahlberg, H.; Grigorieff, N. A maximum-likelihood approach to two-dimensional crystals. *J. Struct. Biol.* **2007**, *160*(3), 362–374.

[128] Gipson, B. R.; Masiel, D. J.; Browing, N. D.; Spence, J.; Mitsuoka, K.; Stahlberg, H. Automatic recovery of missing amplitudes and phases in tilt-limited electron crystallography of two-dimensional crystals. *Phys. Rev. E Stat. Nonlin. Soft Matter. Phys.* **2011**, *84*(1 Pt 1), 011916.

[129] Henderson, R.; Baldwin, J. M.; Ceska, T. A.; Zemlin, F.; Beckmann, E.; Downing, K. H. Model for the structure of bacteriorhodopsin based on high-resolution electron cryo-microscopy. *J. Mol. Biol.* **1990**, *213*(4), 899–929.

[130] Philippsen, A.; Engel, H. A.; Engel, A. The contrast-imaging function for tilted specimens. *Ultramicroscopy* **2007**, *107*(2–3), 202–212.

[131] Henderson, R.; Unwin, P. N. Three-dimensional model of purple membrane obtained by electron microscopy. *Nature* **1975**, *257*(5521), 28–32.

[132] Amos, L. A.; Henderson, R.; Unwin, P. N. Three-dimensional structure determination by electron microscopy of two-dimensional crystals. *Prog. Biophys. Mol. Biol.* **1982**, *39*(3), 183–231.

[133] Henderson, R.; Baldwin, J. M.; Downing, K. H.; Lepault, J.; Zemlin, F. Structure of purple membrane from *Halobacterium halobium*: Recording, measurement and evaluation of electron micrographs at 3.5 Å resolution. *Ultramicroscopy* **1986**, *19*, 147–178.

[134] Lawson, C. L.; Baker, M. L.; Best, C.; Bi, C.; Dougherty, M.; Feng, P.; van Ginkel, G.; Devkota, B.; Lagerstedt, I.; Ludtke, S. J.; Newman, R. H.; Oldfield, T. J.; Rees, I.; Sahni, G.; Sala, R.; Velankar, S.; Warren, J.; Westbrook, J. D.; Henrick, K.; Kleywegt, G. J.; Berman, H. M.; Chiu, W. EMDataBank.org: Unified data resource for CryoEM. *Nucleic Acids Res.* **2011**, *39*(Database issue), D456–D464.

[135] Schenk, A. D.; Castano-Diez, D.; Gipson, B.; Arheit, M.; Zeng, X.; Stahlberg, H. 3-D reconstruction from 2-D crystal image and diffraction data. *Meth. Enzymol.* **2010**, *482*, 101–129.

[136] Crowther, R.; Henderson, R.; Smith, J. MRC image processing programs. *J. Struct. Biol.* **1996**, *116*(1), 9–16.

[137] Schmid, M. F.; Dargahi, R.; Tam, M. W. SPECTRA: A system for processing electron images of crystals. *Ultramicroscopy* **1993**, *48*(3), 251–264.

[138] Hardt, S.; Wang, B.; Schmid, M. F. A brief description of I.C.E.: The integrated crystallographic environment. *J. Struct. Biol.* **1996**, *116*(1), 68–70.

[139] Hovmöller, S.CRISP Crystallographic image processing on a personal computer. *Ultramicroscopy* **1992**, *41*, 121–135.

[140] Zou, X. D.; Hovmoller, A.; Hovmoller, S. TRICE – a program for reconstructing 3-D reciprocal space and determining unit-cell parameters. *Ultramicroscopy* **2004**, *98*(2-4), 187–193.

[141] Zou, X. D.; Sukharev, Y.; Hovmöller, S. Quantitative electron diffraction – new features in the program system ELD. *Ultramicroscopy* **1993**, *52*, 436–444.

[142] Gipson, B.; Zeng, X.; Stahlberg, H. 2dx_merge: Data management and merging for 2-D crystal images. *J. Struct. Biol.* **2007**, *160*(3), 375–384.

[143] Gipson, B.; Zeng, X.; Stahlberg, H. 2dx – Automated 3-D structure reconstruction from 2-D crystal data. *Microsc. Microanal.* **2008**, *14*(Suppl. 2), 1290–1291.

[144] Gipson, B.; Zeng, X.; Zhang, Z.; Stahlberg, H. 2dx – User-friendly image processing for 2-D crystals. *J. Struct. Biol.* **2007**, *157*(1), 64–72.

[145] Zeng, X.; Gipson, B.; Zheng, Z. Y.; Renault, L.; Stahlberg, H. Automatic lattice determination for two-dimensional crystal images. *J. Struct. Biol.* **2007**, *160*(3), 353–361.

[146] Mitsuoka, K.; Hirai, T.; Murata, K.; Miyazawa, A.; Kidera, A.; Kimura, Y.; Fujiyoshi, Y. The structure of bacteriorhodopsin at 3.0 Å resolution based on electron crystallography: Implication of the charge distribution. *J. Mol. Biol.* **1999**, *286*(3), 861–882.

[147] Philippsen, A.; Schenk, A. D.; Signorell, G. A.; Mariani, V.; Berneche, S.; Engel, A. Collaborative EM image processing with the IPLT image processing library and toolbox. *J. Struct. Biol.* **2007**, *157*(1), 28–37.

[148] Philippsen, A.; Schenk, A. D.; Stahlberg, H.; Engel, A. Iplt – image processing library and toolkit for the electron microscopy community. *J. Struct. Biol.* **2003**, *144*(1-2), 4–12.

[149] Kühlbrandt, W.; Wang, D. N.; Fujiyoshi, Y. Atomic model of plant light-harvesting complex by electron crystallography. *Nature* **1994**, *367*(6464), 614–621.

[150] Ren, G.; Reddy, V. S.; Cheng, A.; Melnyk, P.; Mitra, A. K. Visualization of a water-selective pore by electron crystallography in vitreous ice. *Proc. Natl. Acad. Sci. USA* **2001**, *98*(4), 1398–1403.

[151] Miyazawa, A.; Fujiyoshi, Y.; Unwin, N. Structure and gating mechanism of the acetylcholine receptor pore. *Nature* **2003**, *424*(6943), 949–955.

[152] Gonen, T.; Sliz, P.; Kistler, J.; Cheng, Y.; Walz, T. Aquaporin-0 membrane junctions reveal the structure of a closed water pore. *Nature* **2004**, *429*(6988), 193–197.

[153] Hiroaki, Y.; Tani, K.; Kamegawa, A.; Gyobu, N.; Nishikawa, K.; Suzuki, H.; Walz, T.; Sasaki, S.; Mitsuoka, K.; Kimura, K.; Mizoguchi, A.; Fujiyoshi, Y. Implications of the aquaporin-4 structure on array formation and cell adhesion. *J. Mol. Biol.* **2006**, *355*(4), 628–639.

[154] Holm, P. J.; Bhakat, P.; Jegerschold, C.; Gyobu, N.; Mitsuoka, K.; Fujiyoshi, Y.; Morgenstern, R.; Hebert, H. Structural basis for detoxification and oxidative stress protection in membranes. *J. Mol. Biol.* **2006**, *360*(5), 934–945.

[155] Jegerschold, C.; Pawelzik, S. C.; Purhonen, P.; Bhakat, P.; Gheorghe, K. R.; Gyobu, N.; Mitsuoka, K.; Morgenstern, R.; Jakobsson, P. J.; Hebert, H. Structural basis for induced formation of the inflammatory mediator prostaglandin E2. *Proc. Natl. Acad. Sci. USA* **2008**, *105*(32), 11110–11115.

[156] Abe, K.; Tani, K.; Fujiyoshi, Y. Conformational rearrangement of gastric H(+),K(+)-ATPase induced by an acid suppressant. *Nat. Commun.* **2011**, *2*(1), 155.

[157] Henderson, R. Realizing the potential of electron cryo-microscopy. *Quart. Rev. Biophys.* **2004**, *37*(1), 3–13.

[158] Vinothkumar, K. R.; Henderson, R. Structures of membrane proteins. *Quart. Rev. Biophys.* **2010**, *43*(1), 65–158.

[159] Fleishman, S. J.; Harrington, S. E.; Enosh, A.; Halperin, D.; Tate, C. G.; Ben-Tal, N. Quasi-symmetry in the cryo-EM structure of EmrE provides the key to modeling its transmembrane domain. *J. Mol. Biol.* **2006**, *364*(1), 54–67.

[160] Conroy, M. J.; Jamieson, S. J.; Blakey, D.; Kaufmann, T.; Engel, A.; Fotiadis, D.; Merrick, M.; Bullough, P. A. Electron and atomic force microscopy of the trimeric ammonium transporter AmtB. *EMBO Rep.* **2004**, *5*(12), 1153–1158.

[161] Oling, F.; Santos, J. S.; Govorukhina, N.; Mazeres-Dubut, C.; Bergsma-Schutter, W.; Oostergetel, G.; Keegstra, W.; Lambert, O.; Lewit-Bentley, A.; Brisson, A. Structure of membrane-bound annexin A5 trimers: A hybrid cryo-EM – X-ray crystallography study. *J. Mol. Biol.* **2000**, *304*(4), 561–573.

[162] Saint, N.; Lacapere, J. J.; Gu, L. Q.; Ghazi, A.; Martinac, B.; Rigaud, J. L. A hexameric transmembrane pore revealed by two-dimensional crystallization of the large mechanosensitive ion channel (MscL) of *Escherichia coli*. *J. Biol. Chem.* **1998**, *273*(24), 14667–14670.

[163] Hoogenboom, B. W.; Suda, K.; Engel, A.; Fotiadis, D. The supramolecular assemblies of voltage-dependent anion channels in the native membrane. *J. Mol. Biol.* **2007**, *370*(2), 246–255.

[164] Li, H. L.; Sui, H. X.; Ghanshani, S.; Lee, S. Walian, P. J.; Wu, C. L.; Chandy, K. G.; Jap, B. K. Two-dimensional crystallization and projection structure of KcsA potassium channel. *J. Mol. Biol.* **1998**, *282*(2), 211–216.

[165] Kuo, A.; Domene, C.; Johnson, L. N.; Doyle, D. A.; Venien-Bryan, C. Two different conformational states of the KirBac3.1 potassium channel revealed by electron crystallography. *Structure* **2005**, *13*(10), 1463–1472.

[166] Chiu, P. L.; Pagel, M. D.; Evans, J.; Chou, H. T.; Zeng, X.; Gipson, B.; Stahlberg, H.; Nimigean, C. M. The structure of the prokaryotic cyclic nucleotide-modulated potassium channel MloK1 at 16 A resolution. *Structure* **2007**, *15*(9), 1053–1064.

[167] Mindell, J. A.; Maduke, M.; Miller, C.; Grigorieff, N. Projection structure of a CIC-type chloride channel at 6.5 A resolution. *Nature* **2001**, *409*(6817), 219–223.

[168] Appel, M.; Hizlan, D.; Vinothkumar, K. R.; Ziegler, C.; Kühlbrandt, W. Conformations of NhaA, the Na/H exchanger from *Escherichia coli*, in the pH-activated and ion-translocating states. *J. Mol. Biol.* **2009**, *386*(2), 351–365.

[169] Vinothkumar, K. R.; Smits, S. H.; Kühlbrandt, W. pH-induced structural change in a sodium/proton antiporter from *Methanococcus jannaschii*. *EMBO J.* **2005**, *24*(15), 2720–2729.

[170] Boekema, E. J.; Stuart, M.; Koning, R. I.; Keegstra, W.; Brisson, A.; Verheij, H. M.; Dekker, N.A 7.4-A projection structure of outer membrane phospholipase A from *Escherichia coli* by electron crystallography. *J. Struct. Biol.* **1998**, *123*(1), 67–71.

[171] Zhuang, J.; Prive, G. G.; Werner, G. E.; Ringler, P.; Kaback, H. R.; Engel, A. Two-dimensional crystallization of *Escherichia coli* lactose permease. *J. Struct. Biol.* **1999**, *125*(1), 63–75.

[172] Heymann, J. A.; Sarker, R.; Hirai, T.; Shi, D.; Milne, J. L.; Maloney, P. C.; Subramaniam, S. Projection structure and molecular architecture of OxlT, a bacterial membrane transporter. *EMBO J.* **2001**, *20*(16), 4408–4413.

[173] Hirai, T.; Heymann, J. A.; Shi, D.; Sarker, R.; Maloney, P. C.; Subramaniam, S. Three-dimensional structure of a bacterial oxalate transporter. *Nat. Struct. Biol.* **2002**, *9*(8), 597–600.

[174] Ziegler, C.; Morbach, S.; Schiller, D.; Kramer, R.; Tziatzios, C.; Schubert, D.; Kühlbrandt, W. Projection structure and oligomeric state of the osmoregulated sodium/glycine betaine symporter BetP of *Corynebacterium glutamicum*. *J. Mol. Biol.* **2004**, *337*(5), 1137–1147.

[175] Aller, S. G.; Unger, V. M. Projection structure of the human copper transporter CTR1 at 6-A resolution reveals a compact trimer with a novel channel-like architecture. *Proc. Natl. Acad. Sci. USA* **2006**, *103*(10), 3627–3632.

[176] De Feo, C. J.; Aller, S. G.; Siluvai, G. S.; Blackburn, N. J.; Unger, V. M. Three-dimensional structure of the human copper transporter hCTR1. *Proc. Natl. Acad. Sci. USA* **2009**, *106*(11), 4237–4242.

[177] Hacksell, I.; Rigaud, J. L.; Purhonen, P.; Pourcher, T.; Hebert, H.; Leblanc, G. Projection structure at 8 Å resolution of the melibiose permease, an Na-sugar co-transporter from *Escherichia coli*. *EMBO J.* **2002**, *21*(14), 3569–3574.
[178] Zheng, H.; Taraska, J.; Merz, A. J.; Gonen, T. The prototypical $H^+$/galactose symporter GalP assembles into functional trimers. *J. Mol. Biol.* **2010**, *396*(3), 593–601.
[179] Jeckelmann, J. M.; Harder, D.; Mari, S. A.; Meury, M.; Ucurum, Z.; Müller, D. J.; Erni, B.; Fotiadis, D. Structure and function of the glucose PTS transporter from. *Escherichia coli*. *J. Struct. Biol.* **2011**, *176*(3), 395–403.
[180] Casagrande, F.; Ratera, M.; Schenk, A. D.; Chami, M.; Valencia, E.; Lopez, J. M.; Torrents, D.; Engel, A.; Palacin, M.; Fotiadis, D. Projection structure of a member of the amino acid/polyamine/organocation transporter superfamily. *J. Biol. Chem.* **2008**, *283*(48), 33240–33248.
[181] Ward, A.; Mulligan, S.; Carragher, B.; Chang, G.; Milligan, R. A. Nucleotide dependent packing differences in helical crystals of the ABC transporter MsbA. *J. Struct. Biol.* **2009**, *165*(3), 169–175.
[182] Tate, C. G.; Kunji, E. R.; Lebendiker, M.; Schuldiner, S. The projection structure of EmrE, a proton-linked multidrug transporter from *Escherichia coli*, at 7 A resolution. *EMBO J.* **2001**, *20*(1-2), 77–81.
[183] Tate, C. G.; Ubarretxena-Belandia, I.; Baldwin, J. M. Conformational changes in the multidrug transporter EmrE associated with substrate binding. *J. Mol. Biol.* **2003**, *332*(1), 229–242.
[184] Ubarretxena-Belandia, I.; Baldwin, J. M.; Schuldiner, S.; Tate, C. G. Three-dimensional structure of the bacterial multidrug transporter EmrE shows it is an asymmetric homodimer. *EMBO J.* **2003**, *22*(23), 6175–6181.
[185] Korkhov, V. M.; Tate, C. G. Electron crystallography reveals plasticity within the drug binding site of the small multidrug transporter EmrE. *J. Mol. Biol* **2008**, *377*(4), 1094–1103.
[186] Orelle, C.; Gubellini, F.; Durand, A.; Marco, S.; Levy, D.; Gros, P.; Di Pietro, A.; Jault, J. M. Conformational change induced by ATP binding in the multidrug ATP-binding cassette transporter BmrA. *Biochemistry* **2008**, *47*(8), 2404–2412.
[187] Lee, J. Y.; Urbatsch, I. L.; Senior, A. E.; Wilkens, S. Projection structure of P-glycoprotein by electron microscopy. Evidence for a closed conformation of the nucleotide binding domains. *J. Biol. Chem.* **2002**, *277*(42), 40125–40131.
[188] Wang, D. N.; Sarabia, V. E.; Reithmeier, R. A.; Kühlbrandt, W. Three-dimensional map of the dimeric membrane domain of the human erythrocyte anion exchanger, Band 3. *EMBO J.* **1994**, *13*(14), 3230–3235.
[189] Yamaguchi, T.; Ikeda, Y.; Abe, Y.; Kuma, H.; Kang, D.; Hamasaki, N.; Hirai, T. Structure of the membrane domain of human erythrocyte anion exchanger 1 revealed by electron crystallography. *J. Mol. Biol.* **2010**, *397*(1), 179–189.
[190] Hasler, L.; Walz, T.; Tittmann, P.; Gross, H.; Kistler, J.; Engel, A. Purified lens major intrinsic protein (MIP) forms highly ordered tetragonal two-dimensional arrays by reconstitution. *J. Mol. Biol.* **1998**, *279*(4), 855–864.
[191] Gonen, T.; Cheng, Y.; Kistler, J.; Walz, T. Aquaporin-0 membrane junctions form upon proteolytic cleavage. *J. Mol. Biol.* **2004**, *342*(4), 1337–1345.
[192] Walz, T.; Hirai, T.; Murata, K.; Heymann, J. B.; Mitsuoka, K.; Fujiyoshi, Y.; Smith, B. L.; Agre, P.; Engel, A. The three-dimensional structure of Aquaporin-1. *Nature* **1997**, *387*(6633), 624–627.
[193] Ren, G.; Cheng, A.; Reddy, V.; Melnyk, P.; Mitra, A. K. Three-dimensional fold of the human AQP1 water channel determined at 4 A resolution by electron crystallography of two-dimensional crystals embedded in ice. *J. Mol. Biol.* **2000**, *301*(2), 369–387.
[194] Jap, B. K.; Li, H. Structure of the osmo-regulated $H_2O$-channel, AQP-CHIP, in projection at 3.5 A resolution. *J. Mol. Biol.* **1995**, *251*(3), 413–420.
[195] de Groot, B. L.; Engel, A.; Grubmüller, H. A refined structure of human aquaporin-1. *FEBS Lett.* **2001**, *504*(3), 206–211.
[196] Schenk, A. D.; Werten, P. J.; Scheuring, S.; de Groot, B. L.; Müller, S. A.; Stahlberg, H.; Philippsen, A.; Engel, A. The 4.5 Å structure of human AQP2. *J. Mol. Biol.* **2005**, *350*(2), 278–289.
[197] Tani, K.; Mitsuma, T.; Hiroaki, Y.; Kamegawa, A.; Nishikawa, K.; Tanimura, Y.; Fujiyoshi, Y. Mechanism of aquaporin-4's fast and highly selective water conduction and proton exclusion. *J. Mol. Biol.* **2009**, *389*(4), 694–706.
[198] Mitsuma, T.; Tani, K.; Hiroaki, Y.; Kamegawa, A.; Suzuki, H.; Hibino, H.; Kurachi, Y.; Fujiyoshi, Y. Influence of the cytoplasmic domains of aquaporin-4 on water conduction and array formation. *J. Mol. Biol.* **2010**, *402*(4), 669–681.
[199] Ringler, P.; Borgnia, M. J.; Stahlberg, H.; Maloney, P. C.; Agre, P.; Engel, A. Structure of the water channel AqpZ from *Escherichia coli* revealed by electron crystallography. *J. Mol. Biol.* **1999**, *291*(5), 1181–1190.
[200] Kukulski, W.; Schenk, A. D.; Johanson, U.; Braun, T.; de Groot, B. L.; Fotiadis, D.; Kjellbom, P.; Engel, A. The 5 Å structure of heterologously expressed plant aquaporin SoPIP2;1. *J. Mol. Biol.* **2005**, *350*(4), 611–616.
[201] Fotiadis, D.; Jeno, P.; Mini, T.; Wirtz, S.; Müller, S. A.; Fraysse, L.; Kjellbom, P.; Engel, A. Structural characterization of two aquaporins isolated from native spinach leaf plasma membranes. *J. Biol. Chem.* **2001**, *276*(3), 1707–1714.
[202] Daniels, M. J.; Chrispeels, M. J.; Yeager, M. Projection structure of a plant vacuole membrane aquaporin by electron cryo-crystallography. *J. Mol. Biol.* **1999**, *294*(5), 1337–1349.
[203] Stahlberg, H.; Braun, T.; de Groot, B.; Philippsen, A.; Borgnia, M. J.; Agre, P.; Kühlbrandt, W.; Engel, A. The 6.9 Å structure of GlpF: A basis for homology modeling of the glycerol channel from *Escherichia coli*. *J. Struct. Biol.* **2000**, *132*(2), 133–141.
[204] Braun, T.; Philippsen, A.; Wirtz, S.; Borgnia, M. J.; Agre, P.; Kühlbrandt, W.; Engel, A.; Stahlberg, H. The 3.7 A projection map of the glycerol facilitator GlpF: A variant of the aquaporin tetramer. *EMBO Rep.* **2000**, *1*(2), 183–189.
[205] Brisson, A.; Unwin, P. N. Quaternary structure of the acetylcholine receptor. *Nature* **1985**, *315*(6019), 474–477.
[206] Toyoshima, C.; Unwin, N. Ion channel of acetylcholine receptor reconstructed from images of postsynaptic membranes. *Nature* **1988**, *336*(6196), 247–250.
[207] Unwin, N. Acetylcholine receptor channel imaged in the open state. *Nature* **1995**, *373*(6509), 37–43.
[208] Yin, C. C.; Han, H.; Wei, R.; Lai, F. A. Two-dimensional crystallization of the ryanodine receptor $Ca^{2+}$ release channel on lipid membranes. *J. Struct. Biol.* **2005**, *149*(2), 219–224.
[209] Korkhov, V. M.; Sachse, C.; Short, J. M.; Tate, C. G. Three-dimensional structure of TspO by electron cryomicroscopy of helical crystals. *Structure* **2010**, *18*(6), 677–687.
[210] Levy, D.; Chami, M.; Rigaud, J. L. Two-dimensional crystallization of membrane proteins: The lipid layer strategy. *FEBS Lett.* **2001**, *504*(3), 187–193.
[211] Schmidt-Krey, I.; Haase, W.; Mutucumarana, V.; Stafford, D. W.; Kühlbrandt, W. Two-dimensional crystallization of human vitamin K-dependent gamma-glutamyl carboxylase. *J. Struct. Biol.* **2007**, *157*(2), 437–442.
[212] Leifer, D.; Henderson, R. Three-dimensional structure of orthorhombic purple membrane at 6.5 A resolution. *J. Mol. Biol.* **1983**, *163*(3), 451–466.
[213] Tsygannik, I. N.; Baldwin, J. M. Three-dimensional structure of deoxycholate-treated purple membrane at 6 Å resolution and molecular averaging of three crystal forms of bacteriorhodopsin. *Eur. Biophys. J.* **1987**, *14*(5), 263–272.
[214] Grigorieff, N.; Ceska, T. A.; Downing, K. H.; Baldwin, J. M.; Henderson, R. Electron-crystallographic refinement of the structure of bacteriorhodopsin. *J. Mol. Biol.* **1996**, *259*(3), 393–421.
[215] Kimura, Y.; Vassylyev, D. G.; Miyazawa, A.; Kidera, A.; Matsushima, M.; Mitsuoka, K.; Murata, K.; Hirai, T.; Fujiyoshi, Y. Surface of bacteriorhodopsin revealed by high-resolution electron crystallography. *Nature* **1997**, *389*(6647), 206–211.
[216] Bullough, P. A.; Henderson, R. The projection structure of the low temperature K intermediate of the bacteriorhodopsin photocycle determined by electron diffraction. *J. Mol. Biol.* **1999**, *286*(5), 1663–1671.
[217] Subramaniam, S.; Lindahl, M.; Bullough, P.; Faruqi, A. R.; Tittor, J.; Oesterhelt, D.; Brown, L.; Lanyi, J.; Henderson, R. Protein conformational changes in the bacteriorhodopsin photocycle. *J. Mol. Biol.* **1999**, *287*(1), 145–161.
[218] Subramaniam, S.; Henderson, R. Molecular mechanism of vectorial proton translocation by bacteriorhodopsin. *Nature* **2000**, *406*(6796), 653–657.
[219] Vonck, J. Structure of the bacteriorhodopsin mutant F219L N intermediate revealed by electron crystallography. *EMBO J.* **2000**, *19*(10), 2152–2160.
[220] Baldwin, J.; Henderson, R. Measurement and evaluation of electron diffraction patterns from two-dimensional crystals. *Ultramicroscopy* **1984**, *14*(4), 319–335.
[221] Havelka, W. A.; Henderson, R.; Heymann, J. A.; Oesterhelt, D. Projection structure of halorhodopsin from *Halobacterium halobium* at 6 A resolution obtained by electron cryo-microscopy. *J. Mol. Biol.* **1993**, *234*(3), 837–846.
[222] Havelka, W. A.; Henderson, R.; Oesterhelt, D. Three-dimensional structure of halorhodopsin at 7 A resolution. *J. Mol. Biol.* **1995**, *247*(4), 726–738.
[223] Kunji, E. R.; von Gronau, S.; Oesterhelt, D.; Henderson, R. The three-dimensional structure of halorhodopsin to 5 Å by electron crystallography: A new unbending procedure for two-dimensional crystals by using a global reference structure. *Proc. Natl. Acad. Sci. USA* **2000**, *97*(9), 4637–4642.
[224] Ruprecht, J. J.; Mielke, T.; Vogel, R.; Villa, C.; Schertler, G. F. Electron crystallography reveals the structure of metarhodopsin I. *EMBO J.* **2004**, *23*(18), 3609–3620.

[225] Schertler, G. F.; Villa, C.; Henderson, R. Projection structure of rhodopsin. *Nature* **1993**, *362*(6422), 770–772.
[226] Unger, V. M.; Schertler, G. F. Low resolution structure of bovine rhodopsin determined by electron cryo-microscopy. *Biophys. J.* **1995**, *68*(5), 1776–1786.
[227] Krebs, A.; Villa, C.; Edwards, P. C.; Schertler, G. F. Characterisation of an improved two-dimensional p22121 crystal from bovine rhodopsin. *J. Mol. Biol.* **1998**, *282*(5), 991–1003.
[228] Krebs, A.; Edwards, P. C.; Villa, C.; Li, J.; Schertler, G. F. The three-dimensional structure of bovine rhodopsin determined by electron cryomicroscopy. *J. Biol. Chem.* **2003**, *278*(50), 50217–50225.
[229] Davies, A.; Schertler, G. F.; Gowen, B. E.; Saibil, H. R. Projection structure of an invertebrate rhodopsin. *J. Struct. Biol.* **1996**, *117*(1), 36–44.
[230] Davies, A.; Gowen, B. E.; Krebs, A. M.; Schertler, G. F.; Saibil, H. R. Three-dimensional structure of an invertebrate rhodopsin and basis for ordered alignment in the photoreceptor membrane. *J. Mol. Biol.* **2001**, *314*(3), 455–463.
[231] Schertler, G. F.; Hargrave, P. A. Preparation and analysis of two-dimensional crystals of rhodopsin. *Meth. Enzymol.* **2000**, *315*, 91–107.
[232] Kunji, E. R.; Spudich, E. N.; Grisshammer, R.; Henderson, R.; Spudich, J. L. Electron crystallographic analysis of two-dimensional crystals of sensory rhodopsin II: A 6.9 A projection structure. *J. Mol. Biol.* **2001**, *308*(2), 279–293.
[233] Müller, M.; Bamann, C.; Bamberg, E.; Kühlbrandt, W. Projection structure of channelrodopsin-2 at 6A resolution electron crystallography. *J. Mol. Biol.* **2011**, *414*(1), 86–95.
[234] Breyton, C.; Haase, W.; Rapoport, T. A.; Kühlbrandt, W.; Collinson, I. Three-dimensional structure of the bacterial protein-translocation complex SecYEG. *Nature* **2002**, *418*(6898), 662–665.
[235] Lotz, M.; Haase, W.; Kühlbrandt, W.; Collinson, I. Projection structure of yidC: A conserved mediator of membrane protein assembly. *J. Mol. Biol.* **2008**, *375*(4), 901–907.
[236] Hebert, H.; Schmidt-Krey, I.; Morgenstern, R.; Murata, K.; Hirai, T.; Mitsuoka, K.; Fujiyoshi, Y. The 3.0 A projection structure of microsomal glutathione transferase as determined by electron crystallography of p 21212 two-dimensional crystals. *J. Mol. Biol.* **1997**, *271*(5), 751–758.
[237] Schmidt-Krey, I.; Lundqvist, G.; Morgenstern, R.; Hebert, H. Parameters for the two-dimensional crystallization of the membrane protein microsomal glutathione transferase. *J. Struct. Biol.* **1998**, *123*(2), 87–96.
[238] Schmidt-Krey, I.; Murata, K.; Hirai, T.; Mitsuoka, K.; Cheng, Y.; Morgenstern, R.; Fujiyoshi, Y.; Hebert, H. The projection structure of the membrane protein microsomal glutathione transferase at 3 A resolution as determined from two-dimensional hexagonal crystals. *J. Mol. Biol.* **1999**, *288*(2), 243–253.
[239] Schmidt-Krey, I.; Mitsuoka, K.; Hirai, T.; Murata, K.; Cheng, Y.; Fujiyoshi, Y.; Morgenstern, R.; Hebert, H. The three-dimensional map of microsomal glutathione transferase 1 at 6 A resolution. *EMBO J.* **2000**, *19*(23), 6311–6316.
[240] Holm, P. J.; Morgenstern, R.; Hebert, H. The 3-D structure of microsomal glutathione transferase 1 at 6 A resolution as determined by electron crystallography of p22(1)2(1) crystals. *Biochim. Biophys. Acta* **2002**, *1594*(2), 276–285.
[241] Schmidt-Krey, I.; Kanaoka, Y.; Mills, D. J.; Irikura, D.; Haase, W.; Lam, B. K.; Austen, K. F.; Kühlbrandt, W. Human leukotriene C(4) synthase at 4.5 A resolution in projection. *Structure* **2004**, *12*(11), 2009–2014.
[242] Zhao, G.; Johnson, M. C.; Schnell, J. R.; Kanaoka, Y.; Haase, W.; Irikura, D.; Lam, B. K.; Schmidt-Krey, I. Two-dimensional crystallization conditions of human leukotriene C4 synthase requiring adjustment of a particularly large combination of specific parameters. *J. Struct. Biol.* **2010**, *169*(3), 450–454.
[243] Miller, K. R.; Jacob, J. S. Two-dimensional crystals formed from photosynthetic reaction centers. *J. Cell Biol.* **1983**, *97*(4), 1266–1270.
[244] Karrasch, S.; Bullough, P. A.; Ghosh, R. The 8.5 A projection map of the light-harvesting complex I from Rhodospirillum rubrum reveals a ring composed of 16 subunits. *EMBO J.* **1995**, *14*(4), 631–638.
[245] Walz, T.; Jamieson, S. J.; Bowers, C. M.; Bullough, P. A.; Hunter, C. N. Projection structures of three photosynthetic complexes from Rhodobacter sphaeroides: LH2 at 6 A, LH1 and RC-LH1 at 25 A. *J. Mol. Biol.* **1998**, *282*(4), 833–845.
[246] Stahlberg, H.; Dubochet, J.; Vogel, H.; Ghosh, R. The reaction centre of the photounit of *Rhodospirillum rubrum* is anchored to the light-harvesting complex with four-fold rotational disorder. *Photosynth. Res.* **1998**, *55*, 363–368.
[247] Ikeda-Yamasaki, I.; Odahara, T.; Mitsuoka, K.; Fujiyoshi, Y.; Murata, K. Projection map of the reaction center-light harvesting 1 complex from *Rhodopseudomonas viridis* at 10 A resolution. *FEBS Lett.* **1998**, *425*(3), 505–508.
[248] Jamieson, S. J.; Wang, P.; Qian, P.; Kirkland, J. Y.; Conroy, M. J.; Hunter, C. N.; Bullough, P. A. Projection structure of the photosynthetic reaction centre-antenna complex of *Rhodospirillum rubrum* at 8.5 A resolution. *EMBO J.* **2002**, *21*(15), 3927–3935.
[249] Qian, P.; Addlesee, H. A.; Ruban, A. V.; Wang, P.; Bullough, P. A.; Hunter, C. N. A reaction center-light-harvesting 1 complex (RC-LH1) from a *Rhodospirillum rubrum* mutant with altered esterifying pigments: Characterization by optical spectroscopy and cryo-electron microscopy. *J. Biol. Chem.* **2003**, *278*(26), 23678–23685.
[250] Scheuring, S.; Francia, F.; Busselez, J.; Melandri, B. A.; Rigaud, J. L.; Levy, D. Structural role of PufX in the dimerization of the photosynthetic core complex of *Rhodobacter sphaeroides*. *J. Biol. Chem.* **2004**, *279*(5), 3620–3626.
[251] Qian, P.; Hunter, C. N.; Bullough, P. A. The 8.5A projection structure of the core RC-LH1-PufX dimer of *Rhodobacter sphaeroides*. *J. Mol. Biol.* **2005**, *349*(5), 948–960.
[252] Siebert, C. A.; Qian, P.; Fotiadis, D.; Engel, A.; Hunter, C. N.; Bullough, P. A. Molecular architecture of photosynthetic membranes in *Rhodobacter sphaeroides*: The role of PufX. *EMBO J.* **2004**, *23*(4), 690–700.
[253] Montoya, G.; Cyrklaff, M.; Sinning, I. Two-dimensional crystallization and preliminary structure analysis of light harvesting II (B800-850) complex from the purple bacterium *Rhodovulum sulfidophilum*. *J. Mol. Biol.* **1995**, *250*(1), 1–10.
[254] Savage, H.; Cyrklaff, M.; Montoya, G.; Kühlbrandt, W.; Sinning, I. Two-dimensional structure of light harvesting complex II (LHII) from the purple bacterium *Rhodovulum sulfidophilum* and comparison with LHII from *Rhodopseudomonas acidophila*. *Structure* **1996**, *4*(3), 243–252.
[255] Ranck, J.; Ruiz, T.; Pehau-Arnaudet, G.; Arnoux, B.; Reiss-Husson, F. Two-dimensional structure of the native light-harvesting complex LH2 from *Rubrivivax gelatinosus* and of a truncated form. *Biochim. Biophys. Acta* **2001**, *1506*(1), 67–78.
[256] Böttcher, B.; Graber, P.; Boekema, E. J. The structure of photosystem I from the thermophilic cyanobacterium *Synechococcus* sp. determined by electron microscopy of two-dimensional crystals. *Biochim. Biophys. Acta* **1992**, *1100*(2), 125–136.
[257] Tsiotis, G.; Walz, T.; Spyridaki, A.; Lustig, A.; Engel, A.; Ghanotakis, D. Tubular crystals of a photosystem II core complex. *J. Mol. Biol.* **1996**, *259*(2), 241–248.
[258] Hankamer, B.; Morris, E. P.; Barber, J. Revealing the structure of the oxygen-evolving core dimer of photosystem II by cryoelectron crystallography. *Nat. Struct. Biol.* **1999**, *6*(6), 560–564.
[259] da Fonseca, P.; Morris, E. P.; Hankamer, B.; Barber, J. Electron crystallographic study of photosystem II of the cyanobacterium *Synechococcus elongatus*. *Biochemistry* **2002**, *41*(16), 5163–5167.
[260] Morosinotto, T.; Bassi, R.; Frigerio, S.; Finazzi, G.; Morris, E.; Barber, J. Biochemical and structural analyses of a higher plant photosystem II supercomplex of a photosystem I-less mutant of barley. Consequences of a chronic over-reduction of the plastoquinone pool. *FEBS J.* **2006**, *273*(20), 4616–4630.
[261] Kühlbrandt, W.; Downing, K. H. Two-dimensional structure of plant light-harvesting complex at 3.7 A [corrected] resolution by electron crystallography. *J. Mol. Biol.* **1989**, *207*(4), 823–828.
[262] Kühlbrandt, W.; Wang, D. N. Three-dimensional structure of plant light-harvesting complex determined by electron crystallography. *Nature* **1991**, *350*(6314), 130–134.
[263] Oling, F.; Boekema, E. J.; Ortiz de Zarate, I.; Visschers, R.; van Grondelle, R.; Keegstra, W.; Brisson, A.; Picorel, R. Two-dimensional crystals of LH2 light-harvesting complexes from *Ectothiorhodospira* sp. and *Rhodobacter capsulatus* investigated by electron microscopy. *Biochim. Biophys. Acta* **1996**, *1273*(1), 44–50.
[264] Akiba, T.; Toyoshima, C.; Matsunaga, T.; Kawamoto, M.; Kubota, T.; Fukuyama, K.; Namba, K.; Matsubara, H. Three-dimensional structure of bovine cytochrome bc1 complex by electron cryomicroscopy and helical image reconstruction. *Nat. Struct. Biol.* **1996**, *3*(6), 553–561.
[265] Gohlke, U.; Warne, A.; Saraste, M. Projection structure of the cytochrome bo ubiquinol oxidase from *Escherichia coli* at 6 A resolution. *EMBO J* **1997**, *16*(6), 1181–1188.
[266] Frey, T. G.; Chan, S. H.; Schatz, G. Structure and orientation of cytochrome c oxidase in crystalline membranes. Studies by electron microscopy and by labeling with subunit-specific antibodies. *J. Biol. Chem.* **1978**, *253*(12), 4389–4395.

[267] Warne, A.; Wang, D. N.; Saraste, M. Purification and two-dimensional crystallization of bacterial cytochrome oxidases. *Eur. J. Biochem.* **1995**, *234*(2), 443–451.
[268] Wingfield, P.; Arad, T.; Leonard, K.; Weiss, H. Membrane crystals of ubiquinone:cytochrome c reductase from Neurospora mitochondria. *Nature* **1979**, *280*(5724), 696–697.
[269] Sazanov, L. A.; Walker, J. E. Cryo-electron crystallography of two sub-complexes of bovine complex I reveals the relationship between the membrane and peripheral arms. *J. Mol. Biol* **2000**, *302*(2), 455–464.
[270] Iwane, A. H.; Ikeda, I.; Kimura, Y.; Fujiyoshi, Y.; Altendorf, K.; Epstein, W. Two-dimensional crystals of the Kdp-ATPase of *Escherichia coli*. *FEBS Lett.* **1996**, *396*(2-3), 172–176.
[271] Arechaga, I.; Fotiadis, D. Reconstitution of mitochondrial ATP synthase into lipid bilayers for structural analysis. *J. Struct. Biol.* **2007**, *160*(3), 287–294.
[272] Gerle, C.; Tani, K.; Yokoyama, K.; Tamakoshi, M.; Yoshida, M.; Fujiyoshi, Y.; Mitsuoka, K. Two-dimensional crystallization and analysis of projection images of intact *Thermus thermophilus* V-ATPase. *J. Struct. Biol.* **2006**, *153*(2), 200–206.
[273] Toei, M.; Gerle, C.; Nakano, M.; Tani, K.; Gyobu, N.; Tamakoshi, M.; Sone, N.; Yoshida, M.; Fujiyoshi, Y.; Mitsuoka, K.; Yokoyama, K. Dodecamer rotor ring defines H+/ATP ratio for ATP synthesis of prokaryotic V-ATPase from *Thermus thermophilus*. *Proc. Natl. Acad. Sci. USA* **2007**, *104*(51), 20256–20261.
[274] Stahlberg, H.; Müller, D. J.; Suda, K.; Fotiadis, D.; Engel, A.; Meier, T.; Matthey, U.; Dimroth, P. Bacterial Na(+)-ATP synthase has an undecameric rotor. *EMBO Rep.* **2001**, *2*(3), 229–233.
[275] Meier, T.; Ferguson, S. A.; Cook, G. M.; Dimroth, P.; Vonck, J. Structural investigations of the membrane-embedded rotor ring of the F-ATPase from Clostridium paradoxum. *J. Bacteriol.* **2006**, *188*(22), 7759–7764.
[276] Fritz, M.; Klyszejko, A. L.; Morgner, N.; Vonck, J.; Brutschy, B.; Muller, D. J.; Meier, T.; Müller, V. An intermediate step in the evolution of ATPases: A hybrid F(0)-V(0) rotor in a bacterial Na(+) F(1)F(0) ATP synthase. *FEBS J.* **2008**, *275*(9), 1999–2007.
[277] Matthies, D.; Preiss, L.; Klyszejko, A. L.; Müller, D. J.; Cook, G. M.; Vonck, J.; Meier, T. The c13 ring from a thermoalkaliphilic ATP synthase reveals an extended diameter due to a special structural region. *J. Mol. Biol.* **2009**, *388*(3), 611–618.
[278] Kühlbrandt, W.; Zeelen, J.; Dietrich, J. Structure, mechanism, and regulation of the Neurospora plasma membrane $H^+$-ATPase. *Science* **2002**, *297*(5587), 1692–1696.
[279] Chintalapati, S.; Al Kurdi, R.; van Scheltinga, A. C.; Kühlbrandt, W. Membrane structure of CtrA3, a copper-transporting P-type-ATPase from Aquifex aeolicus. *J. Mol. Biol.* **2008**, *378*(3), 581–595.
[280] Wu, C. C.; Rice, W. J.; Stokes, D. L. Structure of a copper pump suggests a regulatory role for its metal-binding domain. *Structure* **2008**, *16*(6), 976–985.
[281] Nishizawa, T.; Abe, K.; Tani, K.; Fujiyoshi, Y. Structural analysis of 2-D crystals of gastric $H^+$,$K^+$-ATPase in different states of the transport cycle. *J. Struct. Biol.* **2008**, *162*(2), 219–228.
[282] Abe, K.; Tani, K.; Nishizawa, T.; Fujiyoshi, Y. Inter-subunit interaction of gastric $H^+$,$K^+$-ATPase prevents reverse reaction of the transport cycle. *EMBO J.* **2009**, *28*(11), 1637–1643.
[283] Shi, D.; Lewis, M. R.; Young, H. S.; Stokes, D. L. Three-dimensional crystals of Ca2+-ATPase from sarcoplasmic reticulum: Merging electron diffraction tilt series and imaging the (h, k, 0) projection. *J. Mol. Biol.* **1998**, *284*(5), 1547–1564.
[284] Zhang, P.; Toyoshima, C.; Yonekura, K.; Green, N. M.; Stokes, D. L. Structure of the calcium pump from sarcoplasmic reticulum at 8 Å resolution. *Nature* **1998**, *392*(6678), 835–839.
[285] Xu, C.; Rice, W. J.; He, W.; Stokes, D. L. A structural model for the catalytic cycle of Ca(2+)-ATPase. *J. Mol. Biol.* **2002**, *316*(1), 201–211.
[286] Stokes, D. L.; Delavoie, F.; Rice, W. J.; Champeil, P.; McIntosh, D. B.; Lacapere, J. J. Structural studies of a stabilized phosphoenzyme intermediate of $Ca^{2+}$-ATPase. *J. Biol. Chem.* **2005**, *280*(18), 18063–18072.
[287] Stokes, D. L.; Pomfret, A. J.; Rice, W. J.; Glaves, J. P.; Young, H. S. Interactions between $Ca^{2+}$-ATPase and the pentameric form of phospholamban in two-dimensional co-crystals. *Biophys. J.* **2006**, *90*(11), 4213–4223.
[288] Young, H. S.; Rigaud, J. L.; Lacapere, J. J.; Reddy, L. G.; Stokes, D. L. How to make tubular crystals by reconstitution of detergent-solubilized Ca2(+)-ATPase. *Biophys. J.* **1997**, *72*(6), 2545–2558.
[289] Tahara, Y.; Oshima, A.; Hirai, T.; Mitsuoka, K.; Fujiyoshi, Y.; Hayashi, Y. The 11 A resolution projection map of $Na^+/K^+$-ATPase calculated by application of single particle analysis to two-dimensional crystal images. *J. Electron Microsc. (Tokyo)* **2000**, *49*(4), 583–587.
[290] Mohraz, M. Reconstitution of detergent-solubilized Na,K-ATPase and formation of two-dimensional crystals. *J. Struct. Biol.* **1999**, *125*(1), 76–85.
[291] Hebert, H.; Purhonen, P.; Thomsen, K.; Vorum, H.; Maunsbach, A. B. Renal Na,K-ATPase structure from cryo-electron microscopy of two-dimensional crystals. *Ann. New York Acad. Sci.* **2003**, *986*, 9–16.
[292] Rice, W. J.; Young, H. S.; Martin, D. W.; Sachs, J. R.; Stokes, D. L. Structure of $Na^+$,$K^+$-ATPase at 11-A resolution: Comparison with $Ca^{2+}$-ATPase in E1 and E2 states. *Biophys. J.* **2001**, *80*(5), 2187–2197.
[293] Hu, G. B.; Rice, W. J.; Drose, S.; Altendorf, K.; Stokes, D. L. Three-dimensional structure of the KdpFABC complex of *Escherichia coli* by electron tomography of two-dimensional crystals. *J. Struct. Biol.* **2008**, *161*(3), 411–418.
[294] Dorset, D. L.; Engel, A.; Haner, M.; Massalski, A.; Rosenbusch, J. P. Two-dimensional crystal packing of matrix porin. A channel forming protein in *Escherichia coli* outer membranes. *J. Mol. Biol.* **1983**, *165*(4), 701–710.
[295] Sass, H. J.; Buldt, G.; Beckmann, E.; Zemlin, F.; van Heel, M.; Zeitler, E.; Rosenbusch, J. P.; Dorset, D. L.; Massalski, A. Densely packed beta-structure at the protein-lipid interface of porin is revealed by high-resolution cryo-electron microscopy. *J. Mol. Biol.* **1989**, *209*(1), 171–175.
[296] Baboolal, T. G.; Conroy, M. J.; Gill, K.; Ridley, H.; Visudtiphole, V.; Bullough, P. A.; Lakey, J. H. Colicin N binds to the periphery of its receptor and translocator, outer membrane protein F. *Structure* **2008**, *16*(3), 371–379.
[297] Lambert, O.; Moeck, G. S.; Levy, D.; Plancon, L.; Letellier, L.; Rigaud, J. L. An 8-A projected structure of FhuA, A "ligand-gated" channel of the *Escherichia coli* outer membrane. *J. Struct. Biol.* **1999**, *126*(2), 145–155.
[298] Lepault, J.; Dargent, B.; Tichelaar, W.; Rosenbusch, J. P.; Leonard, K.; Pattus, F. Three-dimensional reconstruction of maltoporin from electron microscopy and image processing. *EMBO J.* **1988**, *7*(1), 261–268.
[299] Signorell, G. A.; Chami, M.; Condemine, G.; Schenk, A. D.; Philippsen, A.; Engel, A.; Remigy, H. W. Projection maps of three members of the KdgM outer membrane protein family. *J. Struct. Biol.* **2007**, *160*(3), 395–403.
[300] Behlau, M.; Mills, D. J.; Quader, H.; Kühlbrandt, W.; Vonck, J. Projection structure of the monomeric porin OmpG at 6 A resolution. *J. Mol. Biol.* **2001**, *305*(1), 71–77.
[301] Baldermann, C.; Engelhardt, H. Expression, two-dimensional crystallization, and three-dimensional reconstruction of the beta8 outer membrane protein Omp21 from *Comamonas acidovorans*. *J. Struct. Biol.* **2000**, *131*(2), 96–107.
[302] Collins, R.; Achtman, M.; Ford, R.; Bullough, P. Derrick, J. Projection structure of reconstituted Opc outer membrane protein from *Neisseria meningitidis*. *Mol. Microbiol.* **1999**, *32*(1), 217–219.
[303] Jap, B. K. High-resolution electron diffraction of reconstituted PhoE porin. *J. Mol. Biol.* **1988**, *199*(1), 229–231.
[304] Casagrande, F.; Harder, D.; Schenk, A.; Meury, M.; Ucurum, Z.; Engel, A.; Weitz, D.; Daniel, H.; Fotiadis, D. Projection structure of DtpD (YbgH), a prokaryotic member of the peptide transporter family. *J. Mol. Biol.* **2009**, *394*(4), 708–717.
[305] Unwin, P. N.; Ennis, P. D. Two configurations of a channel-forming membrane protein. *Nature* **1984**, *307*(5952), 609–613.
[306] Perkins, G.; Goodenough, D.; Sosinsky, G. Three-dimensional structure of the gap junction connexon. *Biophys. J.* **1997**, *72*(2 Pt 1), 533–544.
[307] Unger, V. M.; Kumar, N. M.; Gilula, N. B.; Yeager, M. Expression, two-dimensional crystallization, and electron cryo-crystallography of recombinant gap junction membrane channels. *J. Struct. Biol.* **1999**, *128*(1), 98–105.
[308] Unger, V. M.; Kumar, N. M.; Gilula, N. B.; Yeager, M. Three-dimensional structure of a recombinant gap junction membrane channel. *Science* **1999**, *283*(5405), 1176–1180.
[309] Cheng, A.; Schweissinger, D.; Dawood, F.; Kumar, N.; Yeager, M. Projection structure of full length connexin 43 by electron cryo-crystallography. *Cell Commun. Adhes.* **2003**, *10*(4-6), 187–191.
[310] Oshima, A.; Tani, K.; Hiroaki, Y.; Fujiyoshi, Y.; Sosinsky, G. E. Three-dimensional structure of a human connexin26 gap junction channel reveals a plug in the vestibule. *Proc. Natl. Acad. Sci. USA* **2007**, *104*(24), 10034–10039.
[311] Oshima, A.; Tani, K.; Toloue, M. M.; Hiroaki, Y.; Smock, A.; Inukai, S.; Cone, A.; Nicholson, B. J.; Sosinsky, G. E.; Fujiyoshi, Y. Asymmetric configurations and *N*-terminal rearrangements in connexin26 gap junction channels. *J. Mol. Biol.* **2011**, *405*(3), 724–735.
[312] Yeager, M.; Unger, V. M.; Mitra, A. K. Three-dimensional structure of membrane proteins determined by two-dimensional crystallization, electron cryomicroscopy, and image analysis. *Meth. Enzymol* **1999**, *294*, 135–180.

[313] Oshima, A.; Tani, K.; Hiroaki, Y.; Fujiyoshi, Y.; Sosinsky, G. E. Projection structure of a *N*-terminal deletion mutant of connexin 26 channel with decreased central pore density. *Cell Commun. Adhes.* **2008**, *15*(1), 85–93.
[314] Oostergetel, G. T.; Keegstra, W.; Brisson, A. Structure of the major membrane protein complex from urinary bladder epithelial cells by cryo-electron crystallography. *J. Mol. Biol* **2001**, *314*(2), 245–252.
[315] Ounjai, P.; Unger, V. M.; Sigworth, F. J.; Angsuthanasombat, C. Two conformational states of the membrane-associated *Bacillus thuringiensis* Cry4Ba delta-endotoxin complex revealed by electron crystallography: Implications for toxin-pore formation. *Biochem. Biophys. Res. Commun.* **2007**, *361*(4), 890–895.
[316] Martin-Benito, J.; Gavilanes, F.; de Los Rios, V.; Mancheno, J. M.; Fernandez, J. J.; Gavilanes, J. G. Two-dimensional crystallization on lipid monolayers and three-dimensional structure of sticholysin II, a cytolysin from the sea anemone *Stichodactyla helianthus*. *Biophys. J.* **2000**, *78*(6), 3186–3194.
[317] Mancheno, J. M.; Martin-Benito, J.; Martinez-Ripoll, M.; Gavilanes, J. G.; Hermoso, J. A. Crystal and electron microscopy structures of sticholysin II actinoporin reveal insights into the mechanism of membrane pore formation. *Structure* **2003**, *11*(11), 1319–1328.
[318] Wilmsen, H. U.; Leonard, K. R.; Tichelaar, W.; Buckley, J. T.; Pattus, F. The aerolysin membrane channel is formed by heptamerization of the monomer. *EMBO J.* **1992**, *11*(7), 2457–2463.
[319] Bhairi, S. M. *Detergents. A Guide to the Properties and Uses of Detergents in Biological Systems.* Calbiochem-Novabiochem Corporation: San Diego, CA, USA, 2001; p 41.